Title
Mechanistic studies of heme oxygenase

Permalink
https://escholarship.org/uc/item/9625g5px

Author
Torpey, Justin,

Publication Date
1997

Peer reviewed|Thesis/dissertation

Mechanistic Studies of Heme Oxygenase

by

Justin Torpey

DISSERTATION

Submitted in partial satisfaction of the requirements for the degree of

DOCTOR OF PHILOSOPHY
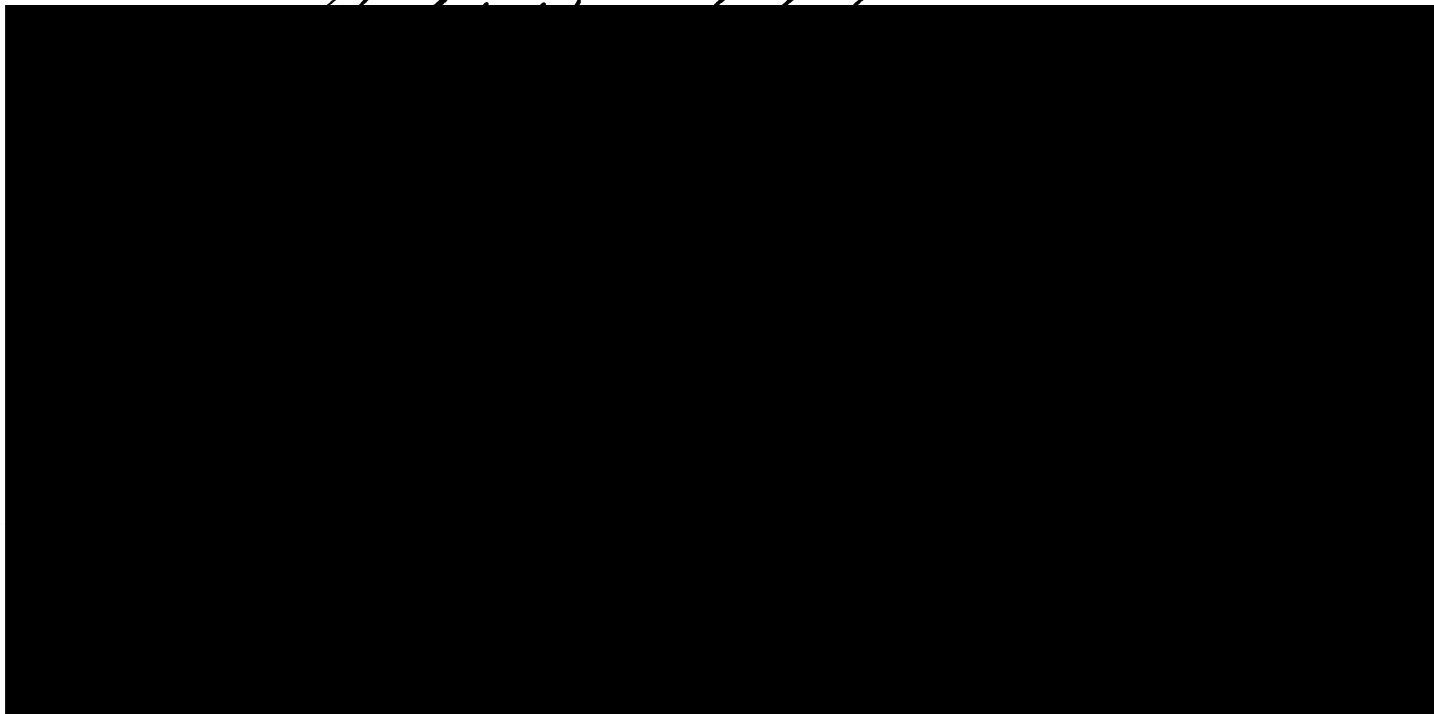
in

Pharmaceutical Chemistry

in the

GRADUATE DIVISION

of the

UNIVERSITY OF CALIFORNIA

San Francisco

ACKNOWLEDGEMENTS

MECHANISTIC STUDIES OF HEME OXYGENASE

Justin W. Torpey

ABSTRACT

The heme oxygenase-catalyzed oxidation of heme is dependent on P450 reductase and NADPH, uses three molecules of dioxygen to yield equimolar amounts of biliverdin IXα, carbon monoxide, and iron. The initial heme hydroxylation step of heme oxygenase-1 (hHO-1) was found to proceed without a primary kinetic isotope effect using a heme molecule deuterated at the *meso* positions. Thus, under the conditions employed for the assay, abstraction of the α-*meso* proton is not rate limiting. The reaction product of the heme-hHO-1 complex and ethylhydroperoxide was identified by mass spectrometry and 2D-^{1}H NMR as α-*meso*-ethoxyheme. The formation of this metabolite is consistent with an electrophilic, but not a nucleophilic, hydroxylation mechanism. Furthermore, the reaction of the α-*meso*-methyl 2,4-dimethyl heme-hHO-1 complex with NADPH-P450 reductase revealed a novel heme cleavage reaction which regiospecifically eliminates the α-*meso* carbon as well as the appended methyl group. While heme hydroxylation at the methyl-substituted position is consistent with an electrophilic hydroxylation mechanism, the absence of detectable CO as a reaction product indicates that hydroxyheme is not an intermediate.

The *meso*-methylmesoheme and *meso*-formylmesoheme regioisomers were synthesized and used as probes of the factors controlling the regiospecificity of hHO-1. The *meso*-substituted mesohemes were reacted with hHO-1 and the mesobiliverdin products were extracted and analyzed by HPLC, UV-visible spectroscopy, and mass spectrometry. The α-*meso*-methylmesoheme gave identical results to those described above. The γ-isomer gave completely inverted regiospecificity, yielding mesobiliverdin IXγ. The δ-isomer gave a mixture of methyl-substituted and unsubstituted mesobiliverdins. These results demonstrate that, in accordance with the electrophilic heme hydroxylation mechanism, the regiospecificity is controlled electronically with the reaction taking place at the most electron-rich *meso*-carbon. The *meso*-formyl isomers, however, have the opposite effect in that the reaction takes place at a *meso*-carbon without the *meso*-formyl substituent, as evidenced by the detection and quantitation of carbon monoxide as a reaction product. Collectively these data are interpreted as compelling evidence that the reaction regiospecificity is dictated by electronic factors, both inherent to the heme and exerted by the protein, as opposed to steric factors as previously believed.

TABLE OF CONTENTS

AND *MESO*-FORMYL MESOHEMES

LIST OF FIGURES

vi

viii

LIST OF TABLES

ABBREVIATIONS

BSA	bovine serum albumin
cGMP	guanosine 3',5'-monophosphate
CO	carbon monoxide
2,4-DNP	2,4-dinitrophenylhydrazine
EPR	electron paramagnetic resonance
GC	gas chromatography
heme	iron protoporphyrin IX
HPLC	high performance liquid chromatography
HTP	hydroxyapatite
KIE	kinetic isotope effect
LSIMS	liquid secondary ion mass spectrometry
LTP	long term potentiation
mesoheme	iron mesoporphyrin
mCPBA	meta-chloroperbenzoic acid
mRNA	messenger RNA
MSPR-DME	mesoporphyrin IX dimethylester
NADPH	β-nicotinamide adenine dinucleotide phosphate (reduced form)
NMR	nuclear magnetic resonance
NO	nitric oxide
NOE	nuclear overhauser effect

NOESY	NOE spectroscopy
PCC	pyridinium chlorochromate
PPIX-DME	protoporphyrin IX dimethylester
THF	tetrahydrofuran
TFA	trifluoroacetic acid
TFAA	trifluoroacetic anhydride
TLC	thin layer chromatography
TPP	tetraphenyl porphine
UV	ultraviolet
Zn-PPIX	Zn-protoporphyrin IX

1.0 INTRODUCTION

1.1 HEME

Heme (iron protoporphyrin IX) is one of the essential biochemical tools of life. It is associated with a variety of proteins that perform such diverse tasks as oxygen transport, electron transport, and oxygen activation for oxidative transformations. Thus, the heme molecule can be utilized in a variety of ways and in each case its function is ultimately determined by the properties of the polypeptide bound to it (Ortiz de Montellano, 1987; Dawson, 1988). This thesis is a study of the unique properties of heme oxygenase [EC 1.14.99.3] , the enzyme responsible for the catabolism of heme.
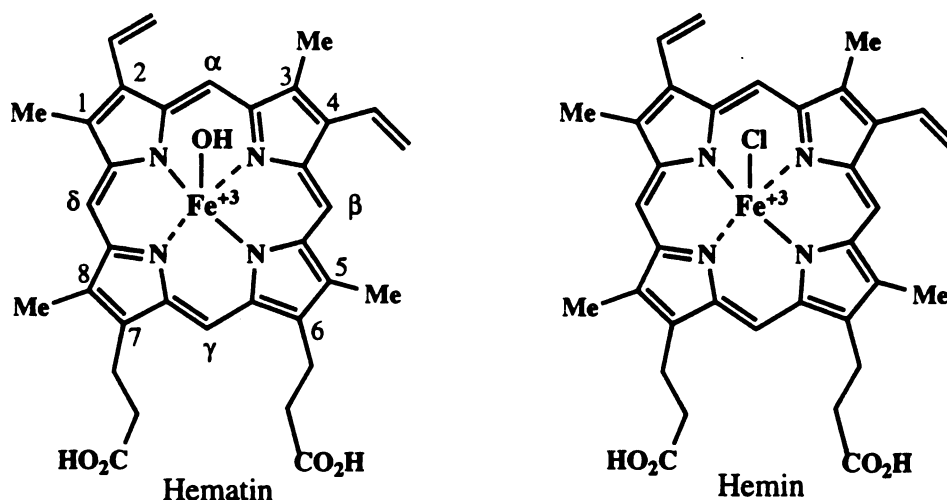
Figure 1.1.1. The structures of the iron(III) protoporphyrin IX salts, hematin and hemin.

1.2 HEME CATABOLISM

Heme catabolism has long been a topic of special interest amongst chemists studying the tetrapyrroles. Perhaps the first connection between heme and bilirubin, the end product of heme catabolism, was made by Küster, who noted sometime near the beginning of the twentieth century that the structures were "closely related" (Gray, 1953). The structures of heme and bilirubin were confirmed by total synthesis in 1927 and 1942, respectively, by Hans Fischer and coworkers (Fischer & Orth, 1937; Fischer & Plieninger, 1942). Proof that bile pigments were the products of heme catabolism *in vivo* was finally provided 20 years later by administration of ^{15}N isotopically labelled hemin and demonstration that at least 20% of the hemin was rapidly metabolized to bile pigments

1

(London, 1950).

The chemistry of the breakdown of heme to bile pigments was entirely speculative until the 30's, when it was shown that a green heme, "Grünes Hämin", could be obtained by oxygenation of a solution of heme in pyridine in the presence of hydrazine or other reducing agents (Warburg & Negelein, 1930). This model for heme catabolism is commonly known as "coupled oxidation". It was taken one step further when crystalline biliverdin dimethylester was obtained upon treatment of the "green hæmin" with methanolic hydrogen chloride (Lemberg, 1935). Lemberg also elucidated an important structural feature of the "green hæmin": it had lost its α-methine group. In addition he incorrectly proposed the structure of the "green hæmin" to be an iron-biliverdin complex and the α-methine group to be formaldehyde. Nevertheless, a compound similar to this "verdohæmochromogen" was formed by adding ascorbic acid to an oxygenated solution of hemoglobin. The product was a bile-pigment-iron-globin complex called "choleglobin" with a well defined visible band at 628 nm for the reduced form and 670 nm for the oxidized form (Lemberg et al., 1941a). The exact structure of "verdohæmochromogen" was rigorously determined much later (Lagarias, 1982), but these landmark experiments established for the first time a working model system for heme catabolism.

1.3 REGIOSPECIFICTY OF HEME CATABOLISM

The total synthesis of bilirubin established that it was probably derived from the heme nucleus and that the porphyrin macrocycle had been cleaved at the α-meso position. Lemberg thought he had isolated exclusively the α-isomer of biliverdin by coupled oxidation (1935). Lemberg was only partially correct, as later studies showed that all four isomeric biliverdins are formed in the coupled oxidation of heme in pyridine and water (Petryka et al., 1962) and these regioisomers (Figure 1.3.1) were later separated and assigned regiochemistries (Bonnett & McDonagh, 1973). However, coupled oxidation of hemoproteins can proceed with some regioselectivity. For example, while coupled oxidation of myoglobin yields biliverdin IXα, and coupled oxidation of hemoglobin yields 60-80% biliverdin IXα and the rest biliverdin IXβ, coupled oxidation of the denatured globins gives roughly equal amounts of the regioisomers (O'Carra & Colleran, 1969). It was therefore shown that globins could exhibit regioselectivity in the heme cleavage reaction, and that this could be relevant to the regiospecificity found in vivo. O'Carra and Colleran on these grounds suggested that "it now seems unnecessary to retain the conventional concept of a haem-cleaving enzyme system since the haemproteins themselves seem to have all the attributes being sought in such an enzyme system". Their inability to

2

detect biliverdin IXβ *in vivo* was rationalized by the fact that only 60-80% of hemoglobin
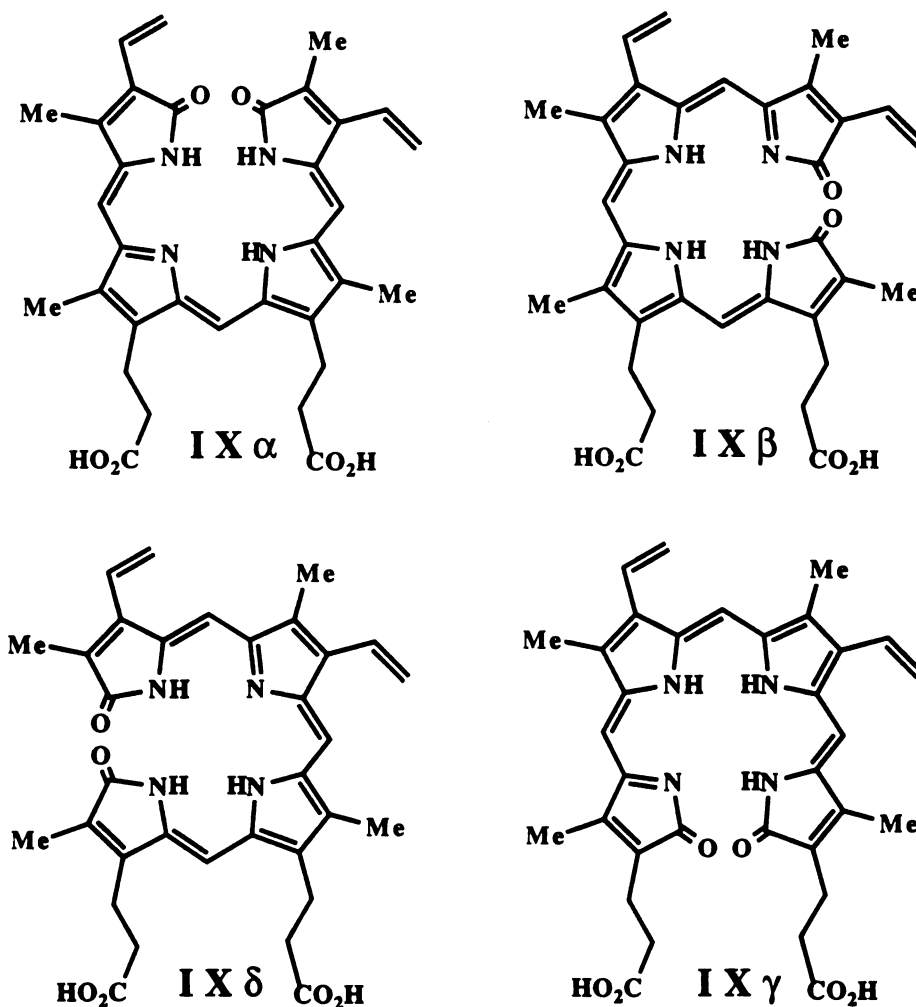
Figure 1.3.1. The structures of the four regioisomers of biliverdin IX.

catabolism is accounted for by the production of bilirubin IXα, and that some other metabolic pathway must exist for the β-isomer. In addition, they determined that the enzymatic reduction of biliverdin IXβ is much slower than for the IXα isomer. Given the unsatisfactory explanation for a lack of biliverdin IXβ *in vivo*, the question remained as to the existence of a heme cleaving enzyme system.

The mechanism of the regiospecificity of heme catabolism *in vivo* has also long been a mystery. Lemberg had proposed an intrinsic enhancement in the reactivity of the α-*meso* position (Lemberg, 1956). Brown (1976) proposed that the regioselectivity was a consequence of the differences in accessibility of each of the *meso* edges to the bound dioxygen. The steric hindrance mechanism of regioselectivity was consistent with the

known active site structures of both myoglobin and hemoglobin (Brown et al., 1981). In addition, the varying biliverdin isomer distributions produced by coupled oxidation of hemoglobin mutants supported the hypothesis that mutated amino acid residues could sterically hinder the heme cleavage reaction at a given site (Brown & Docherty, 1978).

1.4 BILE PIGMENTS

The enzyme heme oxygenase catalyzes the transformation of heme to biliverdin IXα *in vivo*, which is then reduced by the cytosolic enzyme biliverdin reductase to bilirubin (Figure 1.4.1). Reduction of biliverdin to bilirubin occurs in all mammals. Biliverdin is
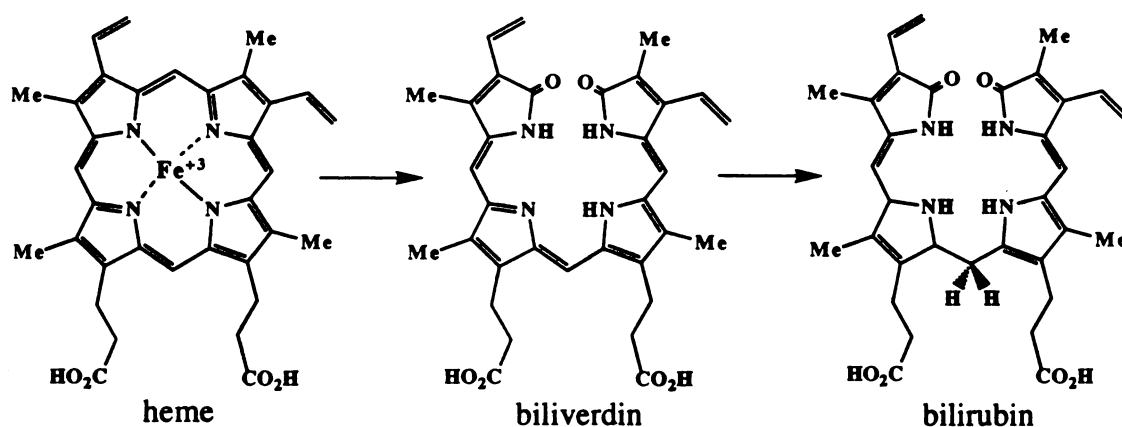
Figure 1.4.1. Conversion of heme to biliverdin, and biliverdin to bilirubin.

the end product of heme catabolism in some non-mammals and is excreted in egg shells and fecal matter. Based on the increased lipophilicity of bilirubin, it was hypothesized that reduction of biliverdin is necessary to move heme metabolites through the placenta (McDonagh et al., 1981). An adult human produces 300-400 mg of bilirubin/day, 80% of which derives from hemoglobin heme (Robinson, 1968). Bilirubin in the serum remains between 5-17 μM, essentially all of which is bound to serum albumin (Maines, 1992a). Bilirubin is excreted as the glucuronide conjugate, which is vastly more water soluble than unconjugated bilirubin. Newborns with impaired glucuronyl transferase activity suffer from neonatal jaundice, or hyperbilirubinemia. In the first few days of life bilirubin production is two- to three- times greater than normal adults, thus hyperbilirubinemia in newborns is considered normal (Maines, 1992a). However, approximately 5% of newborns suffer from bilirubin levels that become dangerously high and threaten neuronal damage. The exact mechanism of how bilirubin passes through the blood-brain barrier and causes harm is unknown.

4

Treatment of neonatal jaundice is two-fold. The most common treatment is phototherapy, in which the jaundiced infant is exposed to blue or white light. The therapeutic effect is mediated by photoisomerization of bilirubin IXα (4Z, 15Z) to bilirubin IXα (4Z, 15E), and other more polar and readily excretable photoisomers (Figure 1.4.2) (McDonagh & Lightner, 1985). In very severe cases, exchange transfusion is also used (A.F. McDonagh, personal communication). A recent experimental treatment is administration of Sn- or Zn-PPIX complexes as inhibitors of both heme oxygenase and biliverdin reductase (Maines, 1992a).
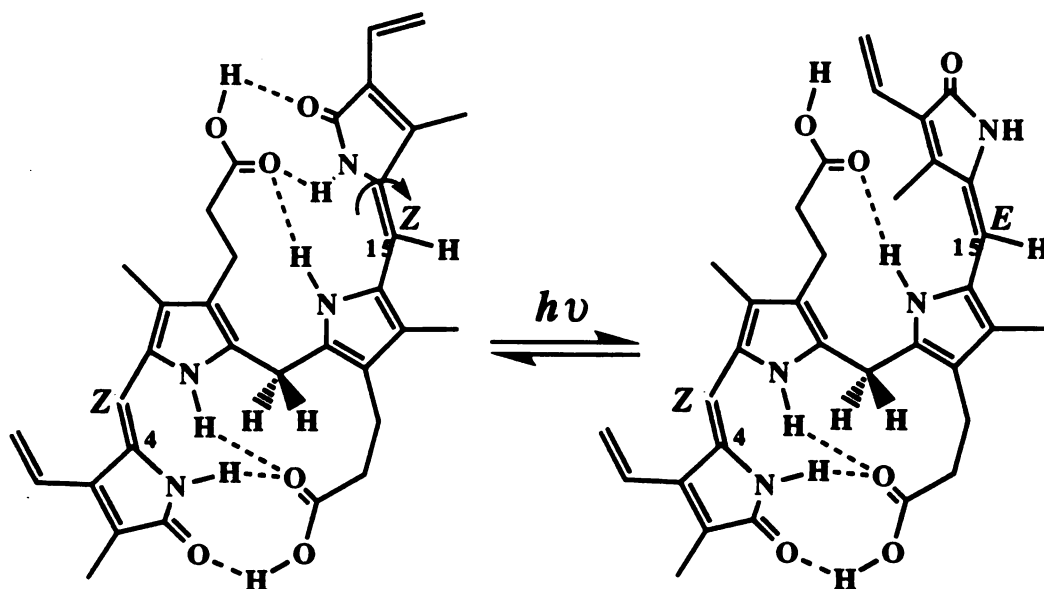
Figure 1.4.2. Photoisomerization of (4Z, 15Z)-bilirubin to (4Z, 15E)-bilirubin occurs in jaundiced infants undergoing phototherapy.

Recently bilirubin was identified as a potentially important antioxidant of possible physiological significance. It was shown *in vitro* that at micromolar concentrations bilirubin efficiently scavenges peroxyl radicals under a physiologically relevant atmosphere of 2% oxygen (Stocker et al., 1987b). In liposomes, bilirubin suppressed oxidation more effectively than α-tocopherol, which is regarded as one of the best antioxidants. This study was extended to albumin-bound bilirubin (Stocker et al., 1987a) and it was found that this complex protected albumin-bound linoleic acid from peroxyl radical induced oxidation *in vitro*. These results indicate the possibility that albumin-bound bilirubin may have physiological antioxidant properties but this remains to be firmly established.

5

1.5 CARBON MONOXIDE AS NEURAL MESSENGER

Carbon monoxide was shown to be an endogenous metabolic product in man by Sjöstrand (1949), who also noted that the rate of carbon monoxide production was elevated in patients with increased erythrocyte destruction. Early hypotheses concerning the source of endogenous carbon monoxide production in mammals were confirmed *in vivo* by investigators who used radioactive tracers to show that the α-*meso* carbon of heme is oxidized to carbon monoxide in stoichiometric amounts with respect to heme consumed and bilirubin produced (Coburn et al., 1967; Landlaw et al., 1970). The rate of CO production in the human body is approximately 16.4 μmol/hr (Marks, 1994). CO had no known physiological function until it was proposed that CO may play a similar role as NO in signal transduction (Marks et al., 1991). It had previously been observed that CO was an apt vasodilator *in vitro*, and furthermore shared the ability of NO to activate guanylyl cyclase. It was therefore postulated that CO could be a vasodilator *in vivo* through the same mechanism as NO, by activating guanylyl cyclase and elevating cGMP levels (Marks et al., 1991).

The first experimental evidence that CO could decrease cGMP levels was provided by a study using the selective heme oxygenase inhibitor Zn-PPIX (Verma et al., 1993). They found two pieces of data that indirectly implicate CO as a neurotransmitter. By *in situ* hybridization in brain slices, they demonstrated the discrete neuronal co-localization of mRNA for the constitutive isozyme of heme oxygenase (HO-2) and mRNA for soluble guanylyl cyclase. In addition, they demonstrated that in primary cultures of olfactory neurons, Zn-PPIX depleted endogenous cGMP. It has since been reported that the neuropharmacological effects of metalloporphyrins may be the result of a direct inhibition of soluble guanylyl cyclase (Luo & Vincent, 1994), thus leaving CO's role as a neurotransmitter in the shadow of circumstance. The indirect effect of Zn-PPIX may mean the proposed CO activity is artifactual.

CO and NO have also been implicated as neurotransmitters mediating activity-dependent long-term synaptic transmission which is thought to contribute to certain forms of learning (Zhuo et al., 1993). This study used Zn-PPIX to block production of CO, and showed that administering Zn-PPIX to hippocampal slices blocked long-term potentiation (LTP). A similar study showed that the same heme oxygenase inhibitor (Zn-PPIX) prevented the induction of LTP and that it reversed LTP that was already established (Stevens & Wang, 1993). However, until a heme oxygenase inhibitor is developed that is

6

entirely specific, the role of CO as neurotransmitter is supported only by indirect evidence.

Another attempt to study the role of carbon monoxide in long-term potentiation used an HO-2 knockout mouse (Poss et al., 1995). The mice lacked any gross neurophysiological abnormalities. Also absent were any observed effects on long-term potentiation. In addition, Zn-PPIX prevented induction of LTP as previously observed. The basic conclusion of the study is that endogenous CO generated by HO-2 in the mouse brain seems not to have any importance with regard to long-term potentiation.

1.6 MICROSOMAL HEME OXYGENASE

Several groups participated in the search for the enzyme system responsible for heme catabolism *in vivo*. Nakajima and co-workers (1963a, 1963b) described a "heme α-methenyl oxygenase" from liver and kidney homogenates which required NADPH, ferrous iron, and an activator extracted from liver cell nuclei by boiling water. They also crystallized a novel intermediate similar to verdoheme but which gave positive aldehyde tests, including the formation of a 2,4-dinitrophenylhydrazone. The intermediate was postulated to retain the α-*meso* carbon on the A pyrrole ring of the porphyrin as an aldehyde. Acid hydrolysis gave biliverdin and stoichiometric amounts of iron and formaldehyde. Attempts to verify these results by other labs resulted in a lack of evidence for a physiological role for the system, including the demonstration that the system actually produced all four biliverdin isomers (O'Carra & Colleran, 1969). Wise and Drabkin (1965) described a system isolated from the hemophagous organ of the dog placenta which required NADP, NAD, oxygen, and ATP. However, the relevance of this system to physiological production of bile pigments was not determined as the hemophagous organ was known to contain biliverdin but had an unknown function.

The enzymatic conversion of heme to bilirubin by microsomal heme oxygenase was first described by Schmid and co-workers here at the University of California at San Francisco (Tenhunen et al., 1968). The enzymatic system was found in rat liver and rat spleen microsomes. The evidence indicating that the activity was indeed enzymatic was (a) its inhibition by CO even in the presence of O_2; (b) its absolute requirement for NADPH; and (c) its heat lability. The biliverdin and bilirubin products produced were identified by spectrophotometric, chromatographic, and chemical means.

Heme oxygenase was first purified from the microsomal fraction of the liver and spleen (Tenhunen et al., 1969). The enzyme had an absolute stoichiometric requirement

7

for NADPH and molecular oxygen and generated equimolar amounts of carbon monoxide and bilirubin. The stoichiometry of oxygen and NADPH consumption was consistent with a mixed function oxidase. Furthermore, the enzyme was inhibited by carbon monoxide and this effect could be reversed by photodissociation of the ferrous-CO complex using monochromatic light in the 450 to 470 nm range (Tenhunen et al., 1972). Thus it was suspected that the microsomal heme oxygenase system was a mixed-function oxidase with a hemoprotein resembling cytochrome P450 as terminal oxidase.

Tenhunen et al. (1969) did, however, report a distinguishing factor between the microsomal heme oxygenase system and the mixed-function oxidase system responsible for the biotransformations of xenobiotics. In particular, these investigators showed that known cytochrome P450 substrates such as hexobarbital, aminopyrine, and a known cytochrome P450 inhibitor SKF 525A, failed to inhibit heme oxygenase. Maines and Kappas (1974, 1975) investigated this further using cobalt, a compound known to decrease both hepatic microsomal drug metabolism and the microsomal content of cytochrome P450 (Tephly and Hibbeln, 1971). By feeding cobalt chloride to rats and analyzing their liver microsomes they found that, indeed, there was a major decrease in cytochrome P450 content whereas, in "striking contrast", the microsomal heme oxygenase system increased activity up to ten-fold. In addition, in urea-treated microsomes, comparable heme oxygenase levels persisted even in the absence of spectrally detectable cytochrome P450. It was therefore shown that the protein components of heme catabolism and drug metabolism were distinct and that P450 was not required for heme oxidation.

Yoshida et al. (1974) partially purified and reconstitued the heme oxygenase system from pig spleen microsomes. These investigators noted that, in contrast to cytochrome P450, the spleen had a high specific activity of heme oxygenase. They demonstrated the absence of cytochrome P450 in their preparation of spleen heme oxygenase, and proposed the existence of a protein in spleen that bound heme to form an enzyme-substrate complex that resembled a hemoprotein. This hemoprotein would then act upon its own prosthetic group and heme would serve as both substrate and cofactor. They also reported the requirement of NADPH-cytochrome c reductase for enzymic activity.

1.7 HEME OXYGENASE ISOZYMES

Maines et al. (1986) first reported the characterization of two forms of heme oxygenase from rat liver microsomes, designated HO-1 and HO-2. HO-2 activity was reported as 2-3 times that of HO-1. However, in response to cobalt, for example, HO-1

was induced by 100-fold, whereas HO-2 levels remained static. They reported similar apparent K_m values (HO-1 = 0.24 μM; HO-2 = 0.67 μM), and different biophysical properties such as thermostability, chromatographic behavior, ammonium sulfate precipitation, and antigenicity for the two isoforms. Similarities included substrate specificity, cofactor requirements, and regiospecificity of heme oxidation. Further studies focused on heme oxygenase levels in the testes. Trakshel et al. (1986) detected both isoforms in the testes and were able to purify the constitutive form (HO-2) to near homogeneity. They noted that, unlike the liver, the testes contained levels of HO-1 that were hardly detectable, and that the apparent M_r values for HO-1 and HO-2 were 30,000 and 36,000, respectively. Again they noted that the immunochemical properties of the isoforms were distinct and that HO-1 anitserum did not recognize HO-2. A similar study of heme oxygenase levels in rat brain failed to detect any HO-1 in this tissue, only high levels of HO-2 (Trakshel et al., 1988).

These studies were unable to determine whether the two heme oxygenase proteins were simply isoforms of heme oxygenase or whether they were true isozymes derived from different genes. Cruse and Maines (1988) found evidence for the latter: i.e., that the two heme oxygenase proteins were different gene products. Using antibody to HO-2, they cloned and sequenced two 274 bp gene fragments that contained a 14-amino acid sequence matching the partial amino acid sequence from purified HO-2. Shibahara et al. (1985) had already cloned rat spleen heme oxygenase (HO-1) and it was now recognized that the HO-2 fragment had only ~40% amino acid homology with this isozyme.

Analysis of the predicted amino acid sequence of HO-1 and a 91-amino acid HO-2 fragment revealed marked differences between the amino acid content of the isozymes, including the absence of cysteine from HO-1 in contrast to the three cysteines detected in HO-2 (Maines, 1988). Approximately 58% homology was determined between the two proteins, including a 24-mer sequence with two unmatched amino acids and a 10-mer sequence with only one unmatched amino acid. It was proposed that the regions with high homology formed the active site of the enzyme (Maines, 1988). HO-2 was cloned and its sequence compared more closely to that of HO-1 (Rotenberg & Maines, 1988; 1991). In sum, they compared rabbit and rat HO-2 to rat, mouse, and human HO-1 and found that the 24-mer sequence of amino acids was omnipresent in the mammalian heme oxygenase proteins sequenced. The sequence corresponds to residues 145-168 in rat and human HO-2. It was also proposed that the hydrophobic C-terminus may serve as the anchor that binds the protein to the membrane of the endoplasmic reticulum (Rotenberg & Maines,

1991). McCoubrey and Maines (1993) expressed modified HO-2 constructs in *E. coli* and determined that His 151, as well as the N-terminal 33 amino acids, but not the C-terminus, were required for enzymic activity. Furthermore they confirmed that the construct without the hydrophobic C-terminus was not associated with bacterial membranes.

1.8 SPECTROSCOPIC STUDIES OF PURIFIED NATIVE ENZYME

While the bulk of mechanistic information about heme catabolism was worked out in model studies, as the enzyme became more readily available its properties began to be studied more closely. Yoshida and co-workers were one of the first groups to purify heme oxygenase and begin spectroscopic studies of the enzyme (Yoshida & Kikuchi, 1978; 1979). The heme oxygenase system, which included the heme:heme oxygenase complex, NADPH-cytochrome c (P450) reductase, and NADPH, was monitored spectrophotometrically and a 688-nm substance was observed and identified as an intermediate in the reaction (Yoshida et al., 1980). This substance was reported to also have a high affinity for carbon monoxide, yielding a CO complexed intermediate with a λ_{max} at 638 nm. In a study using mesoheme instead of protoheme investigators identified the corresponding intermediates, the first with a maximum at 660-nm and the CO complex with a maximum at 617-nm (Yoshida et al., 1981). They also tried to establish that α-*meso* hydroxyheme was an intermediate in the reaction by synthesizing the mixture of *meso*-hydroxymesohemes and incubating them with the heme oxygenase system. They found that the *meso*-hydroxymesohemes were degraded to biliverdins of undetermined regiochemistry and that the reaction required reducing equivalents. This study was later extended using the individually purified regioisomers of *meso*-hydroxyprotoheme and it was found that only the α-isomer was converted efficiently to biliverdin by the heme oxygenase system (Yoshinaga et al., 1990).

Further investigations into the nature of the 688-nm substance followed, yet its precise structure remained elusive. It was shown that CO was liberated at the step of formation of the 688-nm substance from α-hydroxyheme, and therefore that the 688-nm substance had lost its α-methine carbon (Yoshida et al. 1982). In addition, it was shown that the 688-nm substance required reducing equivalents to be transformed to biliverdin (Yoshida & Noguchi, 1984). Lagarias (1982) in his account of the structure of verdohemochrome noted the spectral similarities between verdohemochrome and the heme oxygenase intermediate described by Yoshida.

1.9 SUBSTRATE SPECIFICITY

Through a series of studies (Frydman et al., 1981; Tomaro et al., 1984; Frydman & Frydman, 1987) the substrate specificity of heme oxygenase was determined using rat liver microsomal preparations. A variety of hemes, both natural and synthetic, were assayed and the production of bilirubin was measured and compared to that produced by incubation of the natural substrate, iron(III) protoporphyrin IX. While a wide variety of substituents can be tolerated at C_1, C_2, C_3, and C_4, all substrates have in common the propionates at C_6 and C_7. Furthermore, biliverdin reductase reduced all of the products to bilirubins, and no change in regiospecificity was detected.

1.10 CHEMICAL MECHANISM - HYDROXYHEME

Until recombinant soluble heme oxygenase became available, mechanistic information about heme catabolism was based primarily on model studies using coupled oxidation. These studies suggested the formation of two intermediates along the pathway to biliverdin IXα, meso-hydroxyheme and verdoheme (Figure 1.10.1). Meso-hydroxyheme, or iron oxyporphyrin, was first implicated as a possible intermediate by Lemberg et al. (1938). He proposed a heme structure with a hydroxyl group in place of a methine hydrogen based on isolation of a hydroxyporphyrin (oxyporphyrin; oxophlorin) upon treatment of a "dilute pyridine" solution of hemin with H_2O_2 and ascorbate under an atmosphere of nitrogen. The solution was kept overnight and a 40% final volume of concentrated HCl was added. The solution was kept for another 48 hours and was then extracted with sodium acetate and ether. The visible absorption spectrum of the compound was compared to that of Fischer's oxymesoporphyrin and they subsequently concluded it was a hydroxyporphyrin.

Further insight into the chemical structure of oxophlorins was achieved by synthesis of asymmetric oxophlorins and their ferrihemes (Jackson et al., 1968a & 1968b). These investigators characterized the absorption and ^{1}H-NMR spectra of synthetic β-oxymesoporphyrin and its mono- and dications. They also prepared the iron salt and demonstrated clean conversion of iron(III) β-oxymesoporphyrin to verdohemochrome upon exposure to oxygen at room temperature, supporting Lemberg's earlier hypothesis. Additional experimental evidence that meso-hydroxyhemes were intermediates in heme catabolism came from a study in which tritiated α- and β-hydroxymesohemes were administered to rats and the incorporation of the isotope into bile, bile pigment, urine,

feces, liver, kidney and spleen was measured (Kondo et al., 1971). These investigators found that the α-isomer was efficiently converted into bile pigment and specifically to the expected mesobilirubin. They also found that the β-isomer was poorly converted into bile pigment, and that neither of the free-base α- or β-hydroxymesoporphyrins were converted to bile pigment.
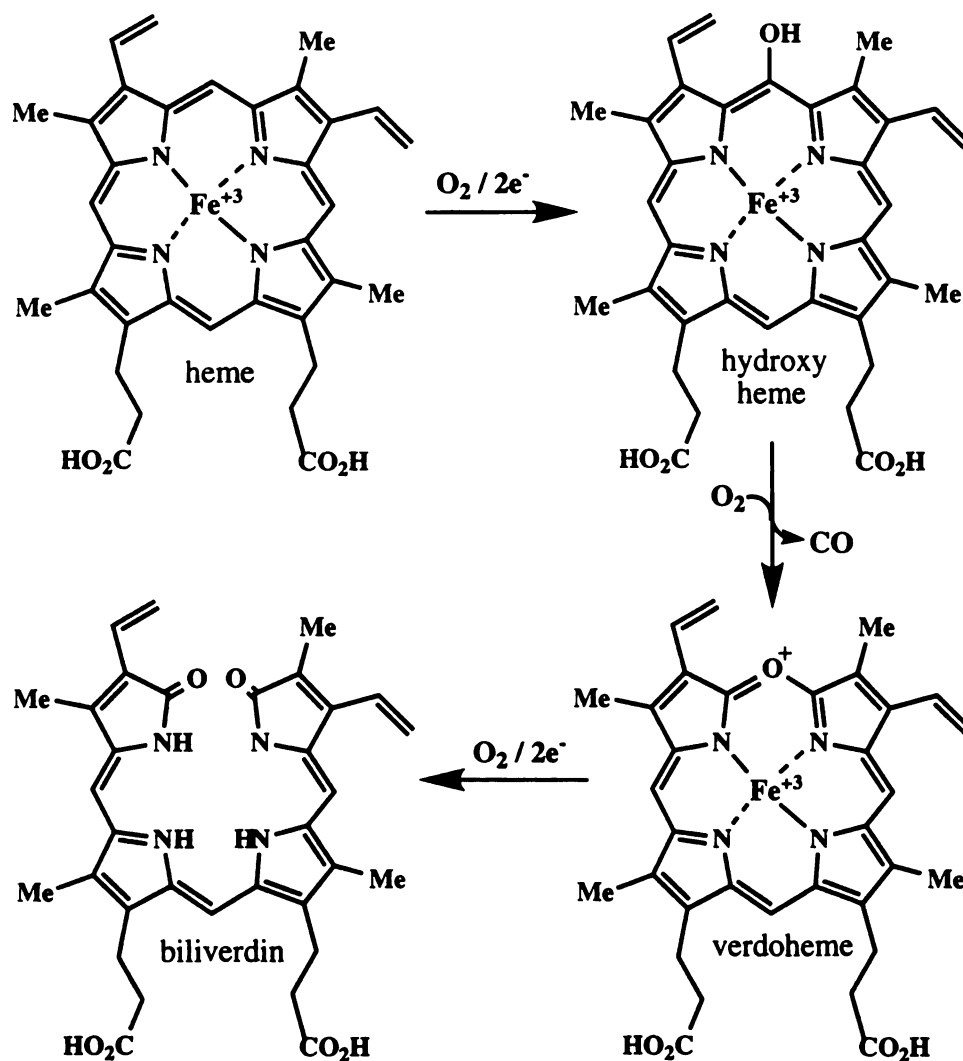
Figure 1.10.1. Probable sequence of intermediates in the heme catabolism reaction.

Bonnett and Dimsdale (1972) confirmed Lemberg's proposal that iron salts of oxyporphyrins were intermediates in the coupled oxidation reaction using iron(II) octaethylporphyrin and H_2O_2, which upon demetallation and treatment with benzoyl chloride gave 5-benzoyloxy-octaethylporphyrin in 75% yield. The product was identical to an authentic sample prepared synthetically (Bonnett & Dimsdale, 1968), proving addition

of a hydroxy group to the *meso* position. They also determined that iron(III) octaethyloxophlorin readily undergoes autoxidation to give octaethylbiliverdin after hydrolysis. Compelling evidence for the involvement of *meso*-hydroxyhemes as intermediates in the coupled oxidation process consequently drove future investigators to illuminate the structure and reactivity of these compounds.

The first assignment of the electronic structure of *meso*-hydroxyheme formed in solution was low spin iron(II) (Sano et al., 1981). These investigators used ESR, NMR, and Mössbauer techniques to analyze synthetic *meso*-hydroxyheme and verdohemochrome. A common observation reported by these investigators was the spontaneous formation of verdohemochrome from *meso*-hydroxyheme in the presence of dioxygen. Sano and Sugiura (1982) monitored the reaction of the *meso*-hydroxyheme-2-methylimidazole complex by UV-visible absorption spectroscopy and EPR and reported that the iron(II) porphyrin radical reacted with dioxygen in a step that liberated carbon monoxide. They suggested that "one-electron transfer may have occurred from the enolate anion at the *meso*-position of the porphyrin to the iron" to explain the formation of the iron(II) porphyrin radical. Further experimental evidence that this was true came from the same group (Morishima et al., 1986). Specifically, the ^{1}H NMR spectrum of iron(III) oxyporphyrin was diamagnetic and showed unusually large pH-dependent *meso* proton hyperfine shifts that were attributed to the deprotonation of the complex and a one electron reduction of the iron to form iron(II) oxyporphyrin radical. It was noted that upon exposure to dioxygen, the iron(II) oxyporphyrin radical spontaneously formed verdohemochrome, indicating that this radical intermediate was attacked by dioxygen.

Following these careful experiments in pyridine solution, the same investigators studied the properties of synthetic iron α-oxyporphyrin reconstituted into myoglobin (Sano et al., 1986). Using ^{1}H NMR, EPR, and UV-visible spectroscopy, they demonstrated that the myoglobin complex of iron(II) α-oxyporphyrin π-neutral radical reacts with one equivalent of dioxygen to give iron(II) verdohemochrome IXα in a reaction that quantitatively yields carbon monoxide. Masuoka and Itano (1987) confirmed the presence of the π-neutral radical and its reactivity with dioxygen in a similar study using iron(III) octaethyloxyporphyrin purified as a dimer. These reactions are regarded as models for the conversion of hydroxyhemes to verdoheheme *in vivo* and *in vitro*.

1.11 CHEMICAL MECHANISM - VERDOHEME

Structural studies of "verdohemochromogen", or verdohemochrome, date back to

13

the early days of Lemberg (1935; 1941c). Without modern spectroscopic tools a wide variety of structures were proposed for this intermediate. The correct structure was first proposed by Lemberg (1943) and confirmed by Lagarias (1982), who synthesized and purified the tetrafluoroborate salt of verdohemochrome derived from the coupled oxidation of octaethylheme. By UV-visible spectroscopy, ^{1}H-NMR, and mass spectrometry, he assigned verdohemochrome the structure of iron(II) oxaporphyrin, an aromatic cationic structure with an oxygen atom bridging the α-*meso* position.

While investigators pursued the structure of verdohemochrome as an intermediate of coupled oxidation, ^{18}O labeling studies with microsomal heme oxygenase temporarily ruled out verdohemochrome as a physiologically relevant intermediate in heme catabolism (Tenhunen et al., 1972). Specifically, they found that incubation of the enzymatic system with ^{18}O$_2$ resulted in the production of bilirubin containing two atoms of ^{18}O as well as ^{18}O labeled carbon monoxide. They also demonstrated that no ^{18}O label was incorporated into any of the products when the incubation was carried out in ^{18}O water. Under the assumption that conversion of verdoheme to biliverdin had to be hydrolytic, they ruled out verdoheme as a possible intermediate *in vivo*. Brown and King (1975; 1976; 1978) and King and Brown (1978), in a series of ^{18}O labeling experiments in live rats, supported the findings of Tenhunen et al. Furthermore, using mixtures of ^{18}O$_2$ and ^{16}O$_2$ they demonstrated that the oxygen atoms in bilirubin came from *different* molecules of O$_2$. This not only ruled out verdoheme but also ruled out a frequently proposed dioxygen bridged iron oxophlorin intermediate (Figure 1.11.1). The two-molecule mechanism was also confirmed using the reconstituted heme oxygenase system purified from bovine spleen (Docherty et al., 1984).
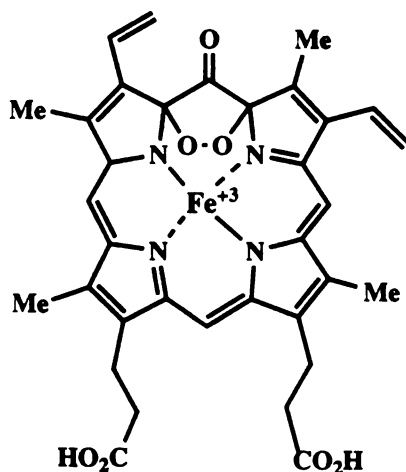
Figure 1.11.1. The dioxygen-bridged iron oxophlorin intermediate ruled out by the two-molecule mechanism.

Saito and Itano (1982) shed tremendous light on the relationship of verdoheme to heme catabolism. They obtained pure verdohemochrome IXα from the coupled oxidation of myoglobin and proposed a structure essentially identical to Lagarias (1982) based on its composition and ^{1}H-NMR spectrum. They then reacted verdohemochrome IXα with ascorbate and $^{18}O_2$ and found that the biliverdin product contained one atom of ^{18}O, thus demonstrating that hydrolysis was not an obligatory step in the conversion of verdoheme to biliverdin, and verdoheme was once again a plausible intermediate.

Significant advances in the chemistry of verdohemes and heme catabolism were also made in a series of publications by Balch and co-workers. Through the use of UV-visible absorption spectroscopy, ^{1}H-NMR, and crystallography, structural characterization of a number of octaethylverdoheme analogs was carried out (Balch et al., 1993). These studies are of particular utility because the oxidation and ligation states of the analogs studied were precisely defined. Correlating the absorption spectra of intermediates observed in the heme oxygenase reaction to the absorption spectra of Balch's derivatives has proven to be useful. In addition, the cobalt analog of verdoheme was formed by coupled oxidation of cobalt(II) octaethylporphyrin (Balch et al., 1994). Biliverdin derivatives are produced in this process (Balch et al., 1995), demonstrating that cobalt can substitute for iron in the heme cleavage reaction. This was also reported for cobalt substituted hemoglobin and myoglobin (Vernon & Brown, 1984).

1.12 STRUCTURAL AND MECHANISTIC STUDIES OF RECOMBINANT HEME OXYGENASE

The human heme oxygenase (HO-1) cDNA was cloned by Shibahara and co-workers (Yoshida et al., 1988). Attempts by a number of groups to express recombinant heme oxygenase in *E. coli* followed. Yoshida & Sato (1989) showed that heme oxygenase synthesized in a cell-free system is post-translationally integrated into the microsomal membrane. Yoshida et al. (1991) expanded this finding by treatment of rat microsomes with trypsin and isolation of a heme oxygenase peptide of 28 kDa. The tryptic peptide bound substrate heme and the absorption spectra of the ferric, ferrous, ferrous-CO, and ferrous-O_2 complexes were comparable to those of native enzyme. Futhermore, the tryptic peptide retained catalytic activity using ascorbate as reductant but was unable to accept the second electron from NADPH-cytochrome P450 reductase. However, the same investigators expressed rat HO-1 in *E. coli* and found the full-length 32 kDa enzyme was catalytically active and localized in bacterial membranes. Amongst a variety of proteolyzed

fragments they found a 30 kDa enzyme that retained the ability to accept the second electron from NADPH-cytochrome P450 reductase (Ishikawa et al., 1991). Wilks and Ortiz de Montellano (1993) reported a high-yield expression system for the rat HO-1 isozyme (HO-30) that produces a fully active, regiospecific, and soluble recombinant enzyme lacking 23 amino acids from the C-terminal end, as well as a similarly truncated human form (hHO-1) (Wilks et al., 1995a). The enzymes were isolated from the green *E. coli* cells as 1:1 complexes with biliverdin. The biliverdin could be exchanged for heme by incubation with an excess of heme and purification of the heme-heme oxygenase complex on a BioRad-HTP column.

The rat enzyme was used in experiments studying the reactivity of the heme-heme oxygenase complex with H_2O_2 and acyl hydroperoxides. It was found that incubation of this complex with one equivalent of H_2O_2 produced an intermediate with a compelling spectroscopic resemblance to iron(III) verdoheme. Subsequent incubation of this enzyme-bound intermediate with NADPH and cytochrome P450 reductase produced biliverdin. In contrast to H_2O_2, acyl hydroperoxides such as mCPBA do not support the formation of bile pigments. Rather, they form a ferryl ($Fe^{IV}=O$) complex and a protein radical analagous to that of cytochrome C peroxidase. In addition, the ferryl intermediate formed in heme oxygenase supports guaiacol (2-methoxyphenol) oxidation, a prototype peroxidase reaction. These results suggest that the ferryl intermediate does not participate in the heme catabolism reaction, and furthermore that the reaction is mediated by the distal oxygen of an iron-peroxo species in either a nucleophilic or electrophilic reaction (Figure 1.12.1).

Resonance Raman and EPR spectroscopy on the heme-heme oxygenase complex by both the Ortiz de Montellano (Sun et al., 1993) and Ikeda-Saito camps (Takahashi et al., 1994a; 1994b) revealed essentially the same structural characteristics. The heme environment in heme oxygenase was found to be similar to myoglobin. Specifically, the studies revealed the presence of a six-coordinate heme ligated to a histidine residue and a water molecule. The resonance Raman band at 216 cm^{-1} was assigned to the metal-histidine stretching mode, and the frequency of this band was used to estimate the degree of ionization of the histidine ligand. The results were interpreted to mean that the proximal histidine has a neutral charge and therefore is not a very strongly electron-donating ligand.

The ^{1}H-NMR of the heme-heme oxygenase complex has also been investigated (Hernández et al., 1994). The initial spectrum showed extensive heterogeneity that was resolved with the use of a hemin that is symmetrical about the α/γ axis. It was shown that

16

the orientational disorder was due to distinct binding modes differing by a 180° flip about this axis. The assignment of all hemin signals by isotopic labelling made it possible to

nucleophilic
H^+

electrophilic
H^+

ferryl
H^+
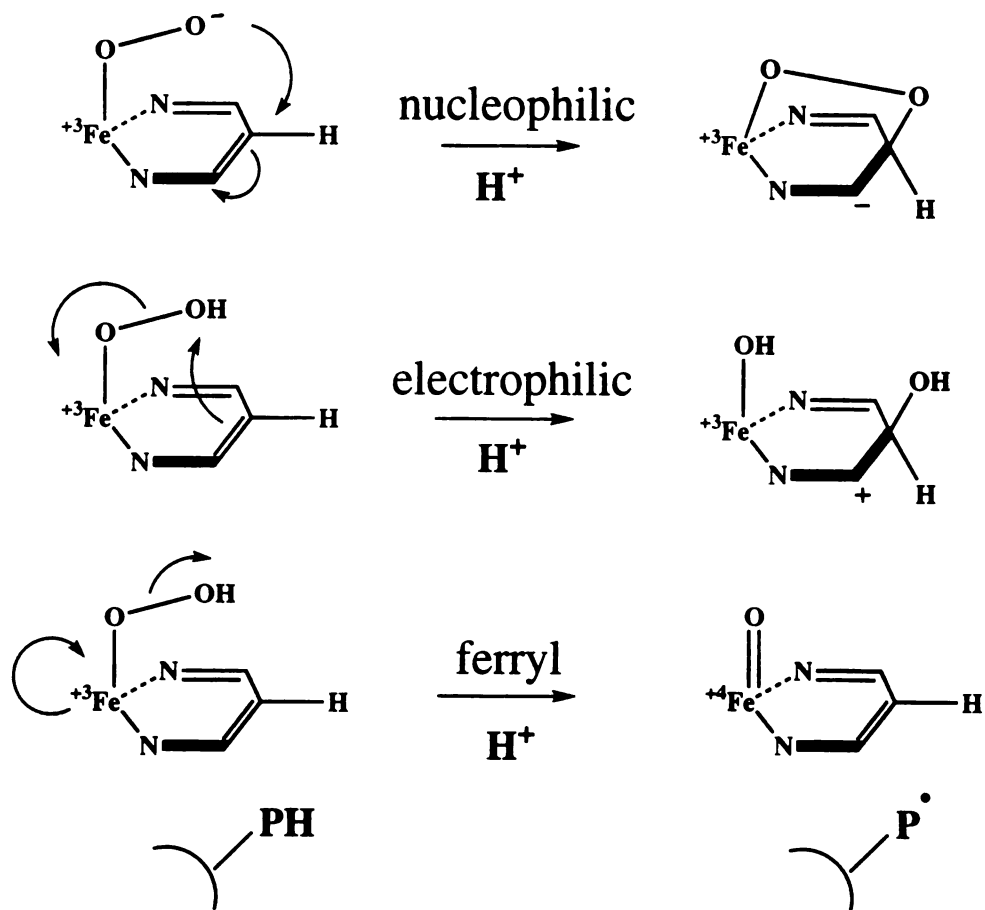
Figure 1.12.1. Possible reaction schemes for an iron-peroxo intermediate.

detect a contact shift pattern that reflects an unusual hemin electronic structure. This effect is characterized by an uneven spin density within the pyrrole rings as illustrated in Figure 1.12.2a. A similar effect has been observed in model systems using unsymmetrically substituted derivatives of iron(III) TPP (Lin et al., 1992; Tan et al., 1994). Specifically, the meso-phenyl groups contained para-NEt2 or para-Cl and the iron(III) TPP derivatives each contained three of one type of phenyl group and one of the other type of phenyl group, causing asymmetric distribution of unpaired electron spin density within the porphyrin π orbitals. The mapping of the spin density distribution at the pyrrole positions was done by ^{1}H COSY and NOESY techniques, similar to the experiments carried out with heme oxygenase. The finding of uneven spin density within the pyrrole rings of the heme-heme oxygenase complex is in contrast to the globins, in which the spin densities of the

17

pyrrolic and *meso* carbons are not polarized (Figure 1.12.2b). The effect in heme oxygenase was shown to be pH dependent, and largely abolished at acidic pH, suggesting

(a)   **(b)**
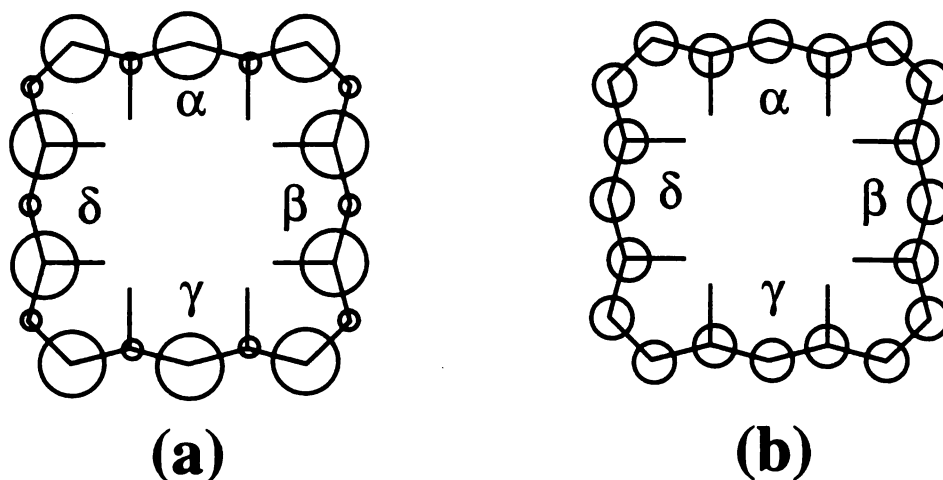
Figure 1.12.2. Illustrations of the spin densities of the porphyrin skeleton.

the participation of an acidic amino acid residue such as glutamate or aspartate as an electron donor at the α-*meso* position. The heme polarization effect is also interpreted as evidence for an electrophilic mechanism of heme hydroxylation due to the increased electron density at the α-*meso* position.

The report that diethylpyrocarbonate, a chemical modifier of histidine, inactivated heme oxygenase suggested that histidine plays a critical role in the enzymatic reaction (Yoshinaga et al., 1982). Furthermore, examination of the sequence homology of the cloned heme oxygenase cDNA's (including rat, human, mouse, and chicken) revealed the presence of four conserved histidine residues: His25, 84, 119, and 132. Ishikawa et al. (1992) tried to investigate the role of each of the conserved histidines by expressing the four individual site-directed His->Ala mutants as 30 kDa soluble truncated proteins in *E. coli*. Activity assays of the partially purified proteins demonstrated the importance of His25, as the His25Ala mutant had no activity. The His84Ala and His119Ala mutants had about 40% of the control (WT) activity, suggesting that they are not essential. The His132Ala mutant was only expressed at low levels, which made it difficult to reach a conclusion regarding its catalytic importance.

Eventual purification of both the His25Ala and His132Ala mutants clarified the role of each histidine residue in the heme oxygenase reaction. Histidine 25 was definitively

18

identified as the proximal ligand by the absence of the iron-imidazole stretching band in the resonance Raman spectrum of the purified His25Ala mutant (Sun et al., 1994). These results were corroborated by the Ikeda-Saito group (Ito-Maki et al., 1995). In addition, exogenous imidazoles bind in the cavity of the His25Ala mutant, coordinate to the iron, and restore catalytic acitivity (Wilks et al., 1995b). In contrast, the His132Ala mutant retains 40-50% specific activity. However, His132 appears to participate in stabilization of the water molecule bound to the iron on the distal side (Wilks et al., 1996). Histidine 132 is essential for the H_2O_2 supported formation of verdoheme, but not for the NADPH-cytochrome P450 reductase supported reaction. The reason for this discrepancy is unclear. The present results suggest that histidine 132 is the distal histidine in heme oxygenase and that it may assist catalysis by stabilizing the ferrous-O_2 intermediate.

A variety of experiments on proteolyzed recombinant HO-2 revealed no major mechanistic or structural differences between HO-1 and HO-2 (Ishikawa et al., 1995). It should be noted, however, that these experiments were conducted on HO-2 protein devoid of 25% of its mass, including both the C-terminal hydrophobic tail and the N-terminal sequence of unknown function.

1.13 THESIS OVERVIEW

Chapter 2 describes the determination of the presence or absence of a kinetic isotope effect upon removal of the α-*meso* proton, the reaction of heme oxygenase with ethylhydroperoxide, and the reaction of heme oxygenase with a 2,4-dimethyl α-*meso* methyl symmetrical heme. The primary aim of this work is to investigate the hydroxylation mechanism and the importance of the α-*meso* proton.

Chapter 3 describes the synthesis and characterization of the regioisomeric *meso*-methyl and *meso*-formyl mesohemes. The primary aim of this work is to obtain substrates for reactions with heme oxygenase.

Chapter 4 describes the reaction of the previously synthesized *meso*-methyl and *meso*-formyl mesohemes with heme oxygenase. The primary aim of this work is to determine the factors controlling the regiospecificty of the heme oxygenase reaction.

2.0 THE ELECTROPHILIC NATURE OF THE HYDROXYLATING SPECIES AND A NOVEL HEME CLEAVAGE REACTION

2.1 INTRODUCTION

Heterologous expression of microsomal heme oxygenase (HO-1) as a truncated soluble protein in *E. coli* has made available for the first time reagent-scale quantities of pure enzyme. Recombinant rat (HO-30) and human (hHO-1) heme oxygenases were expressed and purified as described (Wilks & Ortiz de Montellano, 1993; Wilks et al., 1995) and typically yielded 30-40 mg/L. The enzyme is purified as a 1:1 complex with biliverdin, indicating the presence of a reducing system in *E. coli* that supplies heme oxygenase with the electrons needed to catabolize heme. Due to the plethora of proteases in the *E. coli* system, care must be taken to avoid proteolysis of 30 kDa heme oxygenase to an inactive 28 kDa form during the purification procedures and subsequent experiments. Both recombinant forms of the enzyme are easily reconstituted with the iron(III) porphyrin of choice by addition of an excess of iron(III) porphyrin and purification of the heme:heme oxygenase complex on an HTP column as described.

The ferric heme:heme oxygenase complex spectroscopically resembles a hemoprotein with a Soret band at 404 nm ($\varepsilon = 140$ mM^{-1}·cm^{-1}). Reduction of the ferric complex with sodium thiosulfite (Na$_2$S$_2$O$_4$; dithionite) under an atmosphere of carbon monoxide yields the ferrous-carbon monoxide complex with a Soret band at 418 nm and α/β bands at 568 and 538 nm. Passage of the ferrous-carbon monoxide complex through a Sephadex G25 column results in formation of the ferrous-dioxygen complex with a corresponding shift of the Soret band to 410 nm and a shift of the α/β bands to 574 and 540 nm.

The heme:heme oxygenase complex is converted to biliverdin by addition of catalytic amounts of cytochrome P450 reductase and stoichiometric amounts of NADPH. Kinetic measurements are made using the heme oxygenase coupled assay which includes heme oxygenase apoprotein, cytochrome P450 reductase, biliverdin reductase, a BSA-heme solution, and NADPH. The rate of increased absorbance at 468 nm is used to calculate the rate of bilirubin production ($\varepsilon = 43.5$ mM^{-1}·cm^{-1}).

Reaction of the heme:heme oxygenase complex with cytochrome P450 reductase and NADPH under a partial atmosphere of carbon monoxide stops the reaction, as previously described, at an intermediate stage that is characterized by a visible absorption

20

band at 638 nm (Yoshida et al., 1980; Wilks & Ortiz de Montellano, 1993). This intermediate is thought to be an iron(II) verdoheme:carbon monoxide complex (Lagarias, 1982; Saito & Itano, 1982). Reaction of the mesoheme:heme oxygenase complex yields the identical intermediate with visible absorption bands at 616 and 532 nm (Figure 2.1.1).
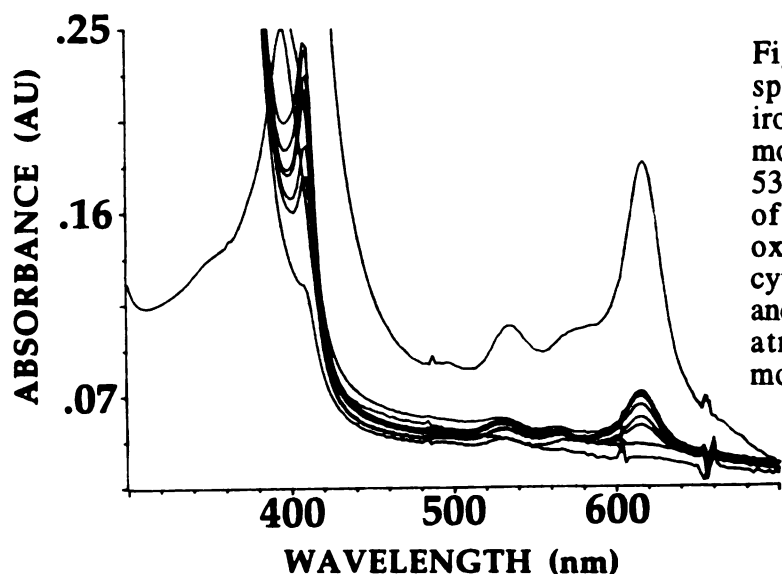
Figure 2.1.1. Absorption spectra of enzyme-bound iron(II) verdoheme:carbon monoxide complex (616 and 532 nm) formed by reaction of the mesoheme:heme oxygenase complex with cytochrome P450 reductase and NADPH under a partial atmosphere of carbon monoxide (30 sec scans).

Reaction of the heme:heme oxygenase complex with one equivalent of H_2O_2 results in essentially quantitative formation of iron(III) verdoheme (Wilks & Ortiz de Montellano, 1993). This reaction is thought to proceed first by hydroxylation of the heme followed by spontaneous oxidation of iron(III) α-meso hydroxyheme to iron(III) verdoheme. Direct evidence for the participation of iron(III) α-meso hydroxyheme in the heme oxygenase reaction has finally been obtained by generation of the intermediate *in situ* in the complete absence of molecular oxygen (Liu et al., 1997). Iron(III) α-meso hydroxyheme is otherwise undetectable, but the iron(III) verdoheme intermediate is characterized by a decrease in the Soret maximum and the appearance of a broad visible absorption band between 620 and 720 nm (Figure 2.1.2). The reaction is stopped in the absence of further reducing equivalents. However, addition of cytochrome P450 reductase and NADPH results in conversion of the intermediate to biliverdin.

Conversely, reaction of the heme:heme oxygenase complex with alkyl and acylhydroperoxides results in a decrease and red-shift of the Soret band but no increase in the visible region (Wilks & Ortiz de Montellano, 1993). The changes in the Soret band are
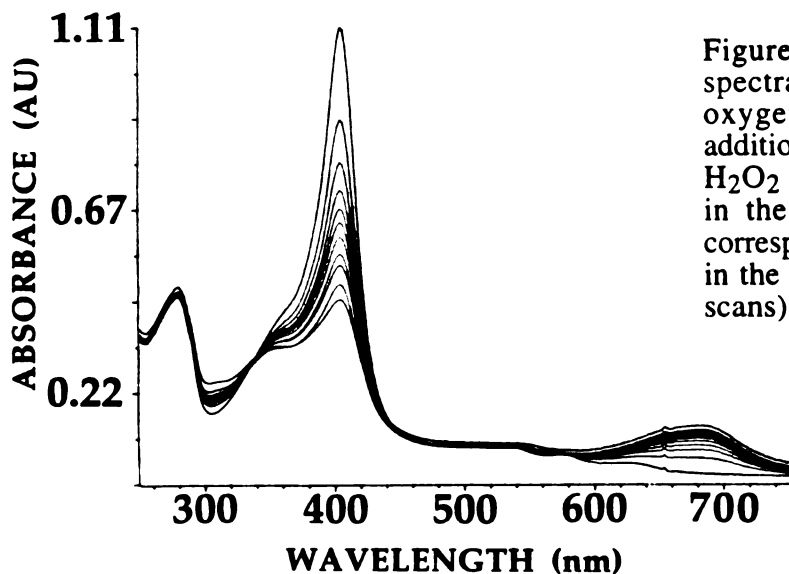
Figure 2.1.2 Absorption spectra of the heme:heme oxygenase complex after addition of one equivalent of H_2O_2 showing the decrease in the Soret band and the corresponding broad increase in the visible region (30 sec scans).

attributed to the formation of a ferryl ($Fe^{IV}=O$) intermediate. Support for this hypothesis is two-fold. Reaction of the ferryl species with phenol or ascorbic acid results in reduction of the ferryl and regeneration of ferric enzyme. In addition, heme oxygenase functions as a peroxidase in the presence of excess mCPBA by reaction of the ferryl species with guaiacol (2-methoxyphenol). The ferryl intermediate does not support the formation of bile pigments and no peroxidase activity is detected in the presence of cytochrome P450 reductase and NADPH. These reaction pathways therefore appear to be mutually exclusive. Furthermore, the presence of a strong protein radical at $g = 2.006$ in the presence of excess mCPBA suggests that the second oxidizing equivalent of the peroxidase reaction is lost to the protein.

The finding that H_2O_2 supports the formation of iron(III) verdoheme suggests that the activated dioxygen is an iron-peroxo species. An iron(III) peroxo complex has since been implicated as the key intermediate of H_2O_2 supported hydroxylation of lauric acid by cytochrome P4502B4 (Pratt et al., 1995). At least three distinct mechanisms can be proposed for the reaction of an iron-peroxo species (see Figure 1.12.1). The possibility that a ferryl species catalyzes the initial heme hydroxylation is discounted due to the results discussed above; i.e. formation of a ferryl intermediate and heme hydroxylation are mutually exclusive. Thus, at least two mechanisms remain in contention: nucleophilic attack or electrophilic addition of an iron-peroxo species. The possibility that heme hydroxylation proceeds by a hydroxy radical mechanism is viewed as unlikely due to the inherent problem of controlling the chemo- and regioselectivity of such a highly reactive

22

intermediate. The hydroxy radical and electrophilic mechanisms, however, can be related by intermediate resonance structures and are therefore difficult to distinguish.

The heme hydroxylation mechanism was examined more closely in an effort to further define the nature of the hydroxylating species as well as to determine the importance of the α-*meso* proton in the enzyme catalyzed reaction. A *meso*-deuterated heme was synthesized for use in experiments to determine the presence or absence of a kinetic isotope effect in the hydroxylation mechanism. In addition, the structural determination of a modified heme formed in the reaction of the heme:heme oxygenase complex with ethylhydroperoxide effectively ruled out one of the possible hydroxylating species. Of particular interest was the reaction of an α-*meso* methyl substituted heme with heme oxygenase. The possibility that the α-methyl would abrogate the catalytic process was investigated, and it was determined that the appended methyl group did not interfere with catalytic turnover. The biliverdin product was purified by HPLC and characterized by UV/vis spectroscopy and mass spectrometry. Finally, an assay was developed to detect carbon monoxide in order to determine whether it was formed in the reaction of heme oxygenase and the α-*meso* methyl heme.

2.2 EXPERIMENTAL

General Methods

A truncated form of rat liver heme oxygenase (HO-30) without the membrane-binding domain was expressed in *E. coli* and purified as previously described (Wilks & Ortiz de Montellano, 1993). Heterologously expressed human cytochrome P450 reductase (1.2 mg/ml) was a gift of Bettie Sue Masters (San Antonio, Texas). Rat liver cytosol was used as an unpurified form of biliverdin reductase and was a gift of the laboratory of Almira Correia (UCSF). Protoporphyrin IX dimethylester (PPIX-DME) was obtained from Porphyrin Products (Logan, Utah). Ethylhydroperoxide was obtained from Polysciences (Warrington, PA). Absorption spectra were recorded on a Hewlett Packard 8452A diode array spectrophotometer. HPLC was done on a semi-prep scale (4.6 x 250 mm) 10-μm ODS-3 reverse phase column eluted with either 75% Solvent A (methanol:water:acetic acid, 50:50:10) and 25% Solvent B (methanol:acetic acid, 100:10), or Solvent C (acetonitrile:water:acetic acid, 55:40:10), or Solvent D (methanol:water, 90:10), or Solvent E (acetone/0.1% aqueous formic acid, 50:50). Solvents A-D were monitored at 404 nm and referenced at 550 nm, and Solvent E was monitored at 364 nm and referenced at 474 nm. Mass spectra were obtained by the electrospray technique on a

Fisons Bio-Q mass spectrometer or by (+)LSIMS on a VG70 instrument using a 1:1 (1% trifluoroacetic acid) glycerol/thioglycerol matrix. ^{1}H NMR spectra were measured in deuterated chloroform on a GN-500 MHz (2D-NMR) or a QE-300 MHz instrument (1D-NMR). ^{1}H NOESY data were obtained using a delay time of 2 sec and a mixing time of 300 ms, and processed on a Sun/AT&T System 4 computer. The NOESY spectra were obtained with 8K data points in the t_2 dimension and 512 blocks of 128 scans each in the t_1 dimension. The free induction decays were zero filled once in both dimensions and apodized with an exponential function with a line broadening of 4 Hz in the t_2 dimension and 10 Hz in the t_1 dimension. A symmetrical heme with methyl groups substituted for the 2,4-vinyls (1) and its α-meso methyl derivative (2) (Figure 2.2.1) were obtained from David Lee and Prof Kevin Smith (University of California, Davis). The iron(III) porphyrins were combined with a truncated recombinant human heme oxygenase (hHO-1) as previously described (Wilks et al., 1995).

Figure 2.2.1   The structures of 2,4-dimethyl symmetrical hemin (1) and the α-meso methyl substituted derivative (2).

Deuteration Catalyst

Deuteration of PPIX-DME at the meso and vinyl positions (Figure 2.2.2) is catalyzed by hexapyridyl-magnesium di-iodide and CD_3OD as previously described (Kenner et al., 1973). A 50 ml double-necked reaction vessel equipped with a stir bar, condenser, and Mg° (800 mg) is flame dried under vacuum and then cooled under an atmosphere of argon. Freshly distilled diethyl ether (30 ml) and I_2 (1.5 g) are then added and the resulting solution refluxed under argon until the solution is colorless (20-30 min). The solution is then filtered under argon using a fritted pressure filter and the filtrate

evaporated to dryness in a sealed round bottom flask under a stream of argon. The resulting yellow solid is quenched by injecting dry pyridine (30 ml) and CD₃OD (2 ml). This standard solution is used as the catalyst in the deuteration step. Care must be taken throughout to prevent exposure to the atmosphere as a small amount of water will diminish the deuteration efficiency of the catalyst.
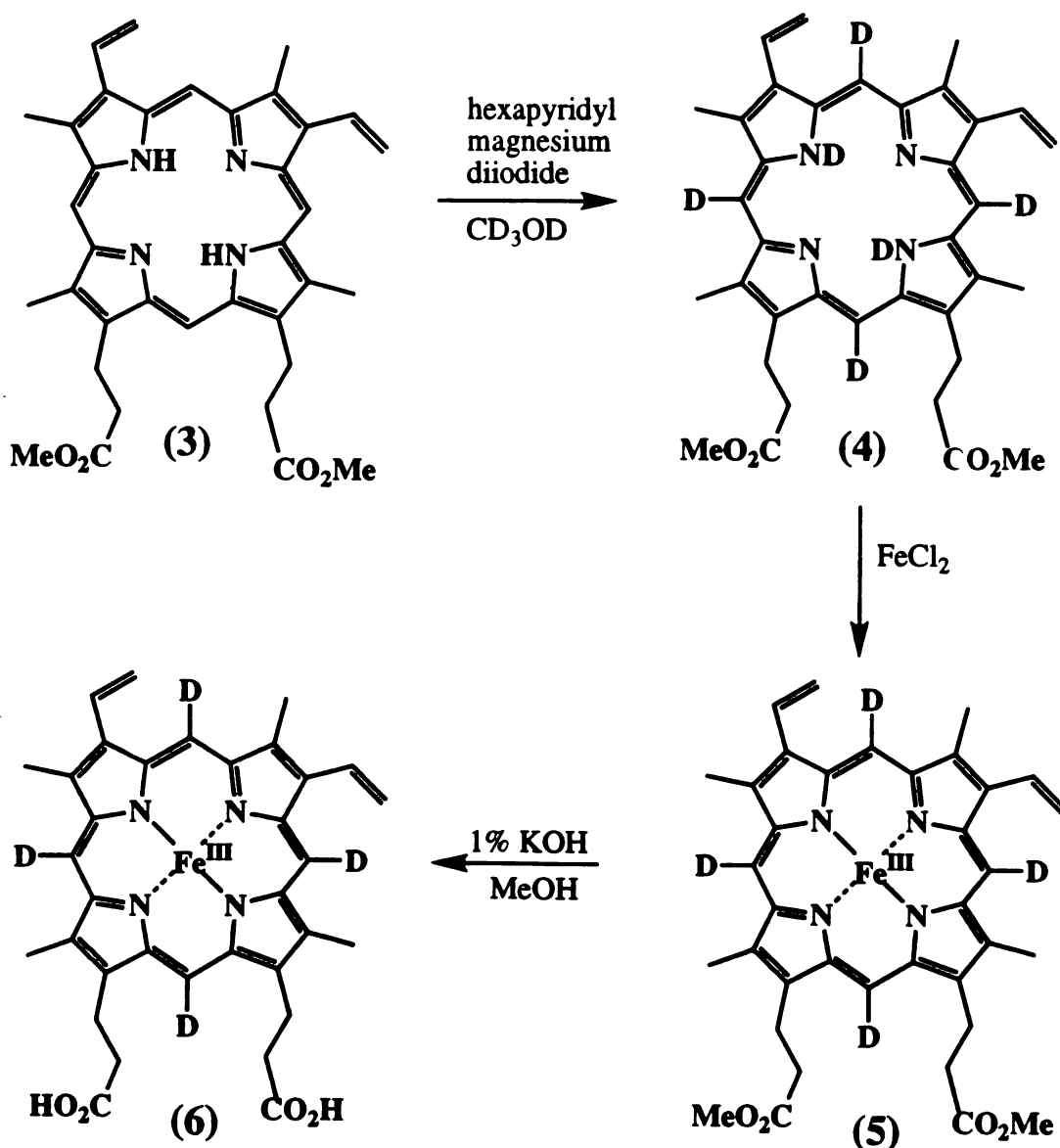

Figure 2.2.2. Deuteration of PPIX-DME (3) and conversion to iron(III) salt. The vinyl groups are also partially deuterated by this procedure.

Deuterated PPIX-DME (4)

To a solution of PPIX-DME (70 mg, 119 μmol) (3) is added dry pyridine (2 ml) and 20 ml of the standard solution described above. This solution is refluxed under argon

overnight (12 hr), at which time the solution is allowed to cool. Upon cooling, the solution is diluted with chloroform (25 ml) and poured into 1.0 N HCl (50 ml). After thorough washing with water (200 ml), the organic phase is dried (Na_2SO_4), evaporated, and the residue allowed to stir overnight in 5% v/v H_2SO_4/MeOH. The solution is then poured into water (200 ml) and the porphyrin extracted into chloroform (100 ml), washed with water (100 ml), dried as before, evaporated to dryness, and purified by flash chromatography on silica gel using 1% MeOH in CH_2Cl_2. Analysis by TLC ($R_f = .40$) shows the deuterated PPIX-DME is pure. ^1H NMR indicates that the product is deuterated approximately equally at the four *meso* positions to an extent of 90%, in addition to partial deuteration at the vinyl positions. This reaction yielded 53 mg (83 μmol) of deuterated porphyrin (69% yield).

Iron(III) Deuterated PPIX-DME (5)

The metallation procedure is done essentially as described by Ator et al. (1989). Deuterated PPIX-DME (4) (53 mg, 83 μmol) is dissolved in freshly distilled THF (20 ml) and the solution bubbled with argon for one hour. In addition, a double-necked flask equipped with stir bar and condenser is charged with a ten-fold excess of $FeCl_2 \cdot 4H_2O$ (166 mg, 0.83 mmol) in methanol (20 ml). This solution is also bubbled with argon for one hour, at which time the solution containing (4) in THF is added slowly under argon pressure via needle to the double-necked flask. The resulting solution is refluxed under argon for one hour. Workup of the reaction is done by first stirring the solution in the open air, which allows the reaction mixture to cool and the iron to autooxidize to Fe^{3+}. The solution is partitioned between CH_2Cl_2 (100 ml) and water (200 ml), then the organic layer is washed with water (200 ml) and evaporated to dryness. The UV λ_{max} shows a shift from 406 nm to 394-396 nm (broad) indicating that the metallation step is complete.

Iron(III) Deuterated PPIX (6)

Hydrolysis of the methyl esters is done also as described by Ator et al. (1989). Deuterated iron(III) PPIX-DME (5) is dissolved in 1% (w/v) methanolic KOH (20 ml) and refluxed for 90 min. The reaction mixture is allowed to cool and acidified with acetic acid, and the heme is extracted with water (50 ml) and diethyl ether (100 ml). The organic phase is concentrated under vacuum and the residue purified by HPLC using 75% Solvent A and 25% Solvent B at 3 ml/min.. Heme elutes at 9.9 min ($\lambda_{max} = 396$ nm) and a minor impurity of unknown identity eluted at 7.8 min ($\lambda_{max} = 392$ nm).

26

HO-30 Kinetic Assay

The HO-30 kinetic assay is performed essentially as described by Wilks & Ortiz de Montellano (1993). This assay is performed in 1 ml final volume of 100 mM potassium phosphate buffer (pH 7.4). Specifically, it contains: 640 μl buffer, 50 μl purified P450 reductase (0.33 mg/ml), 100 μl of partially purified biliverdin reductase (rat liver cytosol), 10 μl rat liver heme oxygenase (HO30, 2.5 mg/ml), and 100 μl of heme solution. The reaction is incubated for five minutes at 37° and is initiated by the addition of 100 μl of 100 mM NADPH. The rate of bilirubin formation is monitored at 468 nm and calculated using $\varepsilon = 43.5$ mM^{-1}cm^{-1}.

The heme solution is prepared by dissolving 1.0 mg of hemin in a few drops of 1.0 M KOH and diluted with 5 ml of buffer. To this solution is added 3.3 mg of BSA. The concentration of the deuterated heme solution can be titrated to equal that of the heme solution using the UV spectrophotometer (monitoring at 398 nm). In order to eliminate as much error as possible, each reaction mixture was prepared in duplicate and split in half between the kinetic assays of heme and deuterated heme.

Reaction of Ethylhydroperoxide With the Heme:HO-30 Complex

The heme:HO-30 complex is obtained as described previously (Wilks & Ortiz de Montellano, 1993). The incubations contained 100 μM heme:HO-30 and a 5- to 10-fold excess of ethylhydroperoxide in a final volume of 5 ml of 0.1 M phosphate buffer. Reactions are allowed to proceed for 30 min on ice after which a few grains of ascorbate are added to quench any remaining peroxide. The solution is acidified with 200 μl of glacial acetic acid and is then extracted with diethyl ether (2 ml). The organic phase is concentrated *in vacuo* and the residue is analyzed by reverse phase HPLC using 100% Solvent C at a flow rate of 1 ml/min for analytical purposes and 5 ml/min for preparative purposes.

Preparation of the Zn-Complexed α-*Meso* Ethoxy PPIX-DME NMR Sample

Formation of the dimethyl esters is carried out by stirring the α-*meso* ethoxyheme in 5% H$_2$SO$_4$/MeOH (100 ml) in the dark for 8 hr at room temperature. The reaction is worked up by partitioning between CH$_2$Cl$_2$ (100 ml) and water (100 ml), washing the organic layer with water (100 ml), and concentrating it to dryness at a rotary evaporator. Removal of the iron from the porphyrin is accomplished by the ferrous sulfate method

27

(Morell et al., 1961) and the zinc complex is prepared by adding 5 ml of a solution of zinc acetate in methanol to a solution of the demetallated porphyrin in 5 ml of chloroform. A color change is immediately observed. The reaction mixture is again partitioned between water and CH_2Cl_2 and the organic layer is washed with water and concentrated *in vacuo*. The zinc-complexed dimethyl ester of α-*meso* ethoxy PPIX is purified by HPLC using 100% Solvent D at 1 ml/min (retention time 21.3 min; λ_{max} 416, 546).

Complexes of hHO-1 and Symmetrical Hemes (1) and (2): Reactions with Cytochrome P450 Reductase and NADPH Under a CO Amosphere

The hHO-1 complexes of **(1)** (300 µg, 9.9 nmol) and **(2)** (220 µg, 7.2 nmol) were reacted with cytochrome P450 reductase (1.6 µg, 20 pmol) and NADPH (83 µg, 0.1 µmol) under a partial atmosphere of carbon monoxide. Under these conditions the reaction is arrested at an intermediate stage and the visible absorption spectrum (λ_{max} 614 nm) indicates the trapping of the ferrous-CO verdoheme:hHO-1 complex.

Complexes of hHO-1 and Symmetrical Hemes (1) and (2): Reactions with One Equivalent of H_2O_2

The hHO-1 complexes of **(1)** (220 µg, 7.2 nmol) and **(2)** (165 µg, 5.4 nmol) were reacted with one equivalent of H_2O_2. Under these conditions the reaction is arrested at an intermediate stage and the visible absorption spectrum (λ_{max} 600-700 nm, broad) indicates the trapping of the ferric verdoheme:hHO-1 complex. Addition of of 20% pyridine results in an increase in intensity of the visible band and a more precisely defined λ_{max} at 640 nm.

Complexes of hHO-1 and Symmetrical Hemes (1) and (2): Extraction and Purification of Biliverdin Products for Mass Spectrometry

The hHO-1 complexes of **(1)** (2.6 mg, 86.8 nmol) and **(2)** (2.9 mg, 96.8 nmol) were reacted with cytochrome P450 reductase (60 µg, 0.75 nmol) and NADPH (4.1 mg, 5.0 µmol) in air for 1 hour at 25˚C. Both solutions turned a deep blue-green and were extracted with diethyl ether after acidification to pH 3 with HCl and AcOH. The biliverdin products were purified by HPLC using 100% Solvent E at 1 ml/min.

Complexes of hHO-1 and Symmetrical Hemes (1) and (2): Carbon Monoxide Assays

Ferrous deoxymyoglobin is used to qualitatively detect carbon monoxide formed

2 8

during the heme oxygenase reaction. To a 1 ml solution of horse skeletal muscle myoglobin (100 µg, 5.9 nmol) in 100 mM potassium phosphate buffer (pH 7.4) is added an excess of sodium thiosulfite ($Na_2S_2O_4$, 5 mg). The Soret shifts from 408 nm (ferric) to 434 nm (ferrous deoxy). Freshly prepared ferrous deoxymyoglobin is added via syringe to the following heme oxygenase reactions of symmetrical hemes (1) and (2).

To the symmetrical heme (1):hHO-1 complex (0.24 mg, 8.0 nmol) is added cytochrome P450 reductase (6.0 µg, 78 pmol) and NADPH (167 µg, 200 nmol). The test tube is immediately sealed with a rubber septum and the reaction allowed to stand for five minutes (turning green) before adding the ferrous deoxymyoglobin solution. The resulting mixture is mixed by swirling and the UV-visible spectrum recorded. The identical procedure is carried out with the symmetrical heme (2):hHO-1 complex (0.28 mg, 9.2 nmol).

2.3 RESULTS

Investigation of a Primary Kinetic Isotope Effect

Using the deuterated heme (6) synthesized above, the possibility of a primary kinetic isotope effect was investigated using conventional Lineweaver-Burke analysis. The first three experiments used four different substrate concentrations (3.0 µM, 1.5 µM, 1.2 µM, 0.9 µM) for each heme, and the fourth experiment used five different substrate concentrations (3.0 µM, 1.5 µM, 1.2 µM, 0.9 µM, 0.6 µM). A narrow concentration range was used because of the inhibitory effects of increasing concentrations of heme as well as the difficulty of detecting diminished reaction rates at low substrate concentrations. The calculated rates of bilirubin production (V_{max}) from each substrate concentration (S) were graphed as Lineweaver-Burke plots using the graphing program KinetAsyst. The Lineweaver-Burke plots for the four experiments with heme are shown in Figure 2.3.1 and the plots for the four experiments with deuterated heme are shown in Figure 2.3.2. The K_m and V_{max} values obtained from each set of experiments are listed in Table 2.3.1. If an average of the V_{max} kinetic ratios $^{(H)}/_{(D)}$ of the four experiments is taken, one obtains a value of 1.06, consistent with the absence of a primary kinetic isotope effect.

Figure 2.3.1. Lineweaver-Burke plots of kinetic isotope effect data obtained from heme oxygenase assays with heme.

$1/V$ = mg•hr/nmol
$1/S$ = $1/\mu M$
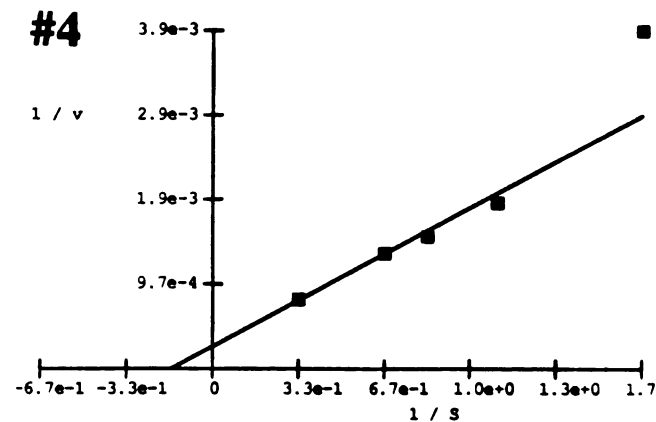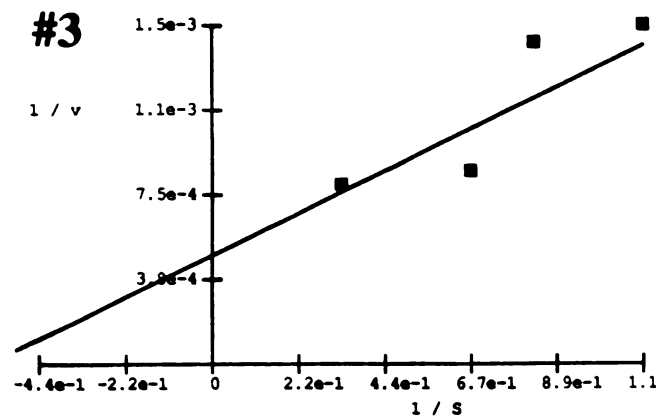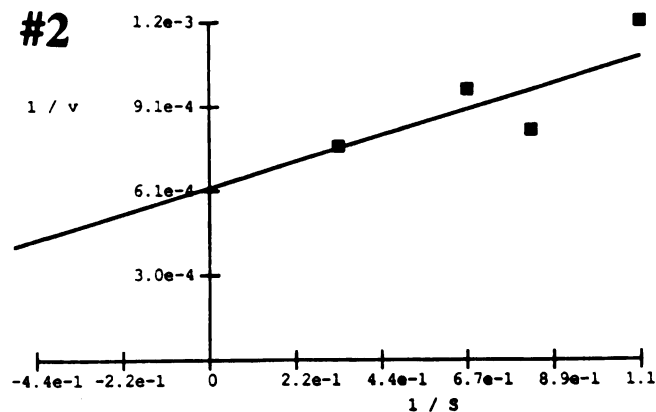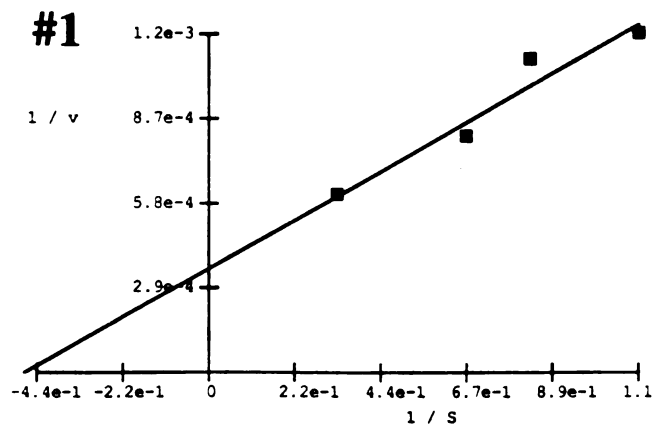
30

Figure 2.3.2. Lineweaver-Burke plots of kinetic isotope effect data   obtained from heme oxygenase assays with deuterated heme.

$1/V = mg \cdot hr/nmol$
$1/S = 1/\mu M$

31

	K_m (μM)	V_{max} (nmol·hr^{-1}·mg^{-1})	$V_{(H)}/V_{(D)}$
Trial #1	(H) 2.1	2788	.78
	(D) 2.6	3569	
Trial #2	(H) 0.70	1613	1.07
	(D) 0.90	1499	
Trial #3	(H) 1.7	2050	1.03
	(D) 1.7	1984	
Trial #4	(H) 6.2	3933	1.37
	(D) 4.4	2855	

Table 2.3.1. Kinetic isotope effect data for HO-30.

Reaction of Ethylhydroperoxide With the Heme:HO-30 Complex

HPLC analysis of the prosthetic group extracted from the heme:HO-30 complex after reaction with ethylhydroperoxide shows the presence of unreacted heme (retention time = 8.3 min) as well as a new iron porphyrin (retention time = 14.3 min) (Figure 2.3.3). The Soret band of the modified heme is at 401 nm rather than, as in unreacted heme, at 397 nm. The mass spectrum of the modified heme exhibits a molecular ion at m/z 660.5, the molecular ion expected if a hydrogen of the porphyrin is replaced by an ethoxy group. The carboxyl groups of the porphyrin were esterified with acidic methanol and the iron of the esterified porphyrin was replaced by divalent zinc for ^{1}H NMR studies.

Identification of the Modified Heme Product

The NMR data, in conjunction with the mass spectrometric results, unambiguously identify the adduct as α-*meso*-ethoxyheme. The one dimensional NMR spectrum (Figure 2.3.4) clearly exhibits signals for three *meso* protons, well-resolved signals for the external and internal vinyl protons, and the other resonances characteristic of a protoporphyrin IX derivative. The absence of one *meso* proton indicates that the ethoxy substituent is located at a *meso* position. Furthermore, the discrete, well-resolved nature of the vinyl and *meso* resonances indicates that the sample is a single *meso* ethoxy substituted porphyrin rather than a mixture of two or more isomers. The NOESY map of the molecule confirms this

32

Figure 2.3.3. HPLC analysis of the iron(III) porphyrins extracted from the heme:heme oxygenase complex after reaction with ethylhydroperoxide.

inference and identifies the specific isomer involved. Thus, the *meso* proton region of the NOESY map (Figure 2.3.5) immediately rules out two of the *meso* positions for the ethoxy substituent. The γ-*meso* proton at 9.65 ppm is unambiguously identified by the cross-peak (resonance A) with the 6- and 7- propionate inner methylene protons at 4.28 ppm, and the δ-*meso* proton at 9.88 ppm is uniquely identified by cross-peaks (resonances B and B') with protons at 3.65 and 3.53 ppm belonging to two different methyl groups. Therefore, the third *meso* proton at 10.00 ppm (resonance C) must be at either the α- or β-*meso* position and the ethoxy substituent at the alternative site.

The strategy undertaken to locate the ethoxy group and the unassigned *meso* proton relies on differentiating the 2- and 4-vinyl groups because the α- and β-*meso* substituents can be distinguished by their NOE connectivity to one or the other of these vinyl groups (Table 2.3.2). In effect, the 2-vinyl outer protons at 5.95 ppm are readily identified by an NOE (Figure 2.3.5, resonance D) with the 1-methyl protons at 3.65 ppm that, in turn, are uniquely identified as the protons of one of the two methyl groups that exhibit NOE signals to the δ-*meso* proton (Figure 2.3.5, resonance B). The 2-vinyl inner proton at 8.48 ppm is then identified by the NOE (Figure 2.3.6, resonance E) interaction with the 2-vinyl outer protons at 5.95 ppm . Finally, the ethoxy adduct is shown to be at the α-*meso* position by an NOE (Figure 2.3.6, resonance G) between the 2-inner vinyl proton at 8.48 ppm and the methyl protons of the ethoxy group at 1.90 ppm. A similar connectivity pattern can be used

3 3

Figure 2.3.4. Partial one-dimensional ^{1}H-NMR spectrum of the modified iron(III) porphyrin formed in the reaction of the heme:heme oxygenase complex with ethylhydroperoxide. The NMR spectrum was obtained after replacing the iron with divalent zinc and converting the carboxyl groups to the methyl esters.

to assign the unidentified *meso* proton. Thus, the 4-vinyl inner proton at 8.19 ppm is identified by NOE interaction with the 4-vinyl outer protons at 6.19 ppm (Figure 2.3.6, resonance **F**). The unassigned *meso* proton at 10.00 ppm is then shown to be at the β-position by an NOE (Figure 2.3.7, resonance **H**) between it and the 4-inner vinyl proton at 8.19 ppm. The porphyrin formed in the reaction of the heme:HO-30 complex with ethylhydroperoxide is therefore α-*meso*-ethoxyheme.
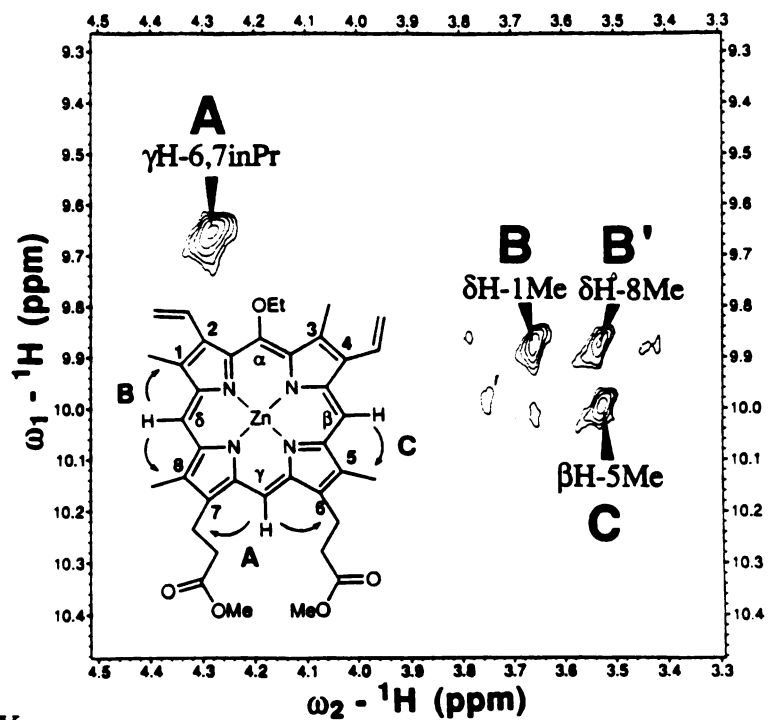
Figure 2.3.5. NOESY crosspeaks identifying *meso* protons (**A-B-C**), as well as the 2-vinyl group (**D**). See text for discussion of assignments.

F
4in-4out vinyl

E
2in-2out vinyl

G
2vinyl-αOEt
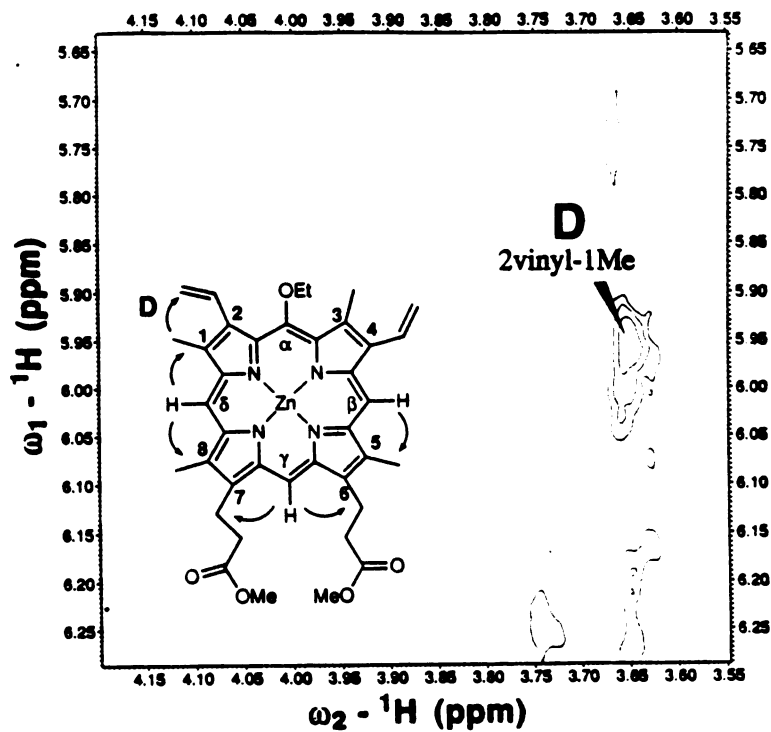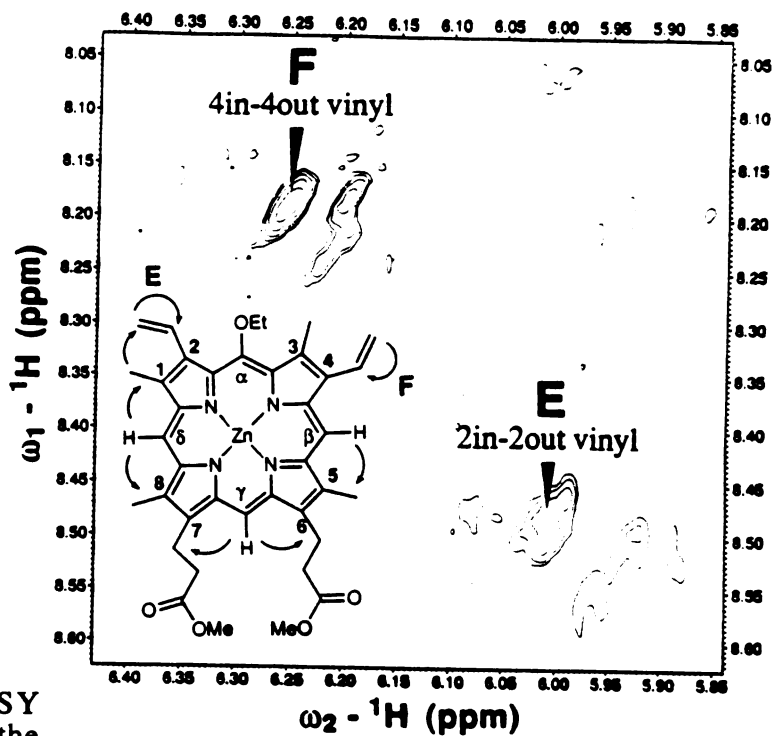
Figure 2.3.6. NOESY crosspeaks correlating the 2,4- inner and outer vinyl protons (E-F), and the 2-vinyl protons to the ethoxy group (G). See text for discussion of assignments.
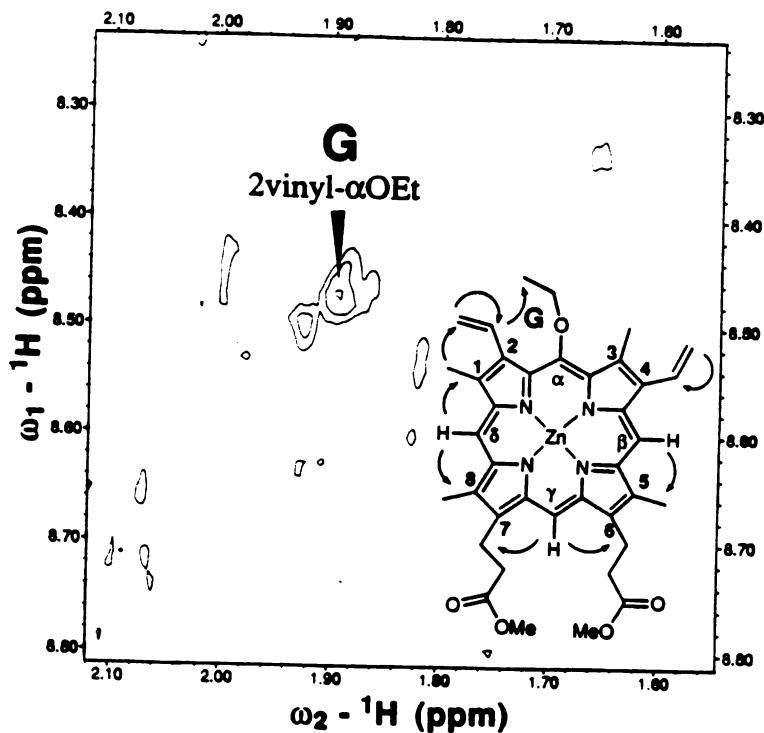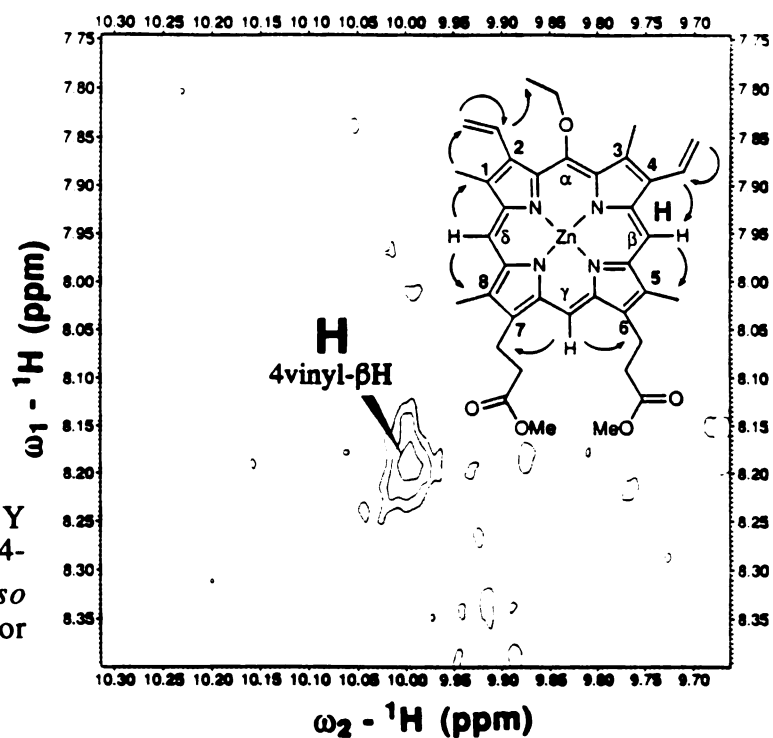
Figure 2.3.7. NOESY crosspeak correlating the 4-vinyl protons to the β-*meso* proton (H). See text for discussion of assignments.

Proton	Chemical Shift (ppm)	NOE
α-O-CH₂-CH₃	4.4, 4.5	α-O-CH₂CH₃
α-O-CH₂-CH₃	1.9	2-CH=CH₂, α-O-CH₂CH₃
β-*meso* H	10.00	4-CH=CH₂, 5-CH₃
γ-*meso* H	9.65	6,7-CH₂CH₂CO₂H
δ-*meso* H	9.88	1-CH₃, 8-CH₃
1-CH₃	3.65	δ-*meso* H, 2-CH=CH₂
2-CH=CH₂	8.48	α-OCH₂CH₃
2-CH=CH₂	5.95, 6.01	1-CH₃
3-CH₃	3.74	4-CH=CH₂
4-CH=CH₂	8.19	β-*meso* H
4-CH=CH₂	6.19, 6.25	3-CH₃
5-CH₃	3.52	β-*meso* H
6,7-CH₂CH₂CO₂CH₃	4.28	γ-*meso* H, 5-CH₃
6,7-CH₂CH₂CO₂CH₃	3.18	γ-*meso* H
8-CH₃	3.53	δ-*meso* H

Table 2.3.2. ¹H NMR assignments for zinc α-*meso*-ethoxy PPIX-DME.

Complexes of hHO-1 and Symmetrical Hemes (1) and (2): Formation of the Iron(II) Verdoheme-CO Complex Using Cytochrome P450 Reductase and NADPH

The absorption maxima of the hHO-1 complex of (1) are ferric (394 nm), ferrous-CO (410, 526, 558 nm), ferrous-O_2 (402, 532, 566 nm), and the absorption maxima of the hHO-1 complex of (2) are ferric (400 nm), ferrous-CO (414, 534 nm), and ferrous-O_2 (408, 536 nm). Reaction of the hHO-1 complex of symmetrical heme (1) with cytochrome P450 reductase and NADPH under an atmosphere of O_2 and CO results in loss of Soret intensity and the gradual accumulation of an intermediate with a distinct visible band at λ_{max} = 614 nm (Figure 2.3.8). This intermediate is the ferrous-CO verdoheme:hHO-1
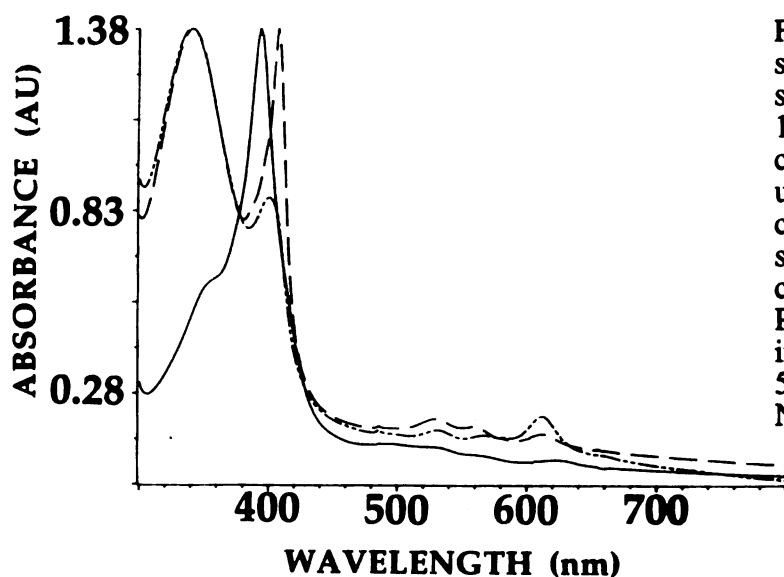
Figure 2.3.8. Absorption spectra of the reaction of the symmetrical heme (1):hHO-1 complex with NADPH and cytochrome P450 reductase under a partial atmosphere of carbon monoxide. The spectra are of the ferric heme complex and cytochrome P450 reductase before (—), immediately after (– –), and 5 min after (·—·) addition of NADPH.

complex. Reaction of the hHO-1 complex of α-*meso* methyl symmetrical heme (2) under identical conditions produces an identical absorption spectrum (Figure 2.3.9) demonstrating the formation of a ferrous-CO verdoheme:hHO-1 complex.
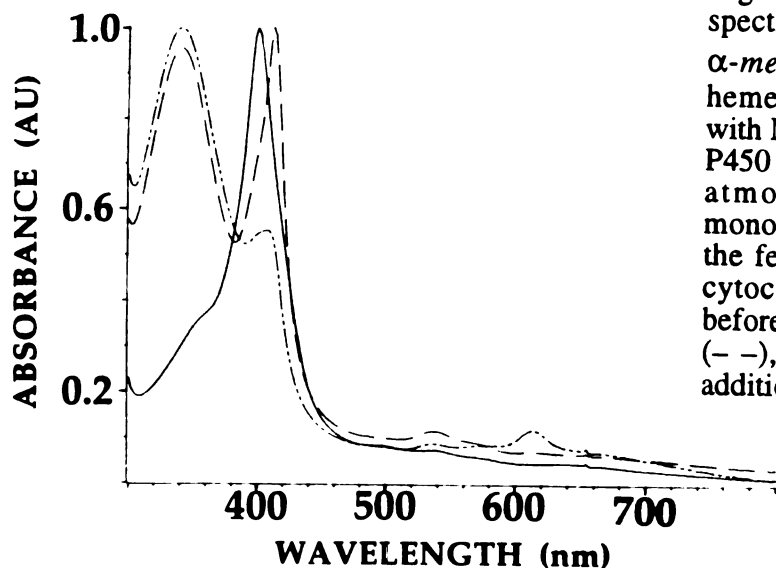
Figure 2.3.9. Absorption spectra of the reaction of the α-*meso*-methyl symmetrical heme (2):hHO-1 complex with NADPH and cytochrome P450 reductase under a partial atmosphere of carbon monoxide. The spectra are of the ferric heme complex and cytochrome P450 reductase before (—), immediately after (– –), and 5 min after (·····) addition of NADPH.

Complexes of hHO-1 and Symmetrical Hemes (1) and (2): Formation of the Iron(III) Verdoheme Complex Using One Equivalent of H_2O_2

Previous studies have shown that the oxidation of heme to verdoheme by heme oxygenase can be supported by H_2O_2, although the conversion of verdoheme to biliverdin still requires cytochrome P450 reductase and NADPH (Wilks & Ortiz de Montellano, 1993). It is not necessary to run the reaction in the presence of CO; due to the lack of reducing equivalents the iron remains in the ferric state and cannot bind or activate molecular oxygen. Reaction of the hHO-1 complex of symmetrical heme (1) with one equivalent of H_2O_2 results in decay of the Soret in conjunction with a broad increase in the visible region from 600-700 nm (Figure 2.3.10). Addition of 20% pyridine sharpens the intensity of the visible band (λ_{max} = 640 nm) as the pyridine complexes the ferric verdoheme complex. In contrast to these results, reaction of the hHO-1 complex of the α-*meso* methyl symmetrical heme (2) with one equivalent of H_2O_2 results in a time-dependent decay in the Soret but without any detectable change in the visible region (Figure 2.3.11).

39
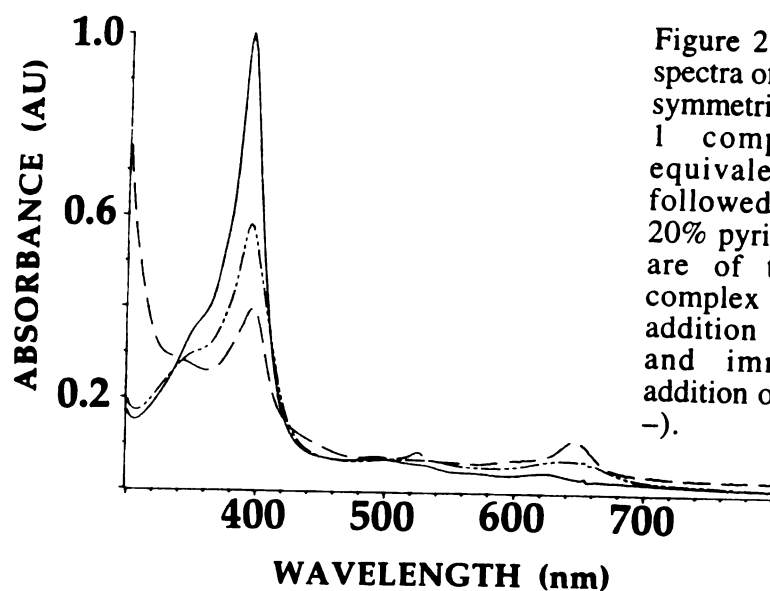
Figure 2.3.10. Absorption spectra of the reaction of the symmetrical heme (1):hHO-1 complex with one equivalent of H_2O_2 followed by addition of 20% pyridine. The spectra are of the ferric heme complex (—), 5 min after addition of H_2O_2 (·—·), and immediately after addition of 20% pyridine (– –).
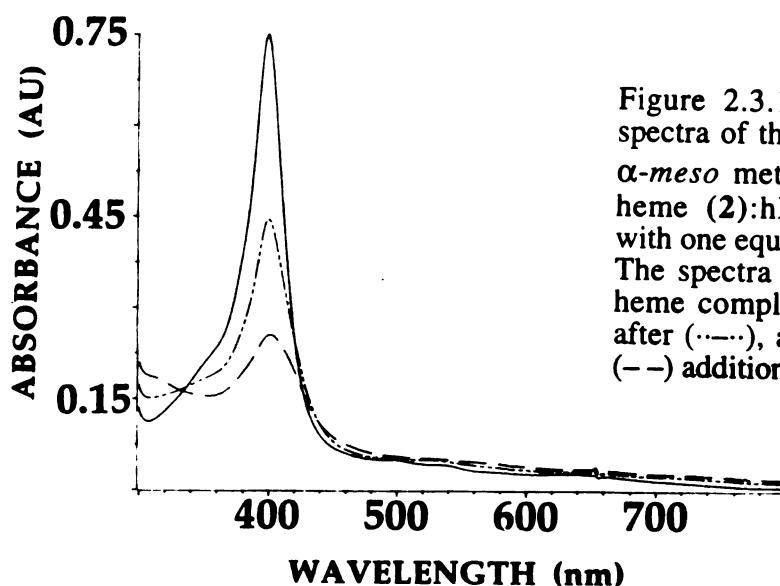
Figure 2.3.11. Absorption spectra of the reaction of the α-*meso* methyl symmetrical heme (2):hHO-1 complex with one equivalent of H_2O_2. The spectra are of the ferric heme complex (—), 10 min after (·—·), and 30 min after (– –) addition of H_2O_2.

Complexes of hHO-1 and Symmetrical Hemes (1) and (2): Extraction and Purification of Biliverdin Products for Mass Spectrometry

The biliverdin product of the oxidation of each of the symmetrical hemes by heme oxygenase was purified and analyzed by HPLC, absorption spectroscopy, and mass spectrometry. Incubations with cytochrome P450 reductase and NADPH were carried out in the absence of exogenous CO. The reaction mixtures were acidified, extracted, and analyzed by HPLC as already described.

The HPLC chromatogram of the biliverdin obtained from the reaction of the symmetrical heme (1):hHO-1 complex shows one biliverdin with a retention time of 10.9 min and absorption maxima (MeOH) at 364 and 638 nm. The purified biliverdin has a mass spectrum m/z (MH$^+$) 559 (calcd for $C_{31}H_{34}O_6N_4$, 558) and is assumed to be the α-isomer. The α-meso methyl symmetrical heme (2):hHO-1 complex was reacted and worked up under identical conditions. The HPLC chromatogram again showed one biliverdin at 10.9 min, the absorption and mass spectra of which are identical to that of the biliverdin product isolated from the reaction of (1) (λ_{max} 364, 638 nm; m/z (MH$^+$) 559).

Complexes of hHO-1 and Symmetrical Hemes (1) and (2): Carbon Monoxide Assays

An assay based on the affinity of ferrous deoxymyoglobin for CO is used to detect the formation of CO in the cytochrome P450 reductase/NADPH supported reactions of hHO-1 and hemes (1) and (2). The assay is based on the shift of the Soret maximum of ferrous deoxymyoglobin (λ_{max} 434 nm) on complexation with CO (λ_{max}422 nm). Addition of deoxymyoglobin to the symmetrical heme (1):hHO-1 reaction mixture after completion of the reaction results in immediate formation of the ferrous-CO myoglobin complex (λ_{max}422 nm). No detectable shift of the deoxymyoglobin Soret maximum was observed when the identical experiment was carried out with the α-meso methyl symmetrical heme (2):hHO-1 reaction mixture. Thus, CO is not detectably formed in the reaction of (2) under conditions where it is easily detected in the corresponding reaction with (1).

2.4 DISCUSSION

The deuterated heme (6) was synthesized and used to determine the absence of a primary kinetic isotope effect using the heme oxygenase coupled assay. The K_m and V_{max} values obtained from each set of experiments are listed in Table 2.3.1. Similar K_m values are obtained for the protonated and deuterated hemins within individual experiments, indicating that the numbers within single experiments are comparable to each other. It is evident that there is a degree of variability between the K_m and V_{max} values obtained from different experiments and the exact reason for this is not known. The variations could be due to the variable and ever-increasing amounts of 28 kDa proteolyzed heme oxygenase existing in enzyme preparations. Similar problems with proteolysis were observed in reactions with heme oxygenase and ethylhydroperoxide. In cases where enzyme preparations were severely proteolyzed, incubations with ethylhydroperoxide resulted in

41

the production of virtually no modified heme. The presence of inactive heme oxygenase in protein preparations could give misleading specific activities, thus affecting the determination of kinetic constants.

Due to the inconsistencies of the KIE data, each set of values was compared internally in the form of a ratio of V_{max} values [$^{(H)}/_{(D)}$] obtained from the protonated and deuterated hemes. Averaging these ratios, one obtains a value of 1.06 suggesting the absence of a primary isotope effect. This result indicates that removal of the α-*meso* proton is not the rate limiting step in the heme hydroxylation mechanism. However, it has since become evident that the heme oxygenase coupled assay may not have been the most effective means of determining the presence or absence of a primary KIE. It is possible that the KIE, if it exists, is obscured by the multitude of other steps in the heme oxygenase coupled assay. For example, the slowest step in the process could be electron transfer, or more likely, transfer of biliverdin from heme oxygenase to biliverdin reductase. Ideally an assay is required that measures the rate of formation of *meso*-hydroxyheme or verdoheme, thus eliminating the interference of other reactions.

Reaction of the heme:HO-30 complex with ethylhydroperoxide results in a decrease in the Soret band and a red-shift of 4 nm (Wilks et al., 1994). This effect is similar to the reactions of heme oxygenase with *tert*-butylhydroperoxide and *m*CPBA in that a ferryl (Fe^{IV}=O) species is generated resembling Compound II of HRP (Wilks et al., 1993). The difference between the ethylhydroperoxide reaction and the reactions of *tert*-butylhydroperoxide and *m*CPBA is that when the ferryl intermediate produced by the ethylhydroperoxide reaction is reduced by phenol or ascorbate, the Soret maximum is only partially regenerated. This observation suggested that the reaction should be explored more thoroughly.

Extraction of the heme from the ethylhydroperoxide reaction and analysis by HPLC revealed the presence of a modified heme (Figure 2.3.3) with a mass spectrum consistent with the presence of an ethoxy substituent in place of a proton. In order to obtain 1-2 mg of the ethoxy-substituted heme for use in ^{1}H NMR studies, gram-scales of recombinant heme oxygenase were employed. The iron of the purified ethoxy heme was replaced with zinc and the carboxylates were converted to the dimethylesters. The one-dimensional ^{1}H NMR spectrum immediately revealed that the ethoxy substituent resided at a *meso* position due to the presence of only three *meso* protons (Figure 2.3.4). In addition, examination of both the *meso* and vinyl regions of the spectrum demonstrates that the ethoxy-substituted porphyrin is a single component and not a mixture of isomers.

Two-dimensional NOESY spectroscopy was employed to determine which *meso* position the ethoxy substitutent occupied. NOESY spectra contain a complete set of homonuclear NOE crosspeaks that correlate spins which are close enough in space to have related relaxation mechanisms. Thus, the NOESY spectrum enables connectivities to be made through space that allow a "walk" from one adjacent group to the next along the porphyrin periphery. The NOESY spectrum of the ethoxy-substituted PPIX-DME proves that the ethoxy substituent is at the α-*meso* position (Figures 2.3.5 - 2.3.7). The conserved regiospecificity of the ethylhydroperoxide reaction implies that the mechanism parallels both the cytochrome P450 reductase and H_2O_2 supported reactions of heme oxygenase. Formation of α-*meso* ethoxy heme also demonstrates that the hydroxylation is mediated by the distal oxygen relative to the iron.
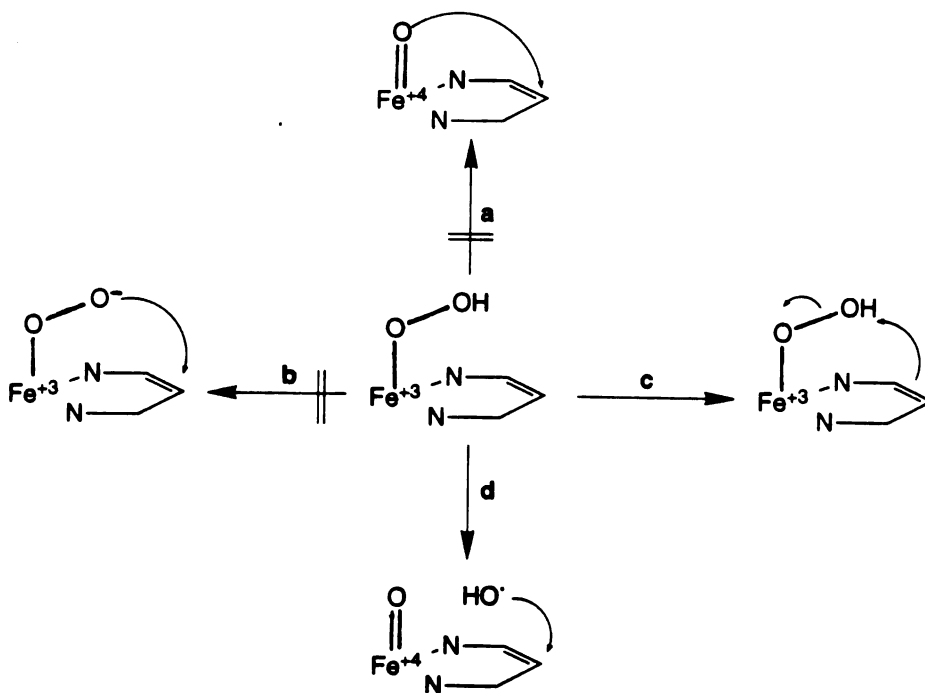
Figure 2.4.1. Four general mechanisms envisioned for heme hydroxylation in the heme oxygenase catalyzed reaction.

Figure 2.4.1 illustrates four possible mechanisms for heme oxygenase catalyzed heme hydroxylation. Pathway (a), participation of a ferryl species, has previously been ruled out based on earlier studies (Wilks et al., 1993). Pathway (b), nucleophilic attack of the iron-peroxo anion at the α-*meso* position, appears much less viable in light of the ethylhydroperoxide reaction, as the ethyl substituent would block such a reaction.

43

Pathways **(c)** and **(d)**, the electrophilic and ethoxy radical mechanisms, respectively, are difficult to distinguish. The difference between the two mechanisms arises from alternative mechanisms of dioxygen cleavage. Strictly heterolytic cleavage gives rise to the electrophilic ethoxonium ion **(c)**, and homolytic cleavage results in formation of the ethoxy radical and a ferryl intermediate **(d)**. The mechanisms converge upon one-electron reduction of the ferryl species, with concomitant formation of a cation adjacent to the α-*meso* position. The recent observation that the attack of a non-heme iron(III) peroxide adduct on a phenol ring is greatly controlled by the substituents on the ring implies that the interaction between the adduct and the ring involves an electronic attractive force, whereby the iron(III) peroxide adduct acts as an electrophile (Ito et al., 1996).

The importance of the α-*meso* proton was investigated by substitution of a methyl group at this position. The hemes used were the 2,4-dimethyl symmetrical hemes **(1)** and **(2)** (Figure 2.2.1). Reaction of the hHO-1 complex of **(1)** with cytochrome P450 reductase and NADPH under an atmosphere of CO results in trapping of the ferrous-CO verdoheme:hHO-1 complex (Figure 2.3.8). Surprisingly, reaction of the hHO-1 complex of **(2)** under identical conditions yields an identical absorption spectrum (Figure 2.3.9). Reaction of the hHO-1 complex of **(1)** with H_2O_2 results in trapping of the ferric verdoheme:hHO-1 complex (Figure 2.3.10), while reaction of the hHO-1 complex of **(2)** with H_2O_2 results in a time-dependent decay of the Soret with no concomitant increase in the visible region (Figure 2.3.11).

Extraction and HPLC purification of the products from scaled-up reactions of heme oxygenase, cytochrome P450 reductase, NADPH, and hemes **(1)** and **(2)** revealed that the reactions produce biliverdin compounds with identical absorption spectra, HPLC retention times, and mass spectra. Furthermore, while CO is detected as a product of heme oxygenase and heme **(1)**, no CO is detected in the reaction of heme oxygenase and heme **(2)**. These results are taken to mean that the α-*meso* methyl group and α-*meso* carbon of heme **(2)** are extruded from the porphyrin macrocycle by a previously undescribed heme cleavage mechanism that does not yield carbon monoxide.

The first important aspect of the α-*meso* methyl reaction is that the methyl group does not inhibit the enzyme, nor does it alter the regiospecificity of the reaction. The relative unimportance of the α-*meso* proton is surprising. The regiospecificity of the reaction, given the electron donating properties of the methyl group and subsequent activation of the α-*meso* position, is consistent with an electrophilic mechanism. However, the methyl group cannot eliminate in a manner analogous to that of a proton. The absence

of detectable amounts of CO indicate that the mechanism does not proceed first by demethylation followed by normal catalytic conversion to biliverdin. Rather, the reaction proceeds by a mechanism that does not involve formation of α-meso-hydroxyheme, yet converges on the normal catalytic pathway upon the formation of verdoheme.

The reaction of the α-meso-methylheme-hHO-1 complex with H_2O_2 resulted in a decrease in intensity of the Soret band without the formation of a verdoheme intermediate. The heme is therefore degraded to unknown products. As previously observed, the heme oxygenase reaction with peroxides results in one or both of the following: formation of a ferryl intermediate and/or electrophilic hydroxylation of the heme. Alkyl and acylhydroperoxides typically react to form exclusively the ferryl intermediate. As the alkylhydroperoxide decreases in size, the ferryl species becomes less favored. Thus, the reaction of ethylhydroperoxide with heme oxygenase results in a partitioning between both pathways. Furthermore, formation of a ferryl species has never been observed in the reaction of heme oxygenase with H_2O_2.

Previous studies have suggested that the heme hydroxylation proceeds through an iron-peroxo intermediate (Wilks & Ortiz de Montellano, 1993). The present experiments have addressed two further aspects of the heme hydroxylation mechanism. The results obtained from substitution of the α-meso proton by a deuteron and a methyl lend further support to the electrophilic mechanism. The absence of a kinetic isotope effect is consistent with a mechanism in which removal of the proton is not rate limiting. Furthermore, reaction of heme oxygenase with an α-meso methyl heme reveals a novel heme cleavage reaction that proceeds through a mechanism that does not include the meso-hydroxyheme intermediate. Finally, determination of the structure of the ethoxy-substituted heme obtained from the reaction of the heme:HO-30 complex with ethylhydroperoxide rules out the possibility that the heme hydroxylation is the result of a nucleophilic attack of the iron-peroxo species.

3.0 SYNTHESIS OF THE FOUR REGIOISOMERIC *MESO*-METHYL AND *MESO*-FORMYL MESOHEMES

3.1 INTRODUCTION

Heme is hydroxylated by heme oxygenase at its α-*meso* position with concomitant elimination of the α-*meso* proton. The placement of a methyl group at the α-*meso* position therefore poses an interesting question. Will the enzyme still turn over? What are the products? *Meso*-substituted porphyrins are known to have distorted planarities (Senge et al., 1995) as well as altered electronic structures (Tan et al., 1994). A variety of results could therefore be envisioned for incubation of *meso*-methyl substituted hemes with heme oxygenase. Each regioisomer could be an inhibitor or a substrate, and the electron donating effect of the *meso*-methyl substituent could have an effect on the reaction regioselectivity. Although relatively small, this effect is envisioned to be analagous to the electron donating effect of a methyl-substitued benzene ring, whereby the π system is polarized making the *ortho* and *para* positions electron rich and the *meta* positions electron poor. Conversely, the *meso*-formyl isomers were synthesized as a set of sterically similar non-planar hemes with the opposite electronic effect.

Despite their potential utility, *meso*-methyl and *meso*-formyl porphyrins are not available commercially. Rather than attempt the total synthesis, a scheme was devised to produce a mixture of regioisomeric *meso*-substituted porphyrins (Figure 3.1.1). The copper complex of MSPR-DME was made to make the porphyrin more electron rich in order to facilitate a Vilsmeier reaction which forms the carbon-carbon bond of the *meso* substituent and the porphyrin. The products of the Vilsmeir reaction were a mixture of regioisomeric *meso*-formyl porphyrins which were then collectively reduced to the *meso*-hydroxymethyl. Removal of the copper ion and separation of the mixture on silica was achieved at the *meso*-hydroxymethyl stage. The individual components of the mixture were therefore purified and the position of the *meso* substituent of each regioisomer identified. Structural data (^{1}H/^{13}C NMR & HRMS) were obtained for each isomer and the regiochemistry of each isomer was determined by ^{1}H NMR. Advantage was taken of the nuclear overhauser effect, which provides spatial connectivity between protons within 3-4 Å. The γ- and δ-isomers, having unique sets of adjacent substituents, were identified using one-dimensional NOE experiments. The β- and α-isomers, however, having identical adjacent substitutents, could only be distinguished by complete assignments using two-dimensional NOESY spectroscopy.

9a: α *meso* R_α=CHO; R_β=R_γ=R_δ=H
9b: β *meso* R_β=CHO; R_α=R_γ=R_δ=H
9c: γ *meso* R_γ=CHO; R_α=R_β=R_δ=H
9d: δ *meso* R_δ=CHO; R_α=R_β=R_γ=H

10a: α *meso* R_α=CH$_2$OH; R_β=R_γ=R_δ=H
10b: β *meso* R_β=CH$_2$OH; R_α=R_γ=R_δ=H
10c: γ *meso* R_γ=CH$_2$OH; R_α=R_β=R_δ=H
10d: δ *meso* R_δ=CH$_2$OH; R_α=R_β=R_γ=H

11a: α *meso* R_α=CH$_2$OH; R_β=R_γ=R_δ=H
11b: β *meso* R_β=CH$_2$OH; R_α=R_γ=R_δ=H
11c: γ *meso* R_γ=CH$_2$OH; R_α=R_β=R_δ=H
11d: δ *meso* R_δ=CH$_2$OH; R_α=R_β=R_γ=H
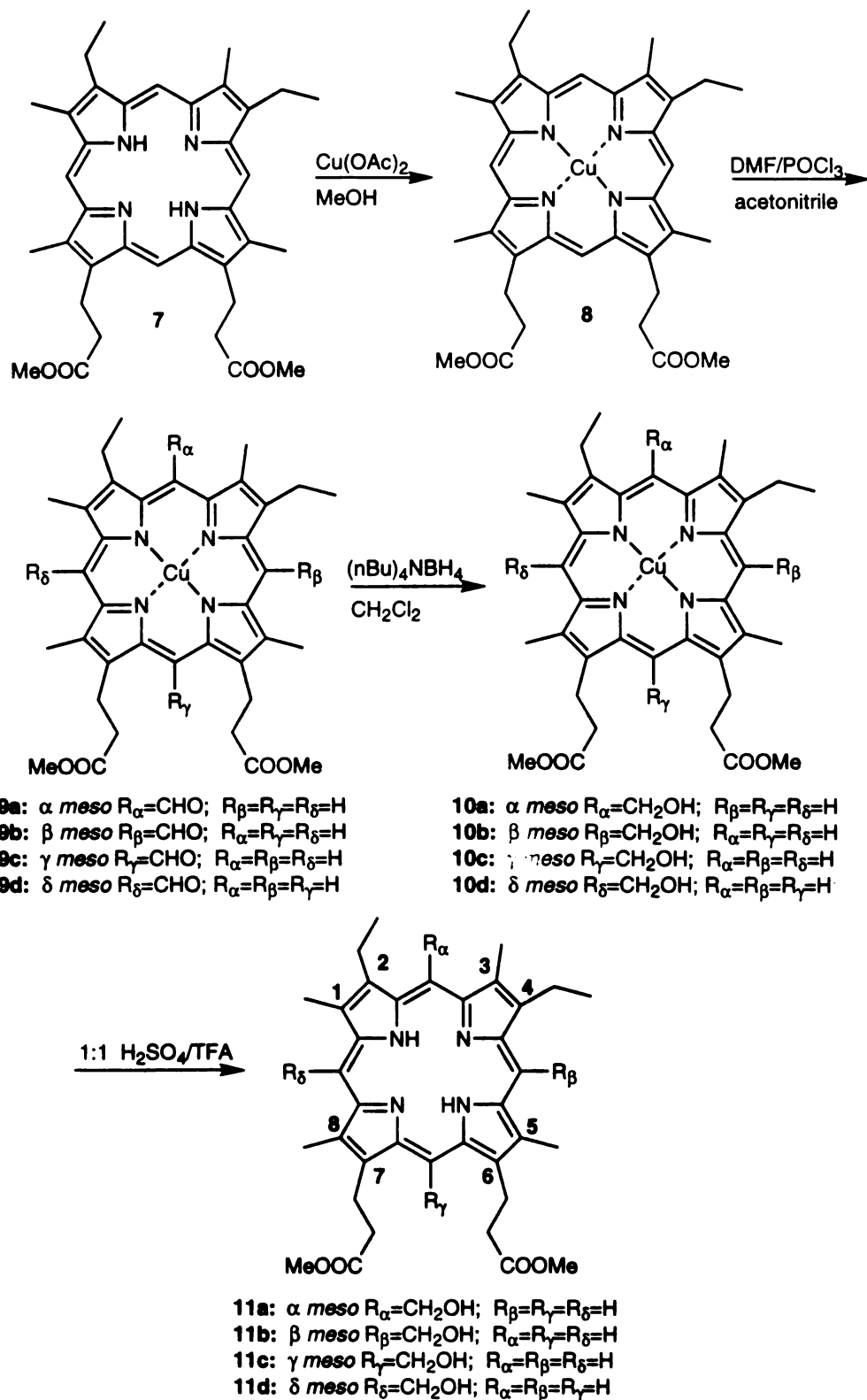
Figure 3.1.1. Synthesis of *meso*-hydroxymethyl MSPR-DME isomers (**11a-d**). The mixture of regioisomers (**11a-d**) is separated on silica gel at this stage of the synthesis.

47

11a: α *meso* R_α=CH$_2$OH; R_β=R_γ=R_δ=H
11b: β *meso* R_β=CH$_2$OH; R_α=R_γ=R_δ=H
11c: γ *meso* R_γ=CH$_2$OH; R_α=R_β=R_δ=H
11d: δ *meso* R_δ=CH$_2$OH; R_α=R_β=R_γ=H

12a: α *meso* R_α=Me; R_β=R_γ=R_δ=H
12b: β *meso* R_β=Me; R_α=R_γ=R_δ=H
12c: γ *meso* R_γ=Me; R_α=R_β=R_δ=H
12d: δ *meso* R_δ=Me; R_α=R_β=R_γ=H
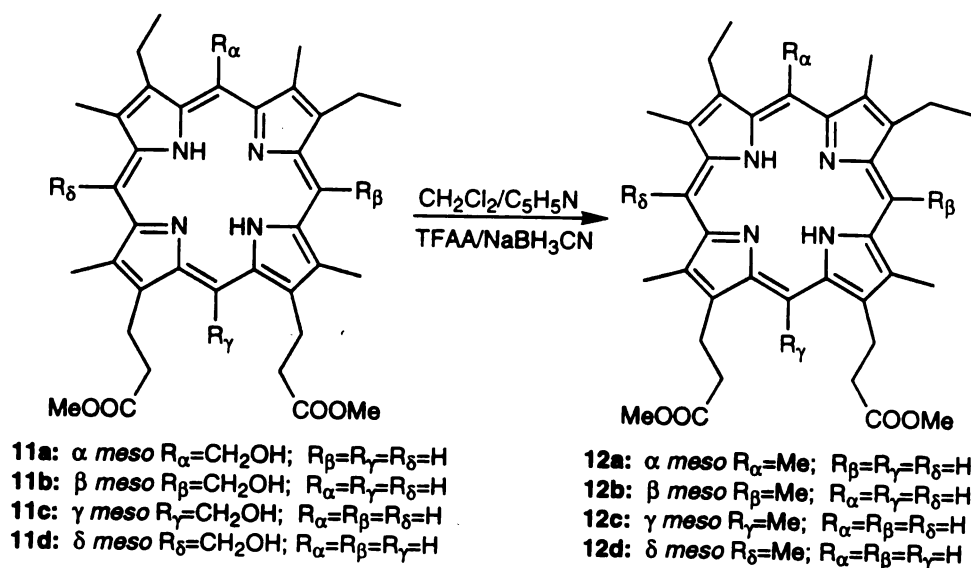
Figure 3.1.2. Synthesis of *meso*-methyl MSPR-DME isomers (**12a-d**) by reduction of the individual *meso*-hydroxymethyl MSPR-DME isomers (**11a-d**).

11a: α *meso* R_α=CH$_2$OH; R_β=R_γ=R_δ=H
11b: β *meso* R_β=CH$_2$OH; R_α=R_γ=R_δ=H
11c: γ *meso* R_γ=CH$_2$OH; R_α=R_β=R_δ=H
11d: δ *meso* R_δ=CH$_2$OH; R_α=R_β=R_γ=H

13a: α *meso* R_α=CHO; R_β=R_γ=R_δ=H
13b: β *meso* R_β=CHO; R_α=R_γ=R_δ=H
13c: γ *meso* R_γ=CHO; R_α=R_β=R_δ=H
13d: δ *meso* R_δ=CHO; R_α=R_β=R_γ=H
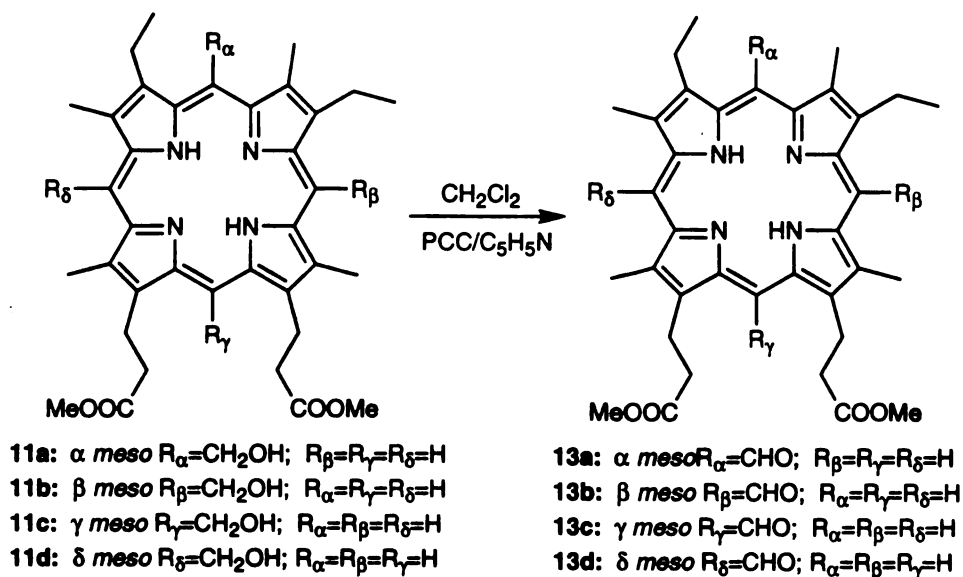
Figure 3.1.3. Synthesis of *meso*-formyl MSPR-DME isomers (**13a-d**) by oxidation of the individual *meso*-hydroxymethyl MSPR-DME isomers (**11a-d**).

The *meso*-methyl porphyrins were obtained by reduction of the *meso*-hydroxymethyl substituent using sodium cyanoborohydride (Figure 3.1.2). The *meso*-formyl porphyrins were obtained by oxidation of the *meso*-hydroxymethyl substituent using PCC (Figure 3.1.3). The *meso*-substituted mesohemes are synthesized by hydrolysis of the dimethylesters to free acids and insertion of iron.

3.2 EXPERIMENTAL

General

^{1}H NMR spectra were measured in deuterated chloroform (porphyrin concentration 3-4 mg/ml) on either a 300 or 500 MHz instrument. One dimensional ^{1}H NOE experiments were carried out using a 4s decoupler pulse and a delay time of 1s. NOE difference spectra were obtained by subtracting the off resonance spectrum from the on resonance spectrum. ^{1}H NOESY data were obtained using a delay time of 2s and a mixing time of 300 ms. The NOESY spectra were obtained with 8K data points in the t_2 dimension and 400 blocks of 16 scans each in the t_1 dimension. The free induction decays were zero filled once in both dimensions and a 70° shifted sine-squared apodization window was applied in both dimensions. ^{13}C NMR spectra were acquired on a 300 MHz instrument and are completely decoupled. MSPR-DME was purchased from Porphyrin Products (Logan, Utah). TLC was carried out on silica gel GF (250 micron) plates (Analtech, Newark, DE).

Cu^{II} MSPR-DME (8)

The synthesis of the *meso*-hydroxymethyl MRPR-DME mixture of regioisomers starting with MSPR-DME (7) is shown in Figure 3.2.1. As described by Fuhrhop and Smith (1975), 20 ml of a saturated solution of cupric acetate in methanol was added to a solution of MSPR-DME (7) (100 mg, 168 μmol) in 20 ml of CH_2Cl_2. After refluxing for 30 min, the reaction was allowed to cool and was then washed with water and extracted with CH_2Cl_2. The organic layer was again washed with water, dried over anhydrous Na_2SO_4, and concentrated *in vacuo* to give (8) in essentially quantitative yield. TLC in chloroform shows a single product (8) with $R_f = 0.41$ and no residual MSPR-DME ($R_f = 0.20$). Compound (8) was used without further purification.

Regioisomers of Cu^{II} *Meso*-Formyl MSPR-DME (9a-d)

Porphyrin (8) was formylated by a Vilsmeier reaction as described by Fuhrhop and Smith (1975) with the following modifications. A solution of (8) (110 mg, 168 μmol) in 50 ml of CH_2Cl_2 in a two necked round bottom flask equipped with a stir bar and condenser was purged with argon while freshly distilled phosphorous oxychloride (2.0 ml, 21.3 mmol) was added to dry dimethylformamide (2.0 ml, 25.8 mmol). The Vilsmeier reagent was stirred at room temperature for 10 min before a 3 ml aliquot was transferred to

the reaction flask, and the resulting mixture was refluxed under argon for 1 h. To the reaction was then added 50 ml of saturated sodium acetate and the mixture was stirred for another hour before it was allowed to cool. The reaction was worked up by diluting it with water (50 ml), extracting it with CH_2Cl_2 (2 x 200 ml), washing the combined organic phase with water, drying it over anhydrous Na_2SO_4, and finally concentrating it *in vacuo*. The residue was used without further purification.

Regioisomers of Cu^{II} *Meso*-Hydroxymethyl MSPR-DME (10a-d)

Meso-formyl porphyrins (**9a-d**) were reduced to the corresponding *meso*-hydroxymethyl porphyrins (**10a-d**) by treatment with tetra-*n*-butylammonium borohydride (50 mg, 196 μmol) in CH_2Cl_2 (30 ml). The reaction mixture was stirred at room temperature for 5 min. Workup of the reaction involved extracting with 100 ml of 3% H_2O_2, thorough washing with water, drying over anhydrous Na_2SO_4, and concentration in *vacuo*. TLC of the residue with diethyl ether as solvent indicates the formation of all four *meso*-hydroxymethyl isomers (R_f = 0.74, 0.68, 0.56, 0.48) as well as detectable amounts of starting material (**8**) (R_f = 0.84) due to incomplete Vilsmeier reaction.

Regioisomers of *Meso*-Hydroxymethyl MSPR-DME (11a-d)

The copper ion was removed from the mixture (**10a-d**) by treatment with 1:1 H_2SO_4 /trifluoroacetic acid as reported by Fuhrhop and Smith (1975). Prolonged exposure of these metalloporphyrins to acidic conditions causes retro-elimination of the *meso*-hydroxymethyl group to give MSPR-DME and formaldehyde, but removal of the copper ion occurs almost instantaneously under the indicated conditions. Therefore, the product mixture (**10a-d**) was dissolved in 10 ml of the acid solution and the solution was immediately diluted with water (100 ml) and extracted with CH_2Cl_2 (2 x 200 ml). The organic layer was washed with water until the pH was neutral and was then dried and concentrated *in vacuo*. Thin layer chromatography with long wave UV light detection shows the presence of five fluorescent spots, indicating that the metal was successfully removed from the four product regioisomers (**11a-d**) as well as the residual starting material (**8**). The first silica column is a short "plug" onto which the porphyrins are loaded in CH_2Cl_2. The short column is washed with large volumes of CH_2Cl_2 until starting material (**7**) completely elutes, at which point the *meso*-hydroxymethyl porphyrins (**11a-d**) are eluted by addition of 10% methanol in CH_2Cl_2. The product mixture (**11a-d**) is then purified by flash column chromatography in 30% hexanes/70% diethyl ether, and each

isomer is subsequently rechromatographed using diethyl ether as solvent: TLC (diethyl ether) R_f = 0.87 (**8**), 0.72 (**11c**), 0.66 (**11a**), 0.55 (**11b**), 0.46 (**11d**); (**11a**):λ_{max} (CH_2Cl_2) 406, 508, 542, 578, 628 nm; ^1H NMR ($CDCl_3$) δ 1.79 (brd t, 3H), 1.89 (brd t, 3H), 1.93 (s, O-H), 3.28 (brd m, 4H), 3.60 (s, 6H), 3.63 (s, 3H), 3.70 (s, 9H), 4.10 (brd m, 4H), 4.37 (brd m, 4H), 5.90 (brd s, 2H), 9.88 (s, 1H), 10.05 (s, 2H); ^{13}C NMR ($CDCl_3$) δ 11.6, 11.9, 16.6, 17.1, 17.5, 20.0, 21.8, 22.9, 36.9, 45.4, 51.7, 59.6, 95.8, 96.7, 96.9, 135.1, 136.5, 136.7, 137.6, 137.7, 138.1, 141.6, 142.0, 142.4, 143.1, 143.6, 144.2, 144.8, 146.5, 147.9, 173.6; LSIMS m/z 607 (MH^+ - H_2O). (**11b**): λ_{max} (CH_2Cl_2) 406, 506, 542, 578, 628 nm; ^1H NMR ($CDCl_3$) δ 1.83 (m, 6H), 1.88 (s, O-H), 3.15 (t, 2H, J = 7.8 Hz), 3.25 (t, 2H, J = 7.5 Hz), 3.53 (s, 3H), 3.56 (s, 6H), 3.65 (s, 3H), 3.67 (s, 3H), 3.68 (s, 3H), 4.02-4.07 (m, 4H), 4.39-4.41 (m , 4H), 5.80 (brd s, 2H), 9.85 (s, 1H), 10.01 (s, 1H) 10.03 (s, 1H); ^{13}C NMR ($CDCl_3$) δ 11.3, 11.5, 12.0, 16.7, 17.1, 17.6, 19.8, 21.9, 22.2, 23.1, 37.0, 45.3, 51.7, 59.5, 96.3, 96.6, 96.8, 134.8, 135.8, 136.0, 138.2, 138.6, 140.7, 141.3, 141.6, 142.3, 142.7, 142.7, 143.3, 145.5, 146.1, 146.5, 147.2, 173.6; LSIMS m/z 607 (MH^+ - H_2O). (**11c**): λ_{max} (CH_2Cl_2) 408, 510, 546, 580, 636 nm; ^1H NMR ($CDCl_3$) δ 1.81(m, 6H), 1.83 (s, O-H), 3.24 (m, 4H), 3.53 (s, 3H), 3.56 (s, 3H), 3.58 (s, 3H), 3.59 (s, 3H), 3.76 (s, 3H), 3.77 (s, 3H), 4.01 (m, 4H), 4.40 (brd m, 4H), 5.70 (s, 2H), 9.83 (s, 1H), 10.01 (s, 2H); ^{13}C NMR ($CDCl_3$) δ 11.4, 11.5, 12.2, 17.5, 17.6, 19.7, 19.8, 25.4, 36.4, 45.5, 51.8, 60.2, 96.2, 96.9, 97.0, 134.7, 135.6, 137.6, 138.9, 141.8, 142.3, 142.7, 143.0, 143.8, 143.8, 145.2, 145.6, 145.8, 146.3, 173.6; LSIMS m/z 607 (MH^+ - H_2O). (**11d**): λ_{max} (CH_2Cl_2) 406, 506, 542, 580, 628 nm; ^1H NMR ($CDCl_3$) δ 1.74 (t, 3H, J = 7.5 Hz), 1.82 (t, 3H, J = 7.5 Hz), 1.92 (s, O-H), 3.14 (t, 2H, J = 7.5 Hz), 3.26 (t, 2H, J = 7.5 Hz), 3.57 (s, 6H), 3.64 (s, 3H), 3.66 (s, 6H), 3.67 (s, 3H), 4.01-4.03 (m, 4H), 4.38-4.40 (m, 4H), 5.75 (s, 2H), 9.86 (s, 1H), 10.02 (s, 1H), 10.04 (s, 1H); ^{13}C NMR ($CDCl_3$) δ 11.5, 11.6, 16.9, 17.5, 17.6, 19.7, 20.0, 21.9, 22.1, 37.0, 45.4, 51.7, 59.5, 96.0, 96.5, 96.6, 134.8,.135.5, 135.7, 135.8, 137.1, 138.7, 140.6, 141.0, 141.9, 141.9, 142.4, 143.9, 144.8, 145.0, 145.7, 146.9; LSIMS m/z 607 (MH^+ - H_2O).

Regioisomers of *Meso*-Methyl MSPR-DME (12a-d)

The *meso*-hydroxymethyl substituent of (**11a-d**) was reduced to the *meso*-methyl of (**12a-d**) by dissolving the porphyrin (16.0 mg, 20.4 µmol) in CH_2Cl_2 (10 ml), adding pyridine (100 µl), trifluoroacetic anhydride (100 µl), and sodium cyanoborohydride (8.0 mg, 127 µmol), and stirring at room temperature for 10 min. The reaction was then sequentially extracted with aqueous $NaHCO_3$, 1.0 N HCl, and brine. The organic layer

was dried and concentrated under vacuum. Each isomer was individually reduced using a similar procedure with yields varying between 60-80%. After workup the products (12a-d) were purified by flash column chromatography with ether as the solvent: (12a): λ_{max} (CH_2Cl_2) 406, 504, 540, 580 nm; ^1H NMR ($CDCl_3$) δ 1.79 (m, 6H), 3.26 (m, 4H), 3.51 (s, 3H), 3.56 (s, 3H), 3.58 (s, 3H), 3.67 (s, 6H), 4.02 (m, 4H), 4.35 (m, 4H), 4.48 (s, 3H), 9.8 (s, 1H), 10.0 (s, 2H); ^{13}C NMR ($CDCl_3$) δ 11.7, 16.0, 17.3, 17.6, 19.9, 21.8, 22.8, 22.9, 36.9, 51.7, 94.6, 96.4, 96.5, 114.4, 135.1, 136.5, 137.1, 137.5, 137.7, 141.2, 141.4, 142.1, 142.2, 144.1, 144.5, 146.0, 173.7; HRMS m/z 608.3371, calcd. for $C_{37}H_{44}O_4N_4$, 608.3363; (12b): λ_{max} (CH_2Cl_2) 406, 506, 540, 576 nm; ^1H NMR ($CDCl_3$) δ 1.78 (t, 3H, J = 9.0 Hz), 1.83 (t, 3H, J = 9.0 Hz), 3.20 (t, 2H, J = 7.5 Hz), 3.26 (t, 2H, J = 7.5 Hz), 3.52 (s, 3H), 3.54 (s, 3H), 3.56 (s, 3H), 3.58 (s, 3H), 3.65 (s, 3H), 3.69 (s, 3H), 4.03 (brd q, 4H), 4.38 (t, 4H, J = 7.5 Hz), 4.49 (s, 3H), 9.81 (s, 1H), 10.00 (s, 1H), 10.01 (s, 1H); ^{13}C NMR ($CDCl_3$) δ 11.4, 11.5, 11.8, 16.0, 17.4, 17.6, 19.8, 21.9, 22.0, 22.8, 22.9, 37.0, 51.7, 95.1, 96.1, 96.4, 114.4, 134.8, 135.3, 137.5, 138.5, 140.4, 141.6, 143.0, 143.8, 144.9, 145.3, 146.8, 147.4, 173.6; HRMS m/z 608.3378, calcd. for $C_{37}H_{44}O_4N_4$, 608.3363; (12c): λ_{max} (CH_2Cl_2) 406, 506, 540, 576 nm; ^1H NMR ($CDCl_3$) δ 1.82 (m, 6H), 3.14 (brd t, 4H), 3.53 (s, 3H), 3.56 (s, 3H), 3.59 (s, 3H), 3.60 (s, 3H), 3.77 (s, 3H), 3.78 (s, 3H), 4.01 (m, 4H), 4.36 (brd t, 4H), 4.53 (s, 3H), 9.79 (s, 1H), 9.99 (s, 2H); ^{13}C NMR ($CDCl_3$) δ 11.4, 11.5, 12.0, 17.5, 17.6, 19.7, 19.8, 25.4, 29.7, 36.0, 51.9, 96.5, 96.6, 98.1, 134.8, 135.2, 135.8, 137.4, 137.5, 138.6; HRMS m/z 608.3345, calcd. for $C_{37}H_{44}O_4N_4$, 608.3363; (12d): λ_{max} (CH_2Cl_2) 404, 504, 538, 576 nm; ^1H NMR ($CDCl_3$) δ 1.79 (t, 3H, J = 9.0 Hz), 1.85 (t, 3H, J = 9.0 Hz), 3.19 (t, 2H, J = 7.5 Hz), 3.26 (t, 3H, J = 7.5 Hz), 3.55 (s, 3H), 3.57 (s, 3H), 3.58 (s, 6H), 3.64 (s, 3H), 3.67 (s, 3H), 4.04 (m, 4H), 4.38 (m, 4H), 4.47 (s, 3H), 9.82 (s, 1H), 10.01 (s, 1H), 10.02 (s, 1H); ^{13}C NMR ($CDCl_3$) δ 11.5, 11.6, 17.1, 17.2, 17.5, 19.7, 19.8, 21.9, 23.6, 37.0, 51.7, 94.9, 96.0, 96.3, 114.7, 134.8, 135.6, 138.7, 140.0, 140.6, 141.5, 142.2, 143.8, 144.1, 145.5, 145.7, 146.3; HRMS m/z 608.3353, calcd. for $C_{37}H_{44}O_4N_4$, 608.3363.

Regioisomers of *Meso*-Formyl MSPR-DME (13a-d)

The *meso*-hydroxymethyl (11a-d) substituent was oxidized to the *meso*-formyl (13a-d) by dissolving the porphyrin (α = 16 mg, 25.6 μmol; β = 14 mg, 22.4 μmol; γ = 5 mg, 8.0 μmol; δ = 42 mg, 67.3 μmol) in CH_2Cl_2 (20 ml), pyridine (5 ml), and 3 equivalents of PCC. The reaction stood at room temperature in the dark overnight at which point the reaction was partitioned between 1.0 N HCl (300 ml) and CH_2Cl_2 (50 ml), the

organic phase washed with water (400 ml), and concentrated under vacuum. TLC of the reaction mixture in diethyl ether showed the product, *meso*-formyl MSPR-DME $(R_f=.88)$. The *meso*-formyl porphyrins were purified on silica columns using hexanes:diethyl ether (30:70) as solvent. Each isomer was oxidized in an identical manner yielding ($\alpha = 6.0$ mg, 9.6 μmol, 38%; $\beta = 9.3$ mg, 15.0 μmol, 67%; $\gamma = 4.0$ mg, 6.4 μmol, 80%; $\delta = 11$ mg, 17.7 μmol, 26%). (**13a**): λ_{max} (CH₃Cl) 404, 504, 538, 576 nm; ¹H NMR (CDCl₃) δ 1.69 (t, 2H, $J = 7.3$ Hz), 1.76 (t, 2H, $J = 7.5$ Hz), 3.23 (t, 4H, $J = 6.5$ Hz), 3.34 (s, 3H), 3.52 (s, 3H), 3.56 (s, 3H), 3.58 (s, 3H), 3.63 (s, 3H), 3.64 (s, 3H), 3.79 (m, 2H) 3.98 (m, 2H), 4.31 (m, 4H), 9.94 (s, 1H), 10.01 (s, 2H), 12.72 (s, 1H); ¹³C NMR (CDCl₃) δ 11.6, 15.2, 16.0, 16.7, 17.5, 18.5, 19.8, 21.7, 29.7, 36.8, 51.8, 98.4, 113.6, 115.2, 137.9, 138.6, 142.2, 143.1, 143.4, 144.0, 144.1, 145.1, 145.5, 150.2, 173.5, 197.6; HMRS *m/z* 622.3163, calcd for C₃₇H₄₂N₄O₆ 622.3155. (**13b**): λ_{max} (CH₃Cl) 404, 506, 538, 574 nm; ¹H NMR (CDCl₃) δ 1.79 (brd m, 2H),1.81 (t, 2H, $J =$ 7.5 Hz), 3.21 (m, 4H), 3.37 (s, 3H), 3.51 (s, 3H), 3.54 (s, 3H), 3.55 (s, 3H), 3.62 (s, 3H), 3.66 (s, 3H), 3.82 (m, 2H), 4.00 (m, 2H), 4.33 (m, 4H), 9.93 (s, 1H), 10.01 (s, 1H), 10.07 (s, 1H), 12.73 (s, 1H); ¹³C NMR (CDCl₃) δ 11.6, 14.1, 17.6, 19.6, 21.7, 22.0, 22.7, 27.4, 31.9, 36.8, 51.7, 97.2, 948.0, 98.5, 113.6, 114.4, 128.7, 135.1, 135.7, 136.2, 138.5, 140.7, 142.0, 142.9, 143.4, 144.7, 146.0, 146.2, 173.5, 174.0, 197.8; HMRS *m/z* 622.3149, calcd for C₃₇H₄₂N₄O₆ 622.3155. (**13c**): λ_{max} (CH₃Cl) 406, 504, 538, 574 nm; ¹H NMR (CDCl₃) δ 1.81 (t, 6H, $J = 9.0$ Hz), 2.33 (t, 2H, $J =$ 7.5 Hz), 3.11 (brd t, 2H), 3.53 (s, 3H), 3.54 (s, 3H), 3.55 (s, 3H), 3.56 (s, 3H), 3.63 (m, 2H), 3.72 (s, 3H), 3.73 (s, 3H), 3.99 (t, 2H, $J = 9.0$ H⁻), 4.12 (t, 2H, $J = 9.0$ Hz), 4.29 (m, 2H), 9.92 (s, 1H), 10.02 (s, 2H), 12.73 (s, 1H); ¹³C NMR (CDCl₃) δ 11.4, 11.9, 17.5, 19.7, 24.4, 29.7, 35.5, 51.8, 98.5, 98.6, 98.8, 136.9, 139.7, 142.9, 143.1, 143.2, 143.8, 145.2, 173.4, 173.5, 196.0; HMRS *m/z* 622.3142, calcd for C₃₇H₄₂N₄O₆ 622.3155. (**13d**): λ_{max} 434, 574, 628 (CH₃Cl) nm; ¹H NMR (CDCl₃) δ 1.77 (t, 2H, $J = 7.5$ Hz), 1.81 (t, 2H, $J = 7.5$ Hz), 3.18 (t, 2H, $J = 7.5$ Hz), 3.24 (t, 2H, $J = 7.5$ Hz), 3.37 (s, 3H), 3.38 (s, 3H), 3.55 (s, 3H), 3.57 (s, 3H), 3.63 (s, 3H), 3.65 (s, 3H), 3.98 (q, 4H, $J = 7.5$ Hz), 4.34 (m, 4H), 9.94 (s, 1H), 10.01 (s, 1H), 10.07 (s, 1H), 12.73 (s, 1H); ¹³C NMR (CDCl₃) δ 11.4, 11.5, 16.5, 16.7, 17.5, 19.7, 21.7, 29.7, 36.8, 51.7, 98.1, 98.3, 98.6, 129.2, 133.9, 135.7, 136.6, 138.8, 141.3, 142.4, 142.8, 143.2, 144.1, 144.7, 144.9, 145.3, 173.4, 174.0, 198.1; HMRS *m/z* 622.3151, calcd for C₃₇H₄₂N₄O₆ 622.3155.

Ferric *Meso*-Substituted Mesohemes

Conversion of the dimethylesters of *meso*-substituted mesoporphyrins to the corresponding mesohemes was done by hydrolyzing the 'imethyl esters in 25% (v/v) HCl at 25°C in the dark for eight hours. The hydrolysis reaction was worked up by neutralizing to pH 4, extracting with CH_2Cl_2, washing the organic phase with water before drying it with anhydrous Na_2SO_4, and removing the solvent under vacuum. The porphyrins were used without further purification for the subsequent reaction in which the iron was inserted by the ferrous sulfate method (Morrell et al., 1961). An argon-purged, saturated aqueous Fe_2SO_4 solution (1 ml) was added to a stirred, argon-purged solution of the porphyrins in 1 ml of pyridine and 20 ml of acetic acid. The mixture was warmed for ten minutes under a stream of argon. The stirred reaction mixture was then exposed to the air while it cooled to promote autooxidative formation of the ferric state before it was combined with 25 ml of brine and extracted with diethyl ether. The organic layer was washed with 25% HCl to remove unreacted porphyrin, washed with water, and dried over Na_2SO_4. Removal of the solvent under vacuum provided the *meso*-substituted mesohemes, which were purified by reverse phase HPLC on a Whatman Partisil 10 semi-prep ODS-3 column at 5 ml/min using 100% Solvent A (55:40:10 - acetonitrile:water:acetic acid). The *meso*-methyl and *meso*-formylmesohemes had poorly resolved retention times between 9.9-10.8 min and by HPLC were shown to be >95% pure.

3.3 RESULTS

Synthesis of the *Meso*-Methyl and *Meso*-Formyl MSPR-DME Regioisomers

The four isomers of *meso*-hydroxymethyl MSPR-DME (11a-d) have been synthesized by Vilsmeier formylation of the copper(II) complex of MSPR-DME (8) (Figure 3.2.1). Reduction of the mixture of copper(II) *meso*-formyl MSPR-DME regioisomers (9a-d) with tetra-*n*-butylammonium borohydride gives the mixture of copper(II) *meso*-hydroxymethyl MSPR-DME regioisomers (10a-d). Demetallation of the porphyrins (10a-d) yields the mixture (11a-d) as well as some starting material (7). The components of both mixtures 10a-d and 11a-d are well resolved on silica. Thus, the R_f values of isomers (11a-d) on silica gel thin layer chromatography with diethyl ether as the solvent are γ (0.72), α (0.66), β (0.55), and δ (0.46). Porphyrins (11a-d) were therefore separated and purified by flash column chromatography and each isomer was subsequently rechromatographed for optimum purity. The overall yield of each of the *meso*-

hydroxymethyl MSPR-DME regioisomers correlates with the degree of steric hindrance surrounding the *meso* position substituted in each, giving 30% of the δ-isomer and as little as 5% of the γ-isomer. The individual *meso*-hydroxymethyl porphyrins (**11a-d**) were then reduced to the corresponding *meso*-methyl porphyrins (**12a-d**) by treatment with trifluoroacetic anhydride/pyridine and sodium cyanoborohydride in CH_2Cl_2 (Figure 3.2.2). Furthermore, the individual *meso*-hydroxymethyl porphyrins (**11a-d**) were also oxidized to the corresponding *meso*-formyl porphyrins (**13a-d**) by treatment with PCC and pyridine in CH_2Cl_2 (Figure 3.2.3).

Identification of the *Meso*-Hydroxymethyl MSPR-DME Regiosomers

The mixture of porphyrin isomers was separated at the *meso*-hydroxymethyl stage because advantage could be taken of the relatively high differences in the polarities of the *meso*-hydroxymethyl regioisomers. The regiochemistry of the *meso*-substitution was established at the same stage. As shown in Figure 3.3.1, the ^{1}H NMR spectra of
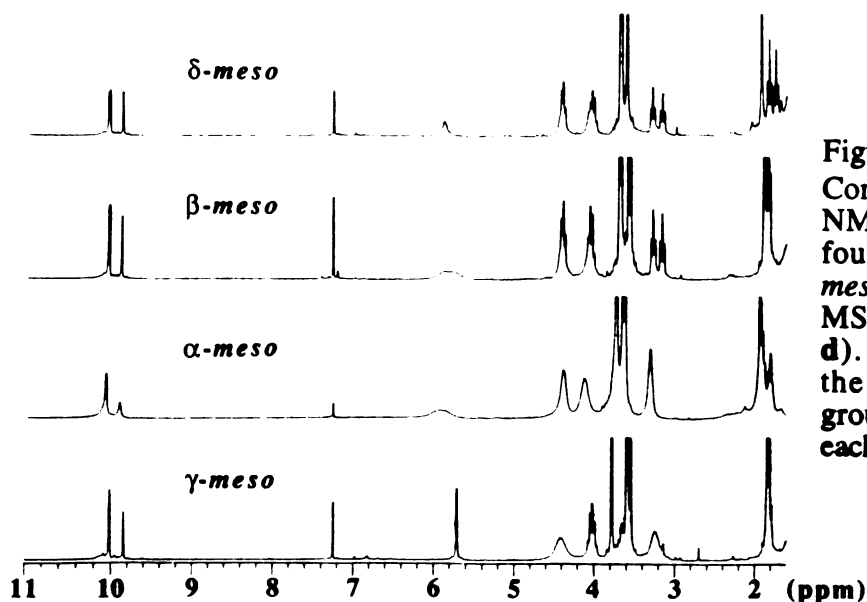
Figure 3.3.1. Comparison of the ^{1}H NMR spectra of the four regioisomers of *meso*-hydroxymethyl MSPR-DME.(**11a-d**). The position of the hydroxymethyl group is indicated on each spectrum.

porphyrins (**11a-d**) are very similar. These pseudo-symmetric molecules exhibit many overlapping resonances, including a highly congested region of methyl signals. As expected, however, porphyrins (**11c**) and (**11d**) are readily identified as the γ– and δ– isomers, respectively, by NOE experiments. Thus, irradiation of the propionate resonance of (**11d**) at 4.39 ppm (Figure 3.3.2, *lower trace*) enhances and identifies the γ-*meso* proton signal (Figure 3.3.2, *upper trace*), while irradiation of the ethyl methylene

resonance at 4.02 ppm (Figure 3.3.3, *lower trace*) enhances and identifies both the α- and β-*meso* proton resonances (Figure 3.3.3, *upper trace*).
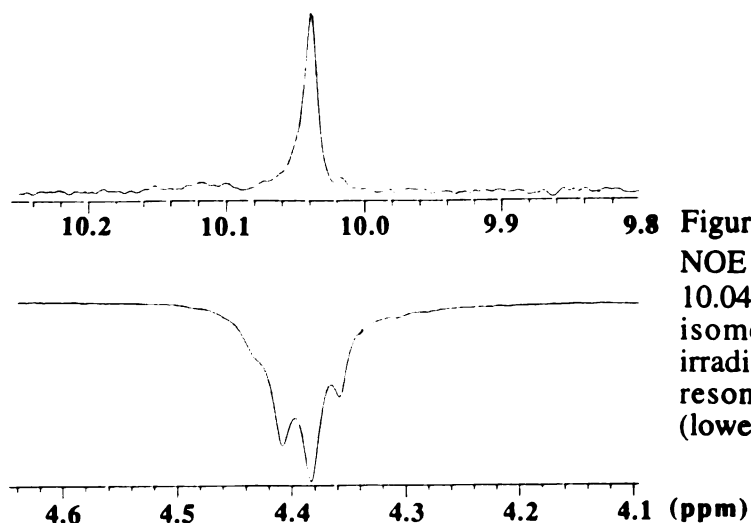
Figure 3.3.2.
NOE of the γ-*meso* proton at 10.04 ppm (upper tracing) of isomer **11d** caused by irradiation of the propionate resonances at 4.39 ppm (lower tracing).
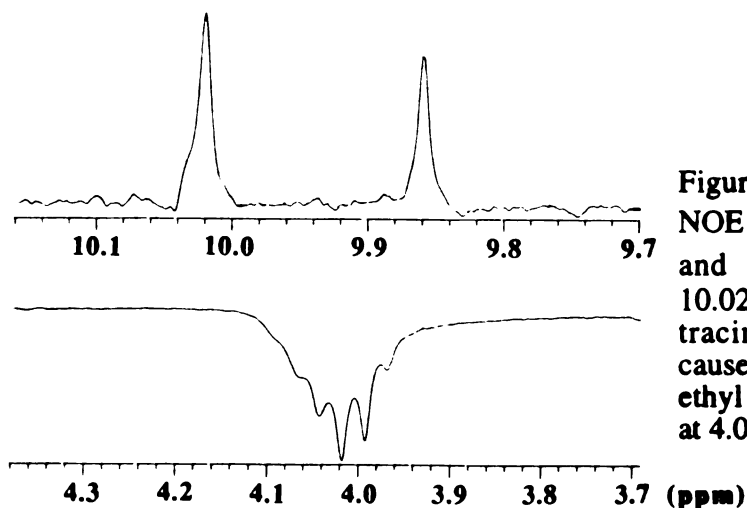
Figure 3.3.3.
NOE enhancement of the α- and β-*meso* protons at 10.02 and 9.86 ppm (upper tracing) of isomer **11d** caused by irradiation of the ethyl methylene resonances at 4.02 ppm (lower tracing).

By exclusion, porphyrin (**11d**) is the δ-*meso* hydroxymethyl isomer. The γ-isomer is unambiguously identified by two independent experiments. The α- and β-*meso* protons are identified in NOESY plots by their NOE interactions with the protons of both a methyl and an ethyl methylene, and the δ-*meso* proton by its NOE interactions with two different methyl groups (not shown). By exclusion, the γ-*meso* position in isomer (**11c**) must bear the hydroxymethyl substituent. This assignment is confirmed by irradiation of the inner methylenes of the propionic acid substituents, which results in enhancement of both the γ-*meso* hydroxymethyl O-H proton at 1.84 ppm and methylene protons at 5.69 ppm (not

shown). The complete resonance assignments for the γ-isomer (11c) are given in Table 3.3.1.

Differentiating the α- and β-isomers, however, requires a NOESY spectrum that contains the NOE's for the entire molecule. The complete proton assignments for the β-isomer (11b) are shown in Table 3.3.2. These proton assignments make possible a "walk" around the porphyrin periphery that identifies the β-*meso* hydroxymethyl group by its NOE crosspeaks to the surrounding substituents. As shown in Figure 3.3.4, the δ-*meso* proton at 9.85 ppm exhibits crosspeaks to the flanking 1- and 8-methyl groups at 3.53 ppm and 3.56 ppm, respectively. The methyl group at 3.56 ppm has an NOE to the

Figure 3.3.4.
Region of the NOESY spectrum of isomer 11b showing the cross-peaks between the δ-*meso* proton at 9.85 ppm and the flanking 1- and 8-methyl groups at 3.53 and 3.56 ppm.
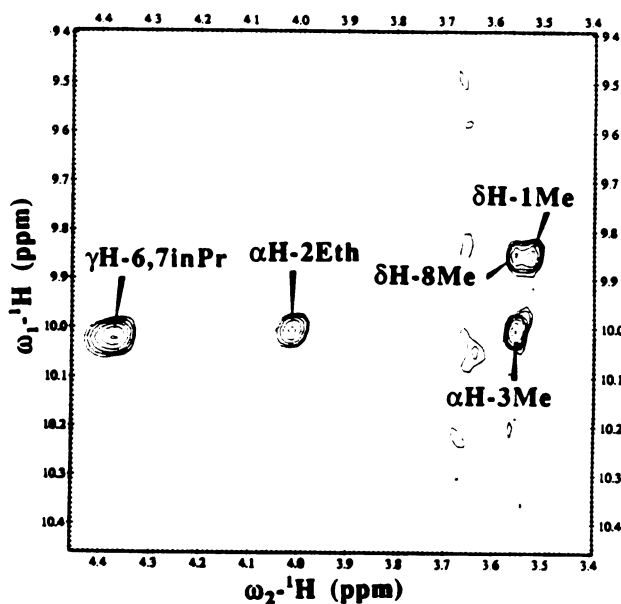
Figure 3.3.5.
Region of the NOESY spectrum of isomer 11b showing the NOE between the methyl group at 3.56 ppm and the 7-propionate inner methylene protons at 4.39 ppm and between the propionate inner methylene protons at 4.41 ppm and the 5-methyl at 3.68 ppm.
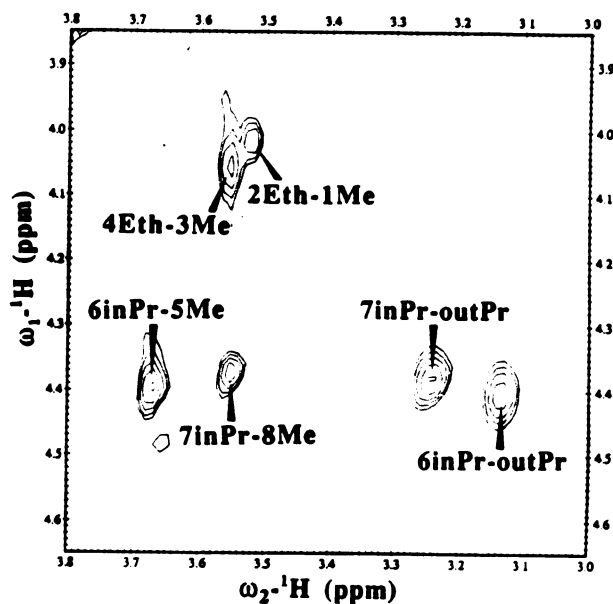
7-propionate inner methylene protons at 4.39 ppm (Figure 3.3.5) and can therefore be identified as the 8-methyl. The other propionate at 4.41 ppm, which must be the 6-propionate, has an NOE to the methyl at 3.68 ppm, which is therefore identified as the 5-methyl (Figure 3.3.5). The 5-methyl at 3.68 ppm exhibits a cross-peak to the *meso* hydroxymethyl O-H proton at 1.88 ppm rather than to a *meso* proton. The *meso* hydroxymethyl group with the O-H signal at 1.88 ppm therefore must be at the β-*meso* position vicinal to the 5-methyl (Figure 3.3.6). The location of the *meso* hydroxymethyl group is independently confirmed by the observation of an NOE between the *meso*-hydroxymethyl O-H proton at 1.88 ppm and the 4-ethyl methylene protons at 4.07 ppm (Figure 3.3.6). The 4-ethyl methylene protons at 4.07 ppm are distinguished from the 2-

Figure 3.3.6.
Region of the NOESY spectrum of isomer **11b** showing the NOE between the 5-methyl at 3.68 ppm and the β-*meso*-hydroxymethyl OH proton at 1.88 ppm.
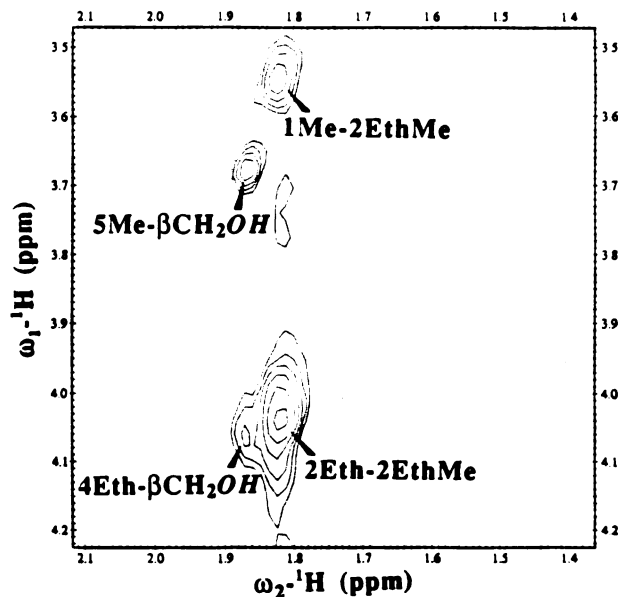
ethyl methylene protons at 4.02 ppm by the presence of an NOE correlating the resonance at 4.02 ppm with that of the 1-methyl at 3.53 ppm (Figure 3.3.5). Both results positively identify (**11b**) as the β-isomer. By exclusion, isomer (**11a**) must be the α-*meso* hydroxymethyl isomer.

Proton	Chemical Shift (ppm)	NOE
α-*meso* **H**	9.84	2-CH$_2$CH$_3$, 3-CH$_3$
β-*meso* **H**	10.01	4-CH$_2$CH$_3$, 5-CH$_3$
γ-*meso* CH$_2$OH	1.84	γ-CH$_2$OH, 6-Pr, 7-Pr
γ-*meso* CH$_2$OH	5.69	γ-CH$_2$OH, 6-Pr, 7-Pr
δ-*meso* **H**	10.01	1-CH$_3$, 8-CH$_3$
1-CH$_3$	3.56	δ-*meso* **H**, 2-CH$_2$CH$_3$
2-CH$_2$CH$_3$	3.99	1-CH$_3$, α-*meso* **H**
2-CH$_2$CH$_3$	1.80	
3-CH$_3$	3.54	α-*meso* **H**, 4-CH$_3$
4-CH$_2$CH$_3$	4.03	3-CH$_3$, β-*meso* **H**
4-CH$_2$CH$_3$	1.81	
5-CH$_3$	3.59	β-*meso* **H**, 6-Pr
6,7-CH$_2$CH$_2$CO$_2$Me	4.47, 4.32	5,8-CH$_3$, γ-CH$_2$OH
6,7-CH$_2$CH$_2$CO$_2$Me	3.24	
8-CH$_3$	3.59	7-Pr, δ-*meso* **H**
diester CH$_3$	3.77, 3.78	

Table 3.3.1. ^{1}H NMR assignments for the γ-*meso* hydroxymethyl isomer.

Proton	Chemical Shift (ppm)	NOE
α-*meso* **H**	10.01	2-CH$_2$CH$_3$, 3-CH$_3$
β-*meso* CH$_2$OH	5.90 (broad)	
β-*meso* CH$_2$OH	1.88	4-CH$_2$CH$_3$, 5-CH$_3$
γ-*meso* **H**	10.03	6-Pr, 7-Pr
δ-*meso* **H**	9.85	1-CH$_3$, 8-CH$_3$
1-CH$_3$	3.53	δ-*meso* **H**, 2-CH$_2$CH$_3$
2-CH$_2$CH$_3$	4.02	1-CH$_3$, α-*meso* **H**
2-CH$_2$CH$_3$	1.83	
3-CH$_3$	3.56	α-*meso* **H**, 4-CH$_2$CH$_3$
4-CH$_2$CH$_3$	4.07	3-CH$_3$, β-CH$_2$OH
4-CH$_2$CH$_3$	1.83	
5-CH$_3$	3.68	β-CH$_2$OH, 6-Pr
6-CH$_2$CH$_2$CO$_2$Me	4.41	5-CH$_3$, γ-*meso* **H**
6-CH$_2$CH$_2$CO$_2$Me	3.15	
7-CH$_2$CH$_2$CO$_2$Me	4.39	γ-*meso* **H**, 8-CH$_3$
7-CH$_2$CH$_2$CO$_2$Me	3.25	
8-CH$_3$	3.56	7-Pr, δ-*meso* **H**
diester CH$_3$	3.67, 3.65	

Table 3.3.2. ^{1}H NMR assignments for the β-*meso* hydroxymethyl isomer.

3.4 DISCUSSION

The Vilsmeier formylation reaction was used to introduce a carbon-carbon bond at the *meso* position. Inhoffen et al. (1966) reported *meso*-substituted mono-formylated products by Vilsmeier formylation of copper(II) octaethylporphyrin. On these grounds it was suspected that Vilsmeier formylation of copper(II) MSPR-DME would yield a mixture of regioisomeric *meso* formyl porphyrins. Use of PPIX-DME was purposely avoided due to the propensity of the electrophilic Vilsmeier reagent to add to the more electron rich vinyl groups rather than the *meso* positions of the porphyrin macrocycle. MSPR-DME has ethyl groups in place of the vinyl substituents of PPIX DME. The copper is believed to be necessary to activate the porphyrin π system by making it more electron rich, thus facilitating the electrophilic addition of the Vilsmeier reagent.

The *meso*-formylated products gave a mixture of porphyrins that were blackish green in color and were not separated on silica gel. Smith et al. (1980) reported the reduction of a copper(II) *meso*-formyl porphyrin directly to copper(II) *meso*-methyl porphyrin using tetra-*n*-butylammonium borohydride, as well as demetalation using 1:1 sulfuric acid and trifluoroacetic acid to give the *meso*-methyl porphyrin. Thus, in attempting to synthesize the *meso*-methyl MSPR-DME regioisomeric mixture, the copper(II) *meso*-formyl MSPR-DME mixture was reduced using tetra-*n*-butylammonium borohydride. Addition of the reducing agent gave an immediate bright burgundy color. TLC of the reaction mixture using diethylether indicated the presence of five products. An identical result was obtained when the mixture of demetallated products was chromatographed. Thus, the copper was removed and the free-base porphyrins were purified on silica gel.

Initially it was thought that the *meso*-hydroxymethyl porphyrins were *meso*-methyl porphyrins because LSIMS gave m/z (MH$^+$) = 608.3, consistent with substitution of a methyl group for a proton. While the presence of only three *meso* protons was consistent with *meso* substitution, the ^{1}H NMR spectrum did not have a methyl group at 4.7 ppm as previously reported for a *meso*-methyl porphyrin (Smith et al., 1984). Instead, the ^{1}H NMR spectra of the *meso*-hydroxymethyl porphyrins contained new, unidentified, peaks at 5.8 (broad) and 1.9 ppm. These peaks were identified as *meso*-hydroxymethyl -CH$_2$ and -OH protons, respectively based on the NOESY spectrum of the γ-isomer. The correct assignments eventually led to the determination that the MS data indicating m/z (MH$^+$) = 608.3 for the *meso*-hydroxymethyl porphyrins was artifactual. This was proven by

reduction of the *meso*-hydroxymethyl porphyrins to give the *meso*-methyl porphyrins with a methyl group in the expected place, 4.7 ppm.

Thus, the purified *meso*-hydroxymethyl MSPR-DME regioisomers (**11a-d**) were used as precursors in the synthesis of the *meso*-methyl (**12a-d**) and *meso*-formyl (**13a-d**) MSPR-DME regioisomers. These porphyrins were converted into the corresponding mesohemes by hydrolysis of the dimethylesters and insertion of an iron atom. These hemes have been used as probes of mechanism and regiospecificity in heme oxygenase and this work is described in the following chapters. In addition, the *meso*-substituted mesohemes may also be highly useful as probes of the structure and mechanism of other hemoproteins. Due to the altered steric and electronic properties of *meso*-substituted hemes, they may have an affect on the many steps of the catalytic pathways of cytochromes P450 and the peroxidases; e.g. electron transport, oxygen binding, substrate binding, and oxygen activation and reactivity.

4.0 OXIDATION OF *MESO*-METHYL AND *MESO*-FORMYLMESOHEME REGIOISOMERS BY HEME OXYGENASE

4.1 INTRODUCTION

Recombinant technology has revolutionized modern enzymology because it makes available reagent-scale quantities of heterologously expressed pure proteins. This allows investigational studies to utilize the powerful tools of spectroscopy that are available to chemists today. It is remarkable to consider the achievements of scientists in this field who were able to learn so much without these basic tools (recombinant technology and modern spectroscopy). Heme oxygenase is certainly an example of an enzyme for which spectroscopic investigations have been impaired by the inability to obtain sufficient quantities from natural sources. Although bearing in mind that heme oxygenase is itself a catalyst and should produce many moles of product per mole of catalyst, nevertheless, recombinantly expressed (30 mg/L) heme oxygenase had made it possible to generate sufficient (mg) quantites of metabolites to facilitate their spectroscopic characterization. In Chapter 2, advantage was taken of the ability to generate enough of the heme oxygenase and ethylhydroperoxide reaction product, α-*meso* ethoxy PPIX-DME, to completely assign the ^{1}H NMR spectrum. Similar circumstances enabled the characterization of a novel heme cleavage reaction: the oxidation of α-*meso*-methyl-1,2-dimethyl heme by heme oxygenase. This chapter extends the work on the novel heme cleavage reaction by investigating the heme oxygenase catalyzed oxidation of the four regioisomeric *meso*-methyl mesohemes and the regioisomeric *meso*-formyl mesohemes synthesized in Chapter 3.

One of the most interesting questions to consider concerning heme oxygenase is the regiospecificity of the reaction. That is, *in vivo* heme catabolism produces exclusively bilirubin IXα. The regiochemistry of the *in vivo* process was established by Fisher following the total synthesis of bilirubin IXα and its correlation with an authentic standard. The question is, of course, how does the *in vivo* system exert control over the activated oxygen species? Until the discovery by Schmid of rat liver heme oxygenase, the debate centered around whether the *in vivo* regiospecificity was mediated by a specific heme-cleaving enzyme, or was simply the final catalytic moment of each and every hemoprotein. Nevertheless, upon the discovery that coupled oxidation in free solution gave a mixture of regioisomers (Petryka et al., 1962), it was universally believed that the hemoprotein matrix was responsible for controlling the regiospecificity of heme catabolism *in vivo* and *in vitro*.

The most pervasive theory on the regiospecificity of heme catabolism to date is the steric-hindrance model (Brown 1976; Brown & Docherty, 1978; Brown et al., 1981) based on the results of the coupled oxidation of hemoproteins. As discussed in Chapter 1.3, coupled oxidation of an aqueous pyridine-solution of heme using ascorbate as reductant results in production of approximately equal amounts of verdoheme regioisomers, which can in turn be hydrolyzed to biliverdin regioisomers (Figure 1.3.1). It was soon discovered that unlike free heme in solution, coupled oxidation of hemoproteins resulted in production of only one or two biliverdin regioisomers. For example, only biliverdin IXα was detected from the coupled oxidation of myoglobin using ascorbate (O'Carra & Colleran, 1969). These authors referenced the X-ray diffraction work of Kendrew et al. (1960) and stated that finding exlusively the α-isomer was a suprising result. Based on Kendrew's crystal structure, they concluded that the heme in the myoglobin active site has an α-meso edge surrounded by hydrophobic groups while the other three meso-positions are fairly open and exposed. They concluded that "the specific cleavage at the α-methine bridge must therefore be a positive effect of the heme binding site rather than a masking of the other three bridges". While no elaboration of the "positive effect" was made, they indicated that they did not believe the regiospecificity of the myoglobin reaction could be attributed to steric-hindrance or "masking" of the three unreacted meso-positions.

Brown's consideration of the steric-hindrance model relied on a slightly different set of assumptions from those of O'Carra and Colleran. O'Carra and Colleran were at University College in Galway, Ireland, and had not apparently read the *Proceedings of the National Academy of the United States*, which had published in the previous calendar year Schmid's description of microsomal heme oxygenase. They therefore did not recognize that a specific heme-cleaving enzyme was responsible for *in vivo* heme catabolism, nor did they recognize that the heme molecule was autocatalytic in its destruction. In their evaluation of the steric-hindrance model they implied that the unreacted meso-bridges were exposed and vulnerable to what they assumed to be an intermolecular reaction. Brown (1976) favored the steric-hindrance model on the basis of accessibility of the various methene bridges to an oxygen molecule *already bound to the iron atom*. Specifically, Brown (1976) proposed that the meso-edges of the heme in sperm-whale myoglobin were blocked by specific amino acid residues: the δ-meso position by Val-68, the γ-meso position by His-64, and the β-meso position by Phe-43, therefore leaving the α-position as the favored site for attack. In later years, the theory was expanded upon by correlating isomer patterns produced by the coupled oxidation of certain abnormal hemoglobins

(Brown & Docherty, 1978). While the hemoglobin mutants did produce different isomer patterns by coupled oxidation, no compelling rationale was made for why any given mutation produced the isomer pattern observed.

Due to the lack of a crystal structure for heme oxygenase, no such comparison can be made for specific amino acid mutations affecting the regiospecificity of the heme oxygenase-catalyzed heme cleavage. Spectroscopic characterization of the wild-type enzyme active site has, however, shed light on this problem and even presented a new theory for the enzyme regiospecificity: that an electronic component is responsible for controlling the enzyme regiospecificity. The first experimental evidence for this theory of heme oxygenase regiospecificity was provided by ^{1}H NMR studies of the heme-heme oxygenase complex (Hernández et al., 1994), as described in Chapter 1.12. In summary, the 2D NMR revealed a contact shift pattern that reflects an unusual hemin electronic structure that is characterized by large differences in delocalized spin density for the two β-positions within a given pyrrole ring, resulting in an increased overall spin density at the α-meso position (see Figure 1.12.2). This was interpreted as evidence for a direct electronic effect mediated by heme oxygenase that activates the α-meso position towards electrophilic attack by an iron-peroxo species. While the specifics of how the protein causes this unusual electronic perturbation are not clear, the idea that the most electron rich meso-position is selectively oxidized by heme oxygenase is consistent with the findings from Chapter 2. In Chapter 2 it was shown that the iron-peroxo intermediate most likely adds to the heme by an electrophilic mechanism (Figure 2.4.1c). In addition, it was shown that a methyl group placed at the α-meso position does not impair the enzyme's ability to oxidize the heme to biliverdin. Oxidation of the α-meso methyl substituted heme occurred regiospecifically at the α-meso position, removing the α-meso carbon and the appended methyl group. The facile removal of the meso-methyl group may be suprising, but regiospecific oxidation at the most electron-rich (methyl substituted) meso-position supports the idea that regiospecificity may be controlled electronically.

The synthesis of the meso-methyl and meso-formyl regioisomeric mesohemes in Chapter 3 makes available the substrates necessary to test the hypothesis that the regiospecificity of heme oxidation is controlled, or at least affected, by the electronic properties of the heme. The absence of a heme oxygenase crystal structure makes site-directed mutagenesis and structure-function arguments based on mutagenesis futile as an approach to the regiospecificity problem. These limitations do not apply to the following experiments, which can be viewed as site-directed mutagenesis of the heme molecule itself.

Each *meso*-substituted mesoheme was reconstituted with heme oxygenase in a 1:1 ratio. The *meso*-methyl and *meso*-formylmesoheme-hHO-1 complexes were assayed for heme oxygenase-catalyzed oxidation using both NADPH-cytochrome P450 reductase and H_2O_2 as oxidants, while monitoring spectroscopically for verdoheme intermediates. Following the determination of catalytic activity, the regioselectivity of each *meso*-methyl reaction with each of three different oxidants (NADPH-cytochrome P450 reductase, H_2O_2, and ascorbate) was determined by extracting the biliverdin products, purifying them by HPLC, and subjecting them to mass spectrometric analysis. The regioselectivity of each *meso*-formyl reaction with NADPH-cytochrome P450 reductase was also determined. CO assays were used to determine whether or not the *meso*-substitutent was removed. In cases where the reaction produced CO and the *meso*-substituent remained appended to the mesobiliverdin, the mesobiliverdin dimethylesters were fragmented using electron impact mass spectrometry in order to determine the mass of the two principal fragments, and thus the axis of heme oxidation as described previously by Bonnett & McDonagh (1973). Furthermore, in an effort to determine the fate of the two carbons cleaved in the α-*meso* methyl reaction, assays were developed and executed for acetic acid and acetaldehyde.

4.2 EXPERIMENTAL PROCEDURES

General Methods

Truncated human HO-1 without the 23 amino acid membrane anchor was expressed in *Escherichia coli* and was purified as previously reported (Wilks et al., 1995a). Mesoheme was obtained from mesoporphyrin IX dimethyl ester (Porphyrin Products, Logan , UT) as reported (Furhop & Smith, 1975; Morell et al., 1961). The *meso*-methylmesoheme and *meso*-formylmesoheme regioisomers were synthesized as described in Chapter 3. Each *meso*-substituted mesoheme was combined with hHO-1 in approximately a 2:1 heme to enzyme ratio and the mixture was purified over a BioRad HTP column to give a 1:1 complex in 100 mM potassium phosphate buffer (pH 7.4), as previously reported (Wilks & Ortiz de Montellano, 1993). HPLC was done on a Varian 9010 solvent delivery system equipped with a Hewlett Packard model 1040A detector and a reverse-phase Whatman analytical (4.6 x 250 mm) Partisil 10 mm ODS-3 column. The mobile phase was either 100% Solvent A (acetone/0.1% aqueous formic acid, 50:50) monitored at 374 nm and referenced at 474 nm or 100% Solvent B (acetonitrile/water/AcOH 55:40:10) monitored at 360 nm and referenced at 550 nm. Absorption spectra were generally recorded on a Hewlett Packard 8452A diode array spectrometer but difference spectra were obtained on an Aminco DW 2000 instrument.

Mass spectra were obtained by (+)LSIMS on a VG-70 or Kratos Concept instrument using a 1:1 (1% trifluoroacetic acid) glycerol:thioglycerol matrix. Gas chromatography was carried out on a Hewlett Packard model 5890A instrument equipped with a J & W Scientific DB-1 column. The GC parameters were initial temp.= 60°C, initial time = 1 min, rate = 10°C/min, final temp. = 250°C, final time = 10 min.

Coupled Oxidation of Mesoheme

Coupled oxidation of mesoheme in pyridine to give a mixture of the mesobiliverdin regioisomers was carried out as previously reported (Bonnett & McDonagh, 1973; Saito & Itano, 1986). A solution of mesoheme (2 mg, 3.2 μmol) in pyridine (20 ml) and deionized water (20 ml) was bubbled vigorously with O_2 for 2 min, after which sodium ascorbate (500 mg, 2.5 mmol) was added and the flask was stoppered and shaken for 5 min. The bright green mixture was poured into CH_2Cl_2 (50 ml) and water (400 ml) and the organic phase was washed with water (400 ml) before it was concentrated under vacuum to give a syrupy residue (5 ml). One volume of MeOH was added and the solution was immediately purged with argon. While under argon, a saturated solution of KOH in MeOH (3 ml) was added and the mixture was allowed to stand for 5 min before pouring it into 25% aqueous HCl (400 ml). The bluish-green solution was allowed to stir at 25 °C for 10 min and was then extracted with CH_2Cl_2 (50 ml), washed with water (400 ml), and concentrated under vacuum. The mesobiliverdin regioisomers were analyzed by HPLC using 100% Solvent A at a flow rate of 0.6 ml/min. Coupled oxidation of free *meso*-methylmesohemes was also attempted but no mesobiliverdin products were obtained.

Meso-Methylmesoheme-hHO-1 Binding Constants

Binding constants were obtained by adding increasing concentrations (0.32 μM to 5.12 μM) of the *meso*-methylmesoheme substrate to a set of matched cuvettes, one containing 11.5 μM hHO-1 apoprotein and the other aqueous buffer, and determining the difference spectrum. The absorbance difference between the minimum and maximum wavelengths was plotted versus the *meso*-methylmesoheme concentration. Biphasic curves were obtained and binding constants were determined by fitting a hyperbolic curve to the data for the initial phase. The second phase represents relatively weak, non-specific binding to the protein.

Fe(II)Mesoverdoheme-CO Complex Formation using NADPH-P450 Reductase

Cytochrome P450 reductase (12 μg, 0.15 nmol) and NADPH (100 nmol) were added to a 1 ml cuvette containing a solution in 100 mM potassium phosphate buffer (pH 7.4) of one of the meso-substituted mesoheme-hHO-1 complexes (α -CH$_3$ = 0.43 mg, 14.3 nmol; β-CH$_3$ = 0.62 mg, 20.5 nmol; γ-CH$_3$ = 0.60 mg, 19.9 nmol; δ-CH$_3$ = 0.59 mg, 19.8 nmol; α -CHO = 0.29 mg, 9.8 nmol; β-CHO = 0.37 mg, 12.2 nmol; γ-CHO = 0.23 mg, 7.8 nmol; δ-CHO = 0.41 mg, 13.8 nmol;1 ml final volume) that had been bubbled with CO. The progress of the reaction was followed spectrophotometrically by monitoring both the appearance of the Fe(II)mesoverdoheme-CO complex at λ_{max} 616 nm and the loss of the Soret band of the starting complex.

Fe(III)Mesoverdoheme Complex Formation using H$_2$O$_2$

H$_2$O$_2$ (10 equiv) was added to a cuvette containing one of the meso-methyl mesoheme-hHO-1 complexes in 100 mM potassium phosphate buffer (pH 7.4) (α-CH$_3$ = 0.58 mg, 19.3 nmol; β-CH$_3$ = 0.22 mg, 7.3 nmol; γ-CH$_3$ = 0.25 mg, 8.2 nmol; δ-CH$_3$ = 0.32 mg, 10.7 nmol; 1 ml final volume). Similarly, H$_2$O$_2$ (1 equiv) was added to a cuvette containing one of the meso-formyl mesoheme-hHO-1 complexes in 100 mM potassium phosphate buffer (pH 7.4) (α-CHO = 0.27 mg, 9.1 nmol; β-CHO = 0.46 mg, 15.2 nmol; γ-CHO = 0.23 mg, 7.8 nmol; δ-CHO = 0.33 mg, 11.11 nmol; 1 ml final volume). The progress of the reaction was monitored spectrophotometrically by the appearance of the Fe(III)mesoverdoheme absorption at 600-700 nm and the decrease in the intensity of the Soret absorbance of the starting complex.

Regiochemical Analysis of the NADPH-P450 Reductase-Supported Meso-Methyl Reactions

Cytochrome P450 reductase (300 μg, 3.9 nmol) and NADPH (30 μmol) were added to a solution in 100 mM potassium phosphate buffer (pH 7.4) of a meso-methyl mesoheme-hHO-1 complex (α-CH$_3$ = 7.1 mg, 237 nmol; β-CH$_3$ = 5.3 mg, 178 nmol; γ-CH$_3$ = 6.7 mg, 222 nmol; δ-CH$_3$ = 7.6 mg, 254 nmol; final volume: α-CH$_3$ = 11.5 ml, β-CH$_3$ = 12.0 ml, γ-CH$_3$ = 10.5 ml, δ-CH$_3$ = 12.5 ml). The reactions were allowed to stand at 25 °C for 1 h and were then extracted and analyzed as described below to give (α-CH$_3$): λ_{max} (CH$_3$OH) 366, 636 nm; m/z (MH$^+$) 587, calcd for C$_{33}$H$_{38}$O$_6$N$_4$ 586; (γ-CH$_3$): λ_{max} (CH$_3$OH) 366, 650 nm; m/z (MH$^+$) 587, calcd for C$_{33}$H$_{38}$O$_6$N$_4$ 586; (δ1-CH$_3$): λ_{max}

(CH_3OH) 322, 358, 570 nm; m/z (MH^+) 601, calcd for $C_{34}H_{40}O_6N_4$ 600; ($\delta 2$-CH_3): λ_{max} (CH_3OH) 366, 610 nm; m/z (MH^+) 587, calcd for $C_{33}H_{38}O_6N_4$ 586.

Regiochemical Analysis of the H_2O_2-Dependent *Meso*-Methyl Reactions

H_2O_2 (2 equiv) was added to a solution in 100 mM potassium phosphate buffer (pH 7.4) of a *meso*-methyl mesoheme-hHO-1 complex (γ-CH_3 = 4.3 mg, 143 nmol; δ-CH_3 = 6.8 mg, 227 nmol; final volume: γ-CH_3 = 7.0 ml, δ-CH_3 = 12.0 ml) and the reaction was monitored spectrophotometrically. The mixture was allowed to stand for 1 h at 25 °C, after which no further changes in the spectrum were observed. P450 reductase (60 μg, 0.78 nmol) and NADPH (10 μmol) were then added and the mixture was allowed to stand for 1 h before it was extracted and analyzed as described below to give (γ-CH_3): λ_{max} (CH_3OH) 366, 650 nm; m/z (MH^+) 587, calcd for $C_{33}H_{38}O_6N_4$ 586; ($\delta 1$-CH_3): λ_{max} (CH_3OH) 322, 358, 570 nm; m/z (MH^+) 601, calcd for $C_{34}H_{40}O_6N_4$ 600; ($\delta 2$-CH_3): λ_{max} (CH_3OH) 366, 610 nm; m/z (MH^+) 587, calcd for $C_{33}H_{38}O_6N_4$ 586.

Regiochemical Analysis of the Sodium Ascorbate-dependent *Meso*-Methyl Reactions

Coupled oxidation with ascorbate was also carried out with each of the *meso*-methyl mesoheme-hHO-1 complexes. To a solution in 100 mM potassium phosphate buffer (pH 7.4) of a *meso*-methyl mesoheme-hHO-1 complex (α-CH_3 = 7.1 mg, 237 nmol; β-CH_3 = 5.3 mg, 178 nmol; γ-CH_3 = 6.7 mg, 222 nmol; δ-CH_3 = 7.6 mg, 254 nmol; final volume: α-CH_3 = 11.5 ml, β-CH_3 = 12.0 ml, γ-CH_3 = 10.5 ml, δ-CH_3 = 12.5 ml) was added sodium ascorbate (50 mg, 0.25 mmol). The solution was gently agitated to facilitate dissolution of the ascorbate. After 1 h at 25 °C the reaction was extracted and analyzed as described below to give (α-CH_3): λ_{max} (CH_3OH) 366, 636 nm; m/z (MH^+) 587, calcd for $C_{33}H_{38}O_6N_4$ 586; (γ-CH_3): λ_{max} (CH_3OH) 366, 650 nm; m/z (MH^+) 587, calcd for $C_{33}H_{38}O_6N_4$ 586; ($\delta 1$-CH_3): λ_{max} (CH_3OH) 322, 358, 570 nm; m/z (MH^+) 601, calcd. for $C_{34}H_{40}O_6N_4$ 600; ($\delta 2$-CH_3): λ_{max} (CH_3OH) 366, 610 nm; m/z (MH^+) 587, calcd. for $C_{33}H_{38}O_6N_4$ 586.

Regiochemical Analysis of the NADPH-P450 Reductase-Supported *Meso*-Formyl Reactions

Cytochrome P450 reductase (24 μg, 312 pmol) and NADPH (25 mg, 30 μmol) were added to a solution in 100 mM potassium phosphate buffer (pH 7.4) of a *meso*-formyl mesoheme-hHO-1 complex (α-CHO = 5.3 mg, 176 nmol; β-CHO = 6.3 mg, 210

nmol; γ-CHO = 5.2 mg, 174 nmol; δ-CHO = 7.5 mg, 251 nmol; final volume: α-CHO = 5.5 ml, β-CHO = 7.0 ml, γ-CHO = 4.7 ml, δ-CHO = 6.5 ml). The reactions were allowed to stand at 37 °C for 30 min and were then extracted and analyzed as the dimethylesters as described below to give: (α-CHO): λ_{max} (CH$_3$OH) 364, 640 nm; (β-CHO): λ_{max} (CH$_3$OH) 366, 650 nm; (δ-CHO): λ_{max} (CH$_3$OH) 366, 635, 680 nm. The γ-isomer was recovered in amounts too small to characterize spectroscopically.

In a separate experiment, cytochrome P450 reductase (900 μg, 13.4 nmol) and NADPH (83.3 mg, 120 μmol) were added to a solution in 100 mM potassium phosphate buffer (pH 7.4) of the α-meso-formyl mesoheme-hHO-1 complex (81 mg, 2.7 μmol; final volume = 40 ml). The reaction was let stand at 25 °C for one hour at which time the reaction was extracted and analyzed as the dimethylesters as described below to give: λ_{max} (CH$_3$OH) 364, 640 nm; m/z (MH$^+$) fragment: 273.

Extraction and HPLC Analysis of the Mesobiliverdin Regioisomers

To each meso-methylmesoheme-hHO-1 reaction mixture was added conc HCl (1 drop) and acetic acid (1 ml) before the solution was extracted with CH$_2$Cl$_2$ (100 ml). The organic phase was washed with brine (300 ml) and water (400 ml) and then concentrated under vacuum. The concentrate was dissolved in 100% Solvent A and analyzed by HPLC as described in General Methods at a flow rate of 0.6 ml/min.

To each meso-formylmesoheme-hHO-1 reaction mixture was added conc HCl (1 drop) and acetic acid (1 ml) before the solution was extracted with CH$_2$Cl$_2$ (50 ml) and the organic phase washed with brine (50 ml). The concentrate was dissolved in 100% Solvent A and analyzed by HPLC at a flow rate of 1.0 ml/min. The UV-visible absorption spectrum was aquired, and each mesobiliverdin was dissolved in 5% H$_2$SO$_4$ (v/v) in MeOH (50 ml) and left at room temperature for 8 h. The mesobiliverdin dimethylesters were extracted into the organic phase after adding CHCl$_3$ (50 ml) and water (50 ml), and the organic phase was washed with water (100 ml) and concentrated under vacuum. The mass spectra of the meso-formyl-mesobiliverdin dimethylesters were acquired.

CO Assays

To a 1 ml solution of mesoheme-hHO-1 complex (0.27 mg, 9.0 nmol) was added P450 reductase (0.24 mg, 3.1 nmol) and NADPH (83.0 μg, 100 nmol). The tube was immediately sealed with a rubber septum. After 5 min at 25 °C the solution had turned green and a freshly prepared solution of ferrous deoxymyoglobin (0.14 mg, 8 nmol) was

injected via syringe through the septum. The solution was shaken, the septum removed, and the UV-visible spectrum recorded. This procedure was repeated with a 1 ml solution of the α-*meso*-methylmesoheme-hHO-1 complex (0.36 mg, 12.0 nmol). The ferrous deoxymyoglobin used to detect CO was prepared by adding sodium dithionite (5 mg) to a 2 ml solution of horse skeletal muscle myoglobin (0.27 mg, 16.0 nmol) in 100 mM potassium phosphate buffer (pH 7.4). This ferrous deoxymyoglobin solution was split in two and subsequently added to one of the hHO-1 reaction mixtures.

To 1 ml solutions of γ-*meso*-methylmesoheme-hHO-1 complex (2.1 mg, 71.0 nmol) and α-*meso*-formylmesoheme-hHO-1 complex (1.6 mg, 54.0 nmol) were added P450 reductase (0.24 mg, 3.1 nmol) and NADPH (0.42 mg, 500 nmol). The tubes were immediately sealed with a rubber septum. After 15 min at 25 °C the solutions had turned green and 700 µl of ferrous deoxymyoglobin (0.60 mg, 36 nmol) was added to the γ-*meso*-methylmesoheme-hHO-1 reaction mixture and 525 µl of ferrous deoxymyoglobin (0.45 mg, 27 nmol) was added to the α-*meso*-formylmesoheme-hHO-1 reaction mixture via syringe through the septa. The solutions were shaken, the septa removed, and the UV-visible spectrum recorded. The ferrous deoxymyoglobin was prepared in the manner described above.

CO assays were similarly performed on 1 ml solutions of the remaining *meso*-formylmesoheme-hHO-1 complexes (β-CHO = 0.27 mg, 9.1 nmol; γ-CHO = 0.21 mg, 7.0 nmol; δ-CHO = 0.26 mg, 8.6 nmol) by adding cytochrome P450 reductase (6.0 µg, 78 pmol) and NADPH (167 µg, 200 nmol) and sealing the tube. After 5 min at 25°C the reactions had turned green and freshly prepared ferrous deoxymyoglobin (88 µg, 5 nmol) was injected via syringe through the septum. The solutions were mixed, the septa removed, and the UV-visible spectrum recorded.

In separate experiments, quantitative CO assays were repeated on 0.5 ml solutions of the α- and δ-*meso*-formylmesoheme-hHO-1 complexes (α-CHO = 1.1 mg, 35 nmol; δ-CHO = 1.0 mg, 34 nmol) were added cytochrome P450 reductase (0.24 mg, 3.1 nmol) and NADPH (0.42 mg, 500 nmol) and the reactions let stand for 15 min at 25 °C with the tubes sealed. Freshly prepared ferrous deoxymyoglobin (0.81 mg, 35 nmol) was injected via syringe through the septum. The solutions were mixed, the septa removed, and the UV-visible spectrum recorded.

Acetaldehyde Assay

Brady's reagent was prepared by mixing 2,4-dinitrophenyl hydrazine (200 mg, 1.01 mmol) and 1 ml of H_2SO_4, followed by dropwise addition of 1.2 ml of water with swirling until dissolved. Upon cooling, 1-propanol (4.6 ml) and acetonitrile (30 ml) are added. This stock solution was used throughout all the experiments.

A standard curve was constructed by adding acetaldehyde (90, 180, 270, 360, 450, and 540 nmol) and sodium ascorbate (26 mg, 0.13 mmol) to 1 ml aliquots of hHO-1 apoprotein (2.5 mg. 83.3 nmol) and incubating at 25°C in sealed vials. A 1 ml solution of α-meso-methylmesoheme-hHO-1 complex (10.7 mg, 357 nmol) was treated identically. After 45 min, 10 μl of the Brady's reagent prepared above and 1 ml of Solvent B were added and the mixtures were incubated for 1 h at 25°C. Each sample (500 μl) was analyzed by HPLC using 100% Solvent B at 1 ml/min as described under General Methods.

Acetic Acid Assay

A standard curve was constructed by adding AcOH (50, 100, 200, 300, 400 nmol) and sodium ascorbate (30 mg, 0.15 mmol) to 1 ml aliquots of hHO-1 apoprotein (2.5 mg. 83.3 nmol) and incubating at 25°C in sealed vials for 1 h. A 1 ml solution of α-meso-methylmesoheme-hHO-1 complex (9.6 mg, 321 nmol) was treated identically. Following the incubation, each solution was taken to pH 14 by adding 100 μl of 10 N KOH. The samples were then frozen and lyophilized. To the residual salts were added 2,4'-dibromoacetophenone (4.2 mg, 15.0 μmol) in CH_2Cl_2 (1 ml) and acetonitrile (15 ml). The samples were then refluxed for 1 h, allowed to cool, transferred to a 5 ml centrifuge tube, and concentrated to dryness under vacuum. The samples were dissolved in 100 μl of CH_2Cl_2 of which 10 μl was used for GC analysis.

4.3 RESULTS

Coupled Oxidation of Mesoheme and *Meso*-Methylmesohemes

Coupled oxidation is the oxidation of heme to biliverdin promoted by ascorbate or other reducing agents (Lemberg et al., 1941a-c). Ascorbate has been specifically shown to support the conversion of heme-hHO-1 complexes to biliverdin IXα (Ito-Maki et al., 1995; Wilks, A., Torpey, J., & Ortiz de Montellano, P. R., unpublished results). To facilitate the identification of the mesobiliverdin isomers from incubations of *meso*-methylmesoheme-hHO-1 complexes, a standard regioisomer mixture was obtained by

coupled oxidation of mesoheme in pyridine:water (Figure 4.3.1). The reactions were
monitored by chromatographic and spectroscopic analysis of the mesobiliverdin products.
The assignment of the regiochemistry of each mesobiliverdin isomer was made by
matching the HPLC retention times of each of the components of the mixture to the HPLC
retention times of authentic samples of mesobiliverdin IXα, IXδ, and IXγ obtained from
hHO-1-catalyzed oxidation of the respective α-, δ-, and γ-meso-methylmesohemes.
Coupled oxidation of free meso-methylmesohemes in pyridine was also attempted under
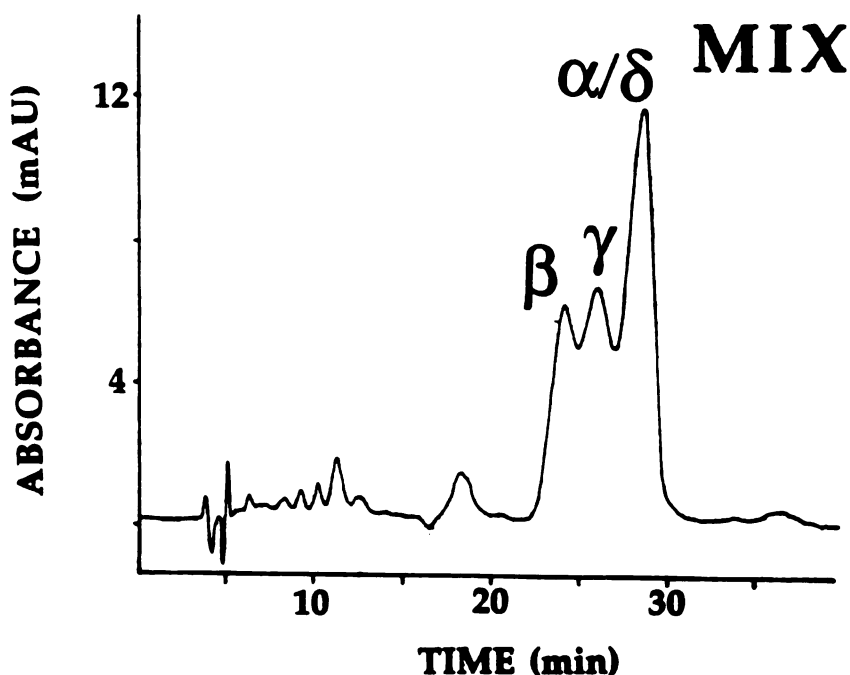identical conditions but the reaction failed to give mesobiliverdin regioisomers.

Figure 4.3.1. HPLC chromatogram of the mesobiliverdin products
extracted from the coupled oxidation of mesoheme in aqueous pyridine
followed by hydrolysis to give the mesobiliverdin regioisomers.

Binding of *Meso*-Methyl Mesohemes to hHO-1

The dissociation constants for the binding of the meso-methylmesoheme
regioisomers were determined by difference spectroscopy. The K_d values for the
regioisomers are: α-CH_3, 1 ± 0.3 μM; β-CH_3, 2 ± 0.5 μM; γ-CH_3, 10 ± 1 μM; and δ-
CH_3, 6 ± 1 μM. These values are similar to the value for mesoheme: K_d = 4 ± 0.2 μM.
The values are approximate due to the biphasic nature of the plots of absorbance difference
versus substrate concentration. It is nevertheless clear that the binding affinities for the
meso-methylmesohemes do not differ greatly from that for mesoheme, with the α-meso-

methyl isomer binding most tightly and the γ-meso-methyl isomer least tightly.

Formation of the Fe(II)Mesoverdoheme-CO Complex using NADPH-P450 Reductase

The meso-methyl and meso-formylmesoheme-hHO-1 complexes were allowed to react with P450 reductase and NADPH under a partial atmosphere of CO to determine whether each of them would undergo hHO-1 catalyzed heme degradation through the Fe(II) mesoverdoheme intermediate. Reaction of the α-meso-methylmesoheme-hHO-1 complex with NADPH and P450 reductase under an atmosphere of O_2 and CO results in loss of Soret intensity and the gradual accumulation of an intermediate with a distinct visible band at λ_{max} = 616 nm (Figure 4.3.2). This intermediate is the Fe(II)mesoverdoheme-CO complex (Yoshida et al., 1981; Lagarias 1982). The CO is included in the incubation to arrest the reaction at the mesoverdoheme stage, as the reaction otherwise proceeds directly to mesobiliverdin. The changes in the absorption spectrum due to the incubation of hHO-1 with γ-meso-methylmesoheme under the same conditions are also shown in Figure 4.3.2. The reactions of hHO-1 with the β-methyl and δ-methyl isomers are shown in Figure 4.3.3. Over the time course of each reaction (3-5 min), the Soret band red-shifts and decreases in intensity and visible bands develop at λ_{max} = 538 and 616 nm. These changes signal formation of the corresponding Fe(II)mesoverdoheme-CO complexes. However, the amount of the Fe(II)mesoverdoheme-CO complex that is formed varies with the isomer, the β-methyl isomer giving the lowest spectroscopic conversion. Of course, the regiochemistries of the Fe(II)mesoverdoheme complexes obtained from the α, δ, and γ, and to some extent β, isomers are not defined by these spectroscopic studies.

The reactions of the four meso-formylmesoheme-hHO-1 complexes with P450 reductase and NADPH under a partial atmosphere of CO are shown in Figures 4.3.4 & 4.3.5. The absorption spectra of all four reactions follow the same pattern: the Soret band red-shifts and decreases dramatically while a prominent increase in the visible region is observed at 616 nm. These changes signal hHO-1 catalyzed degradation of the meso-formyl mesohemes to Fe(II)mesoverdoheme-CO complexes. However, the regiospecificity of each reaction is yet to be determined.
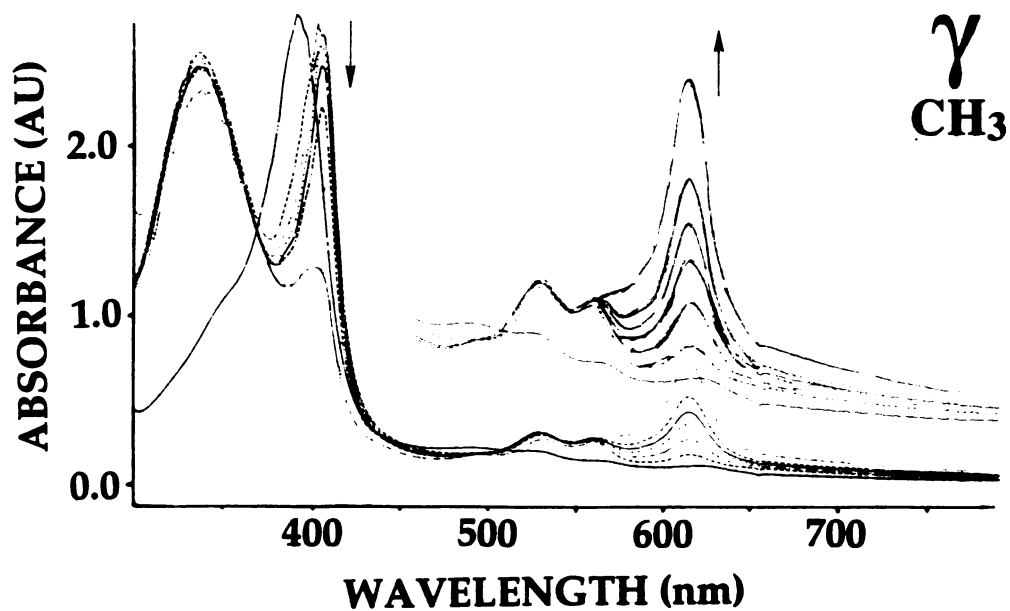
Figure 4.3.2. Spectrophotometric monitoring of the reactions of the α- and
γ-*meso*-methylmesoheme-hHO-1 complexes with NADPH-P450 reductase
under an atmosphere of CO. The reactions were scanned every 10-15 s, the
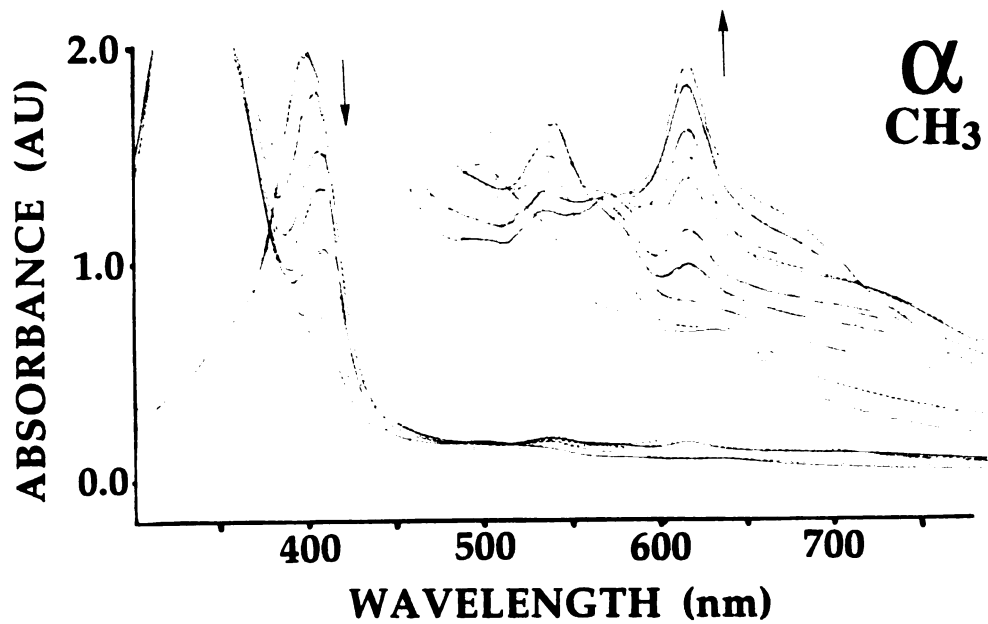first spectrum being recorded before the addition of NADPH.

Figure 4.3.3. Spectrophotometric monitoring of the reactions of the β- and δ-*meso*-methylmesoheme-hHO-1 complexes with NADPH-P450 reductase under an atmosphere of CO. The reactions were scanned every 10-15 s, the first spectrum being recorded before the addition of NADPH.
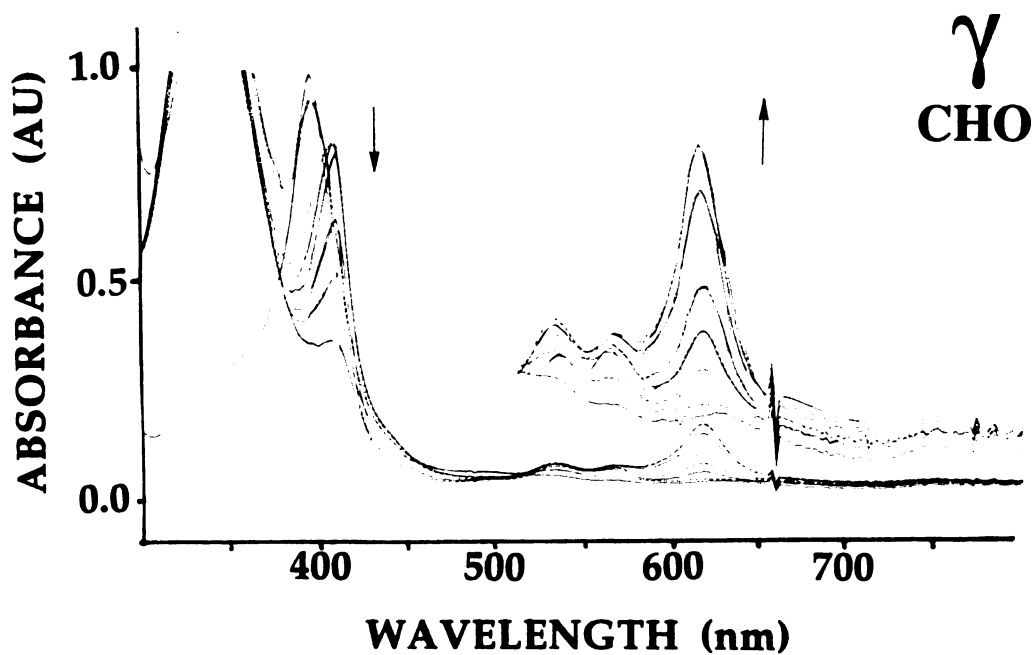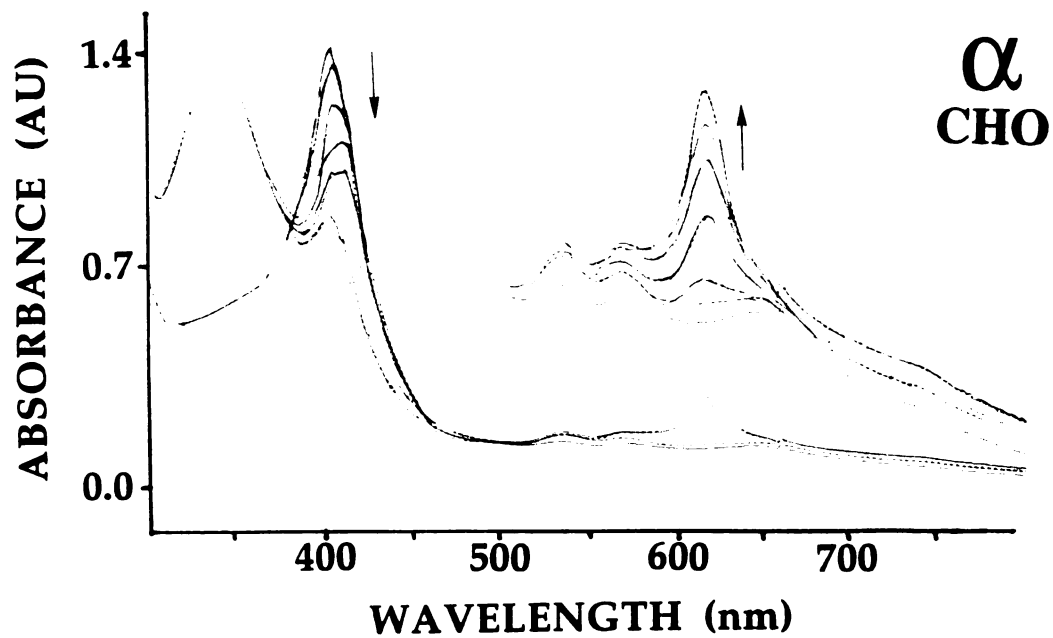
Figure 4.3.4. Spectrophotometric monitoring of the reactions of the α- and γ-*meso*-formylmesoheme-hHO-1 complexes with NADPH-P450 reductase under an atmosphere of CO. The reactions were scanned every 10-15 s, the first spectrum being recorded before the addition of NADPH.
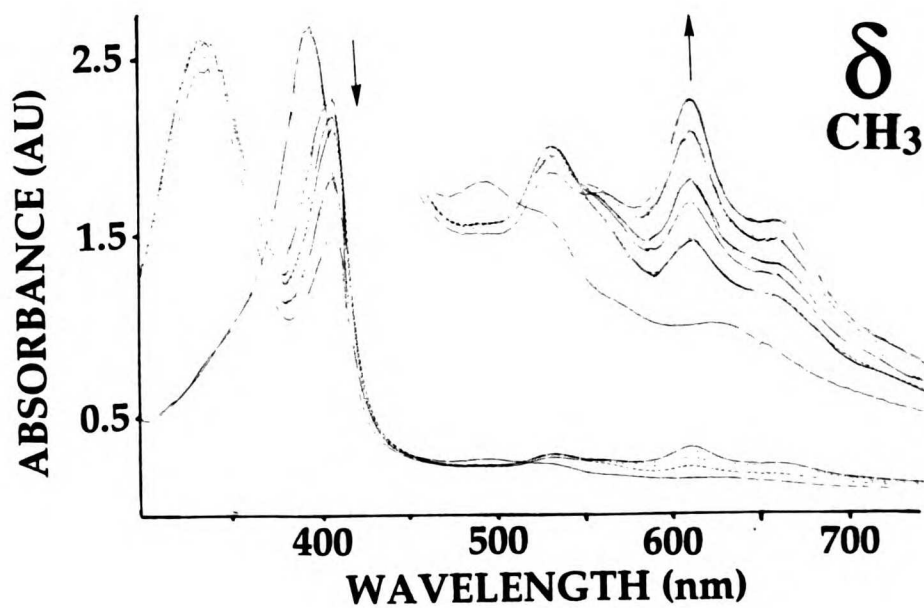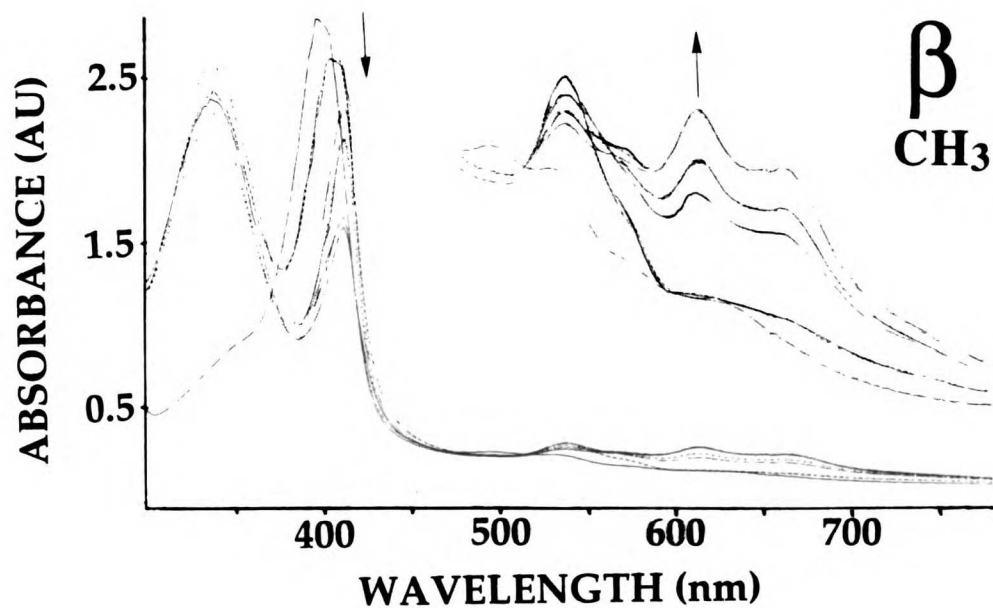
Figure 4.3.5. Spectrophotometric monitoring of the reactions of the β- and δ-*meso*-formylmesoheme-hHO-1 complexes with NADPH-P450 reductase under an atmosphere of CO. The reactions were scanned every 10-15 s, the first spectrum being recorded before the addition of NADPH.
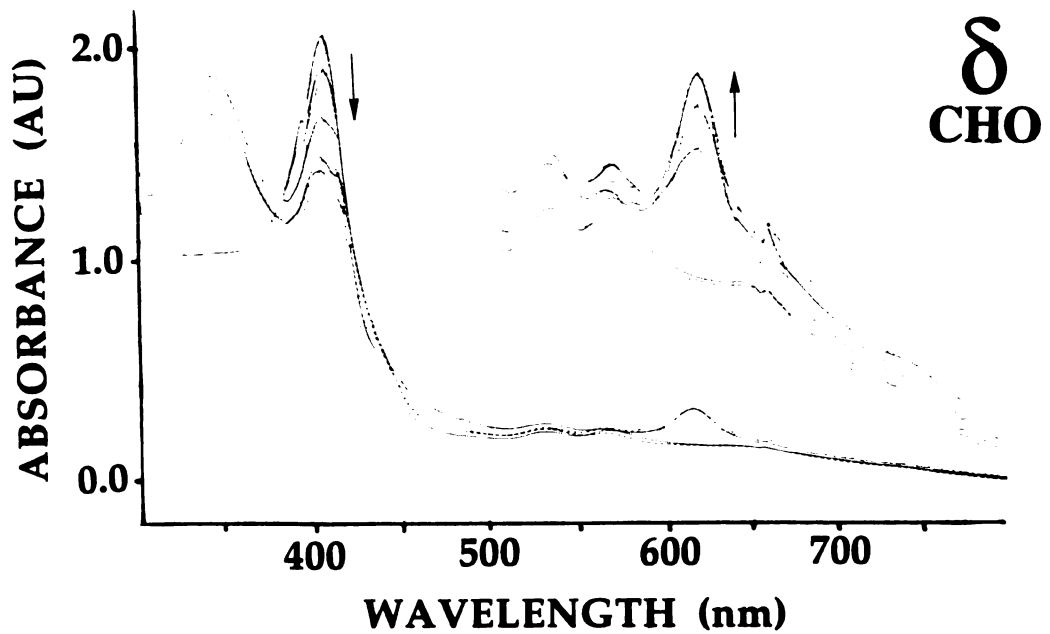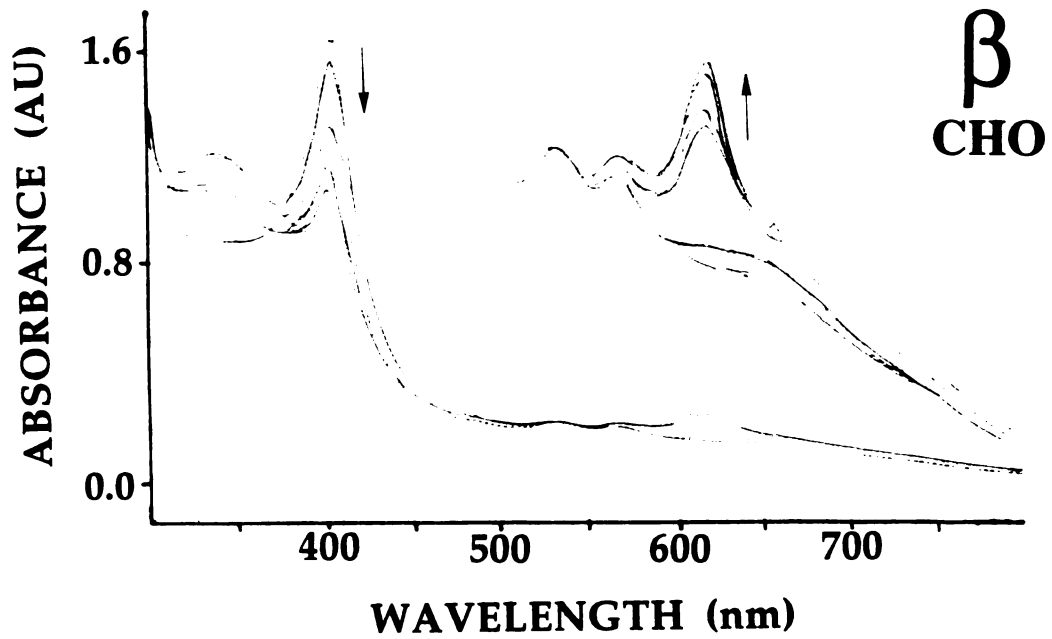
Formation of Fe(III)Mesoverdoheme with H₂O₂

Previous studies have shown that the oxidation of heme to verdoheme by hHO-1 can be supported by H_2O_2, although the conversion of verdoheme to biliverdin still requires P450 reductase and NADPH (Wilks & Ortiz de Montellano, 1993). It is not necessary to run this reaction in the presence of CO because no reducing equivalents are present and the end product is Fe(III)mesoverdoheme (Liu et al., 1997). The *meso*-methyl and *meso*-formyl substituted mesohemes have been incubated with H_2O_2 to determine if it also supports their conversion to mesoverdohemes. The progress of the reactions of the four isomeric *meso*-methylmesoheme-hHO-1 complexes with a 10-fold excess of H_2O_2 has been monitored spectrophotometrically (Figures 4.3.6 & 4.3.7). The earlier studies showed that the H_2O_2-dependent oxidation of heme to Fe(III)verdoheme results in decay of the Soret band and appearance of a broad absorption in the 600-700 nm range (Wilks & Ortiz de Montellano, 1993). In contrast, incubation of α-*meso*-methylmesoheme with hHO-1 and H_2O_2 results in a peroxide concentration-dependent decay of the Soret band without the appearance of the 600-700 nm absorption (Figure 4.3.6). The same spectroscopic change was observed if the excess of H_2O_2 was increased from 10- to 100-fold. Incubation of the γ-methyl isomer led to a similar time-dependent decrease in the Soret band, but in this instance a large increase is observed in the 600-700 nm region (Figure 4.3.6). Incubation of the β-methyl isomer with hHO-1 and H_2O_2 results in the time-dependent decay of the Soret band, but with very little change in the intensity of the visible region (Figure 4.3.7). However, incubation of the δ-methyl isomer with hHO-1 and H_2O_2 gives the spectroscopic changes expected for clean conversion of the substrate to an Fe(III)mesoverdoheme (Figure 4.3.7). Thus, the δ- and γ-isomers appear to be converted to Fe(III)mesoverdohemes of unknown regiochemistry in good yields, but the α- and β-isomers undergo heme degradation without the detectable formation, except for a trace in the case of the β-isomer, of mesoverdoheme-like species.

The reactions of the four *meso*-formylmesoheme-hHO-1 complexes with one equivalent of H_2O_2 are shown in Figures 4.3.8 & 4.3.9. The absorption spectra of all four reactions behave similarly: the Soret band decreases without a detectable shift while a broad increase in the visible region is observed in the 600-700 nm region. These changes signal hHO-1 catalyzed degradation of the *meso*-formylmesohemes to Fe(III)mesoverdoheme complexes by reaction with H_2O_2. Once again, the regiospecificity of each reaction is yet to be determined.
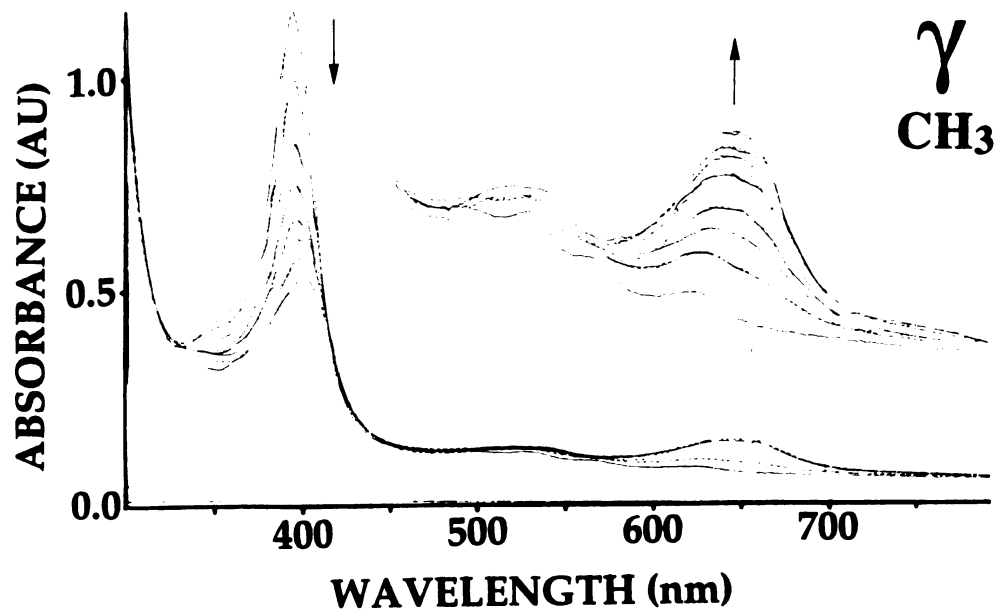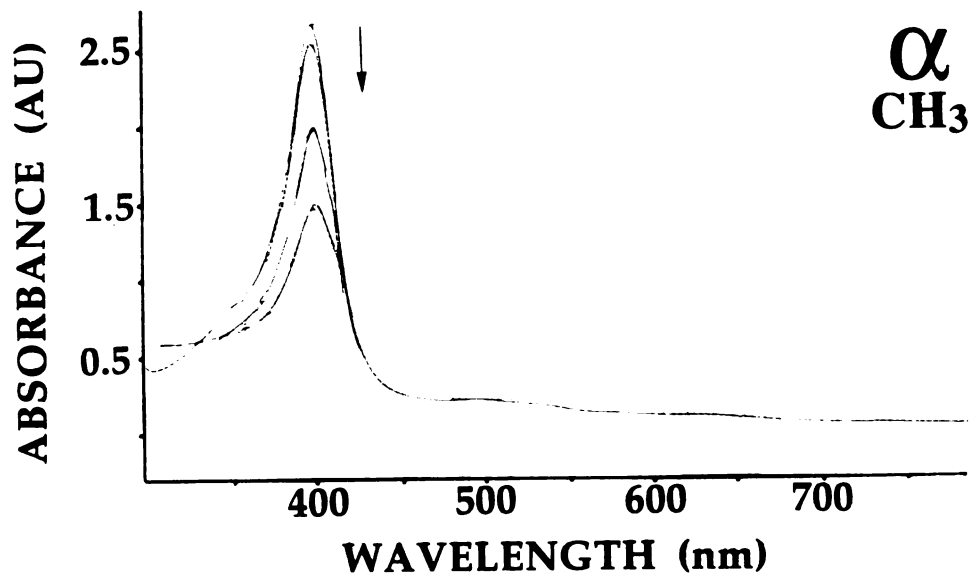
Figure 4.3.6. Spectrophotometric monitoring of the reactions of the α-meso-methylmesoheme-hHO-1 complex with H_2O_2 (2, 50, and 100 equivalents) and the γ-meso-methylmesoheme-hHO-1 complex with 10 equivalents of H_2O_2. Spectra were recorded at intervals of 10 s, the first spectrum being recorded before the addition of H_2O_2.

Figure 4.3.7. Spectrophotometric monitoring of the reactions of the β- and δ- *meso*-methylmesoheme-hHO-1 complexes with 10 equivalents of H_2O_2. Spectra were recorded at intervals of 10 s, the first spectrum being recorded before the addition of H_2O_2.

Figure 4.3.8. Spectrophotometric monitoring of the reactions of the α- and γ- meso-formylmesoheme-hHO-1 complexes with one equivalent of H_2O_2. Spectra were recorded at intervals of 10 s, the first spectrum being recorded before the addition of H_2O_2.
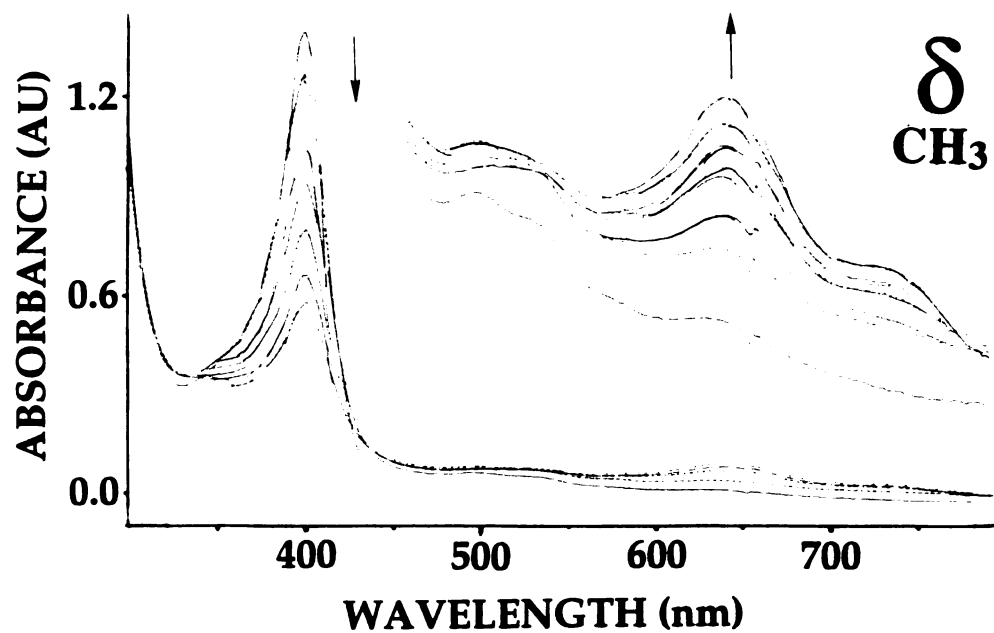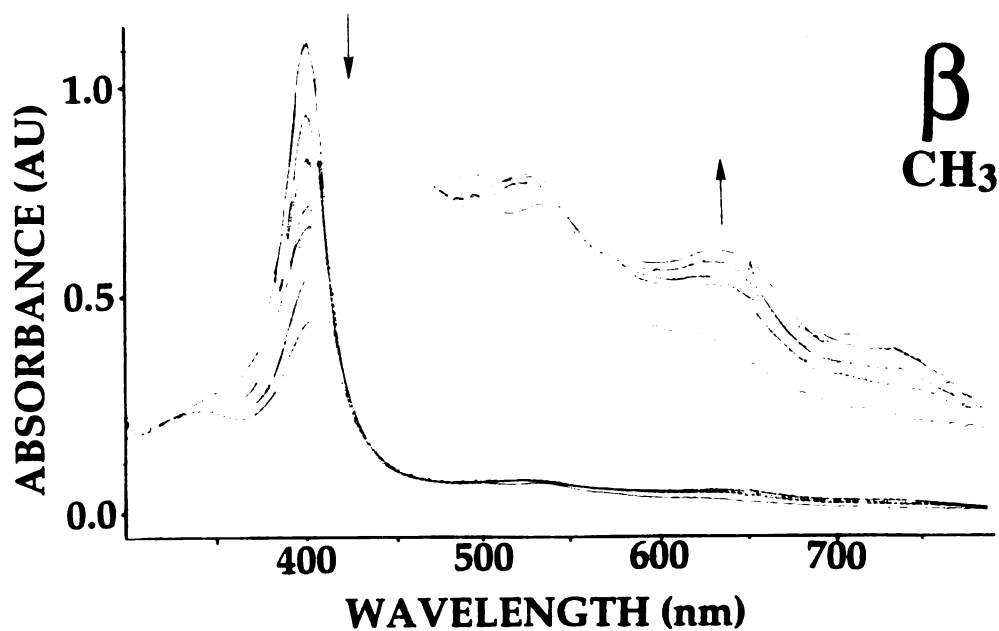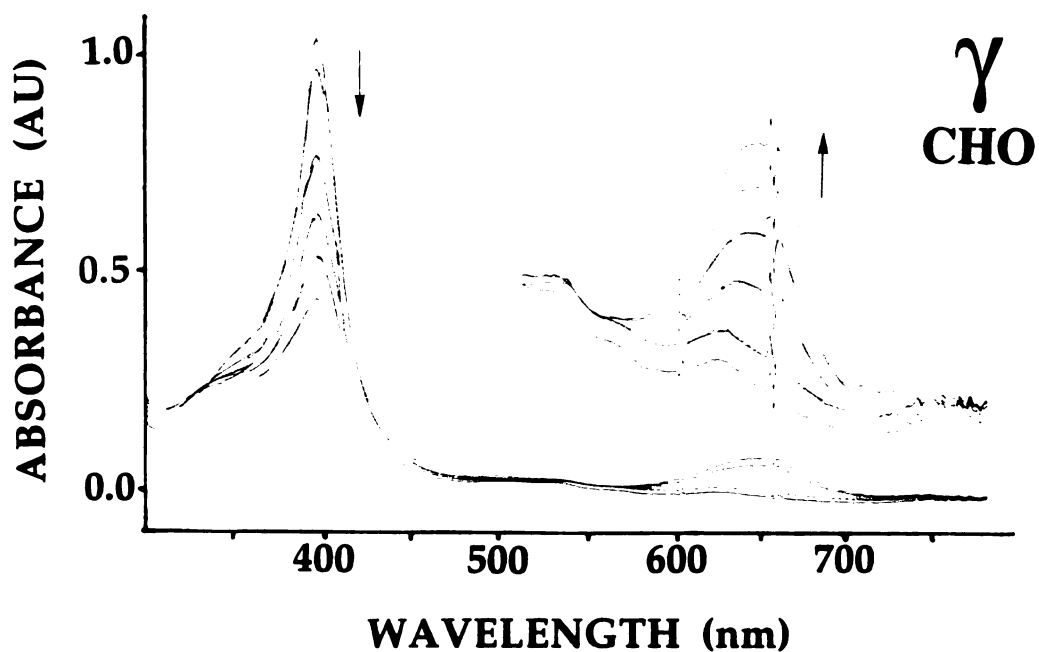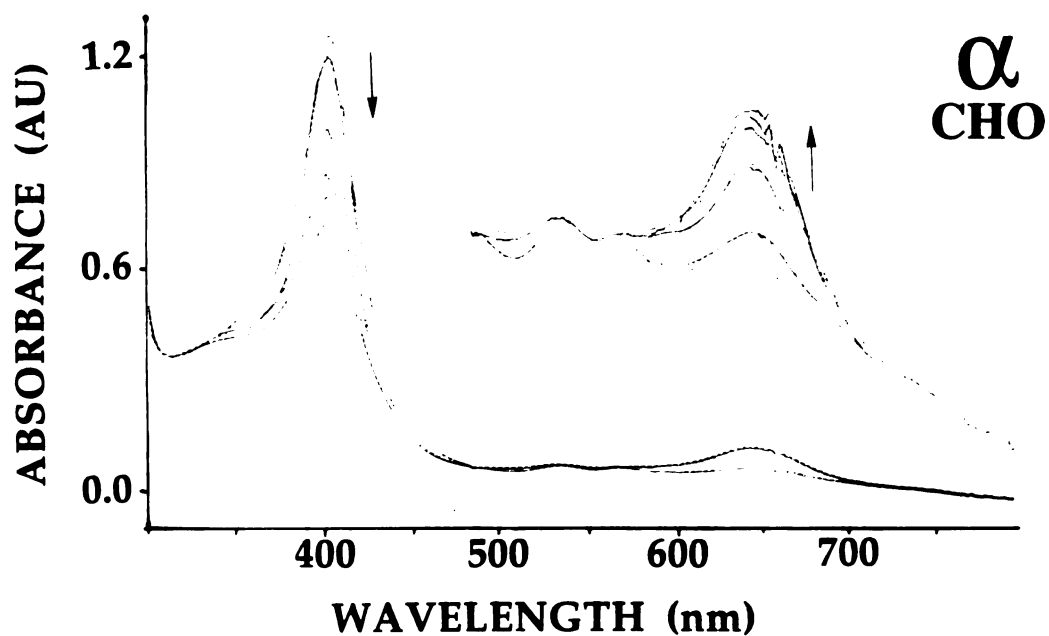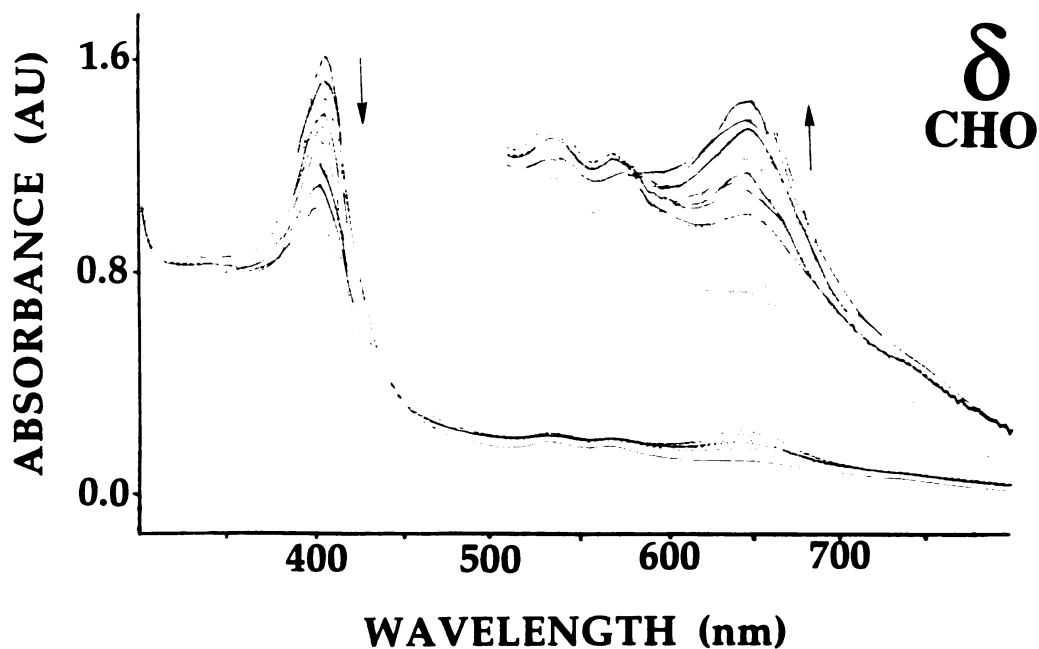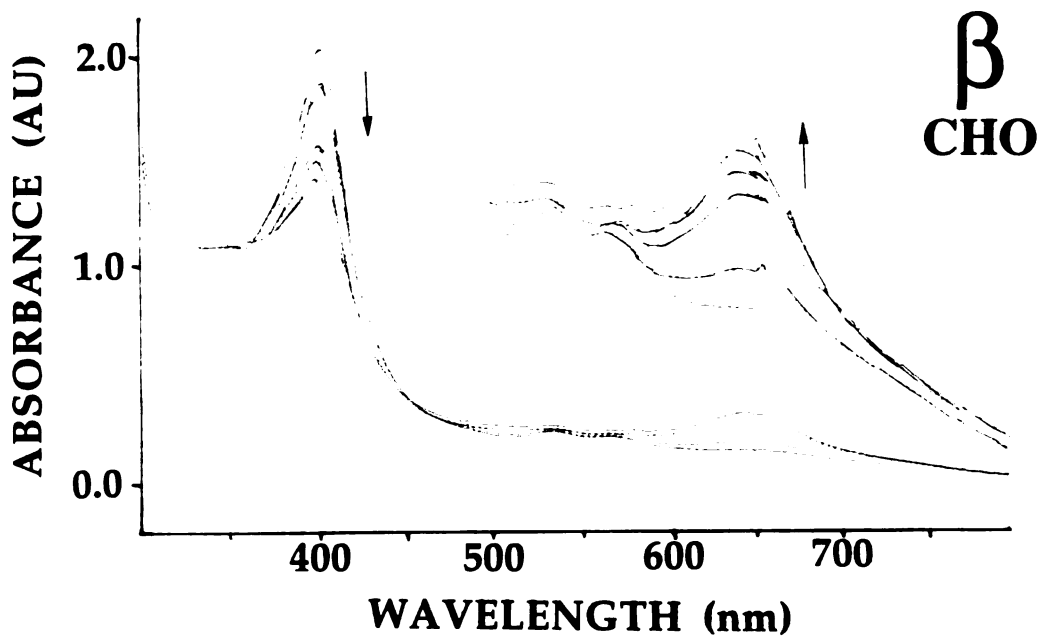
Figure 4.3.9. Spectrophotometric monitoring of the reactions of the β- and δ- *meso*-formylmesoheme-hHO-1 complexes with one equivalent of H_2O_2. Spectra were recorded at intervals of 10 s, the first spectrum being recorded before the addition of H_2O_2.

Regiochemistry of hHO-1-Catalyzed *Meso*-Methylmesoheme Oxidation

The regiospecificity of the oxidation of each of the *meso*-methylmesohemes by hHO-1 was examined with each of the three oxidizing systems: NADPH/P450 reductase, H_2O_2, and ascorbate. The incubations with NADPH and cytochrome P450 reductase were carried out in the absence of exogenous CO, and the Fe(III)mesoverdoheme-hHO-1 complexes obtained with H_2O_2 were incubated with NADPH and cytochrome P450 reductase prior to chromatographic analysis to convert the mesoverdohemes to mesobiliverdins. The products were analyzed by HPLC, absorption spectroscopy, and mass spectrometry. The HPLC system reliably separates the four biliverdin regioisomers derived from heme, and the methyl-substituted from the unsubstituted mesobiliverdins, but only partially separates the mesobiliverdin isomers from each other.

Oxidation of α-*meso*-methylmesoheme by both NADPH-cytochrome P450 reductase and ascorbate results in regiospecific oxidation of the α-*meso* position to give mesobiliverdin IXα (Figure 4.3.10), the product also obtained from mesoheme. The

Figure 4.3.10. HPLC chromatogram of the mesobiliverdin product extracted from the reaction of the α-*meso*-methyl-mesoheme-hHO-1 complex under coupled oxidation conditions (ascorbic acid). The HPLC peak is labeled with the mass spectrometric molecular ion determined for the material in that peak. The reaction that produces the indicated product is shown in the inset.

identity of this product is confirmed by the agreement of its absorption spectrum, HPLC retention time, and mass spectrum with that of authentic mesobiliverdin IXα (Table 4.3.1.). These results, but most particularly the absence of an extra methyl group in the mass spectrum, establish that the α-*meso* carbon and the appended methyl group have been eliminated. In contrast to the reactions supported by NADPH-P450 reductase or ascorbic acid, the H_2O_2-dependent oxidation of α-*meso*-methylmesoheme by hHO-1 results in degradation of the substrate but does not produce a spectroscopically detectable Fe(III)mesoverdoheme intermediate (Figure 4.3.6), or consequently a mesobiliverdin product.

The hHO-1-catalyzed oxidation of the γ-methyl isomer is well behaved. A single mesobiliverdin isomer (Figure 4.3.11) is obtained with all three oxidizing systems, including H_2O_2 (Table 4.3.1). Identification of this isomer as mesobiliverdin IXγ is based on its mesobiliverdin-like spectrum, an HPLC retention time similar to that of one of the isomers derived from mesoheme, and the mass spectrometric molecular ion *m/z* 586. This
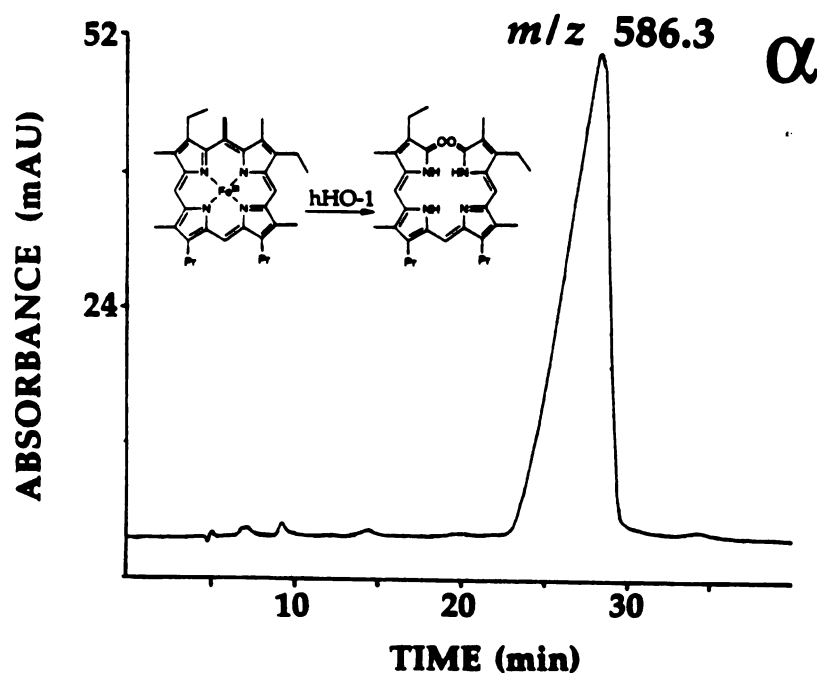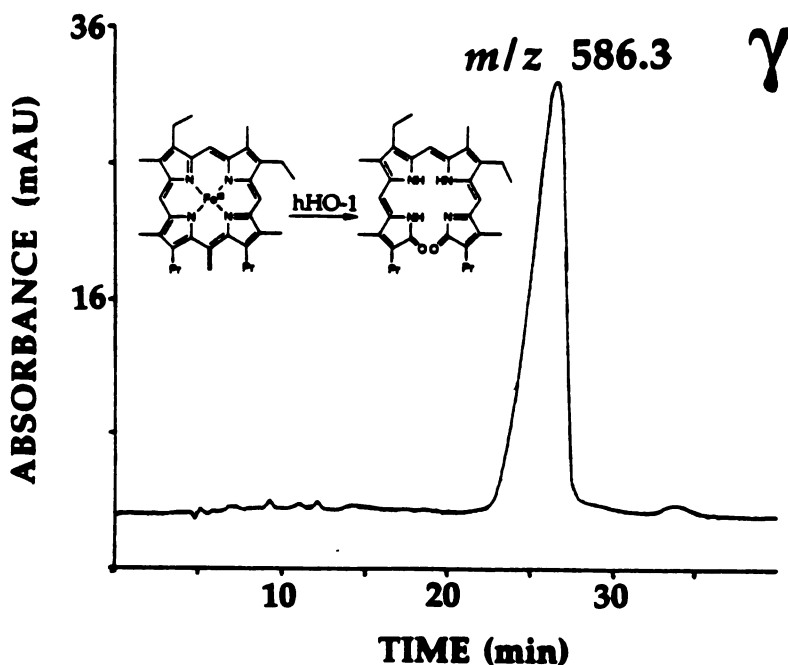

Figure 4.3.11. HPLC chromatogram of the mesobiliverdin product extracted from the reaction of the γ-*meso*-methyl-mesoheme-hHO-1 complex under coupled oxidation conditions (ascorbic acid). The HPLC peak is labeled with the mass spectrometric molecular ion determined for the material in that peak. The reaction that produces the indicated product is shown in the inset.

molecular ion is that of an unsubstituted mesobiliverdin. The hHO-1-catalyzed oxidation of γ-*meso* methyl mesoheme in all three oxidizing systems thus leads to elimination of the γ-*meso* carbon and the attached methyl group.

The hHO-1-catalyzed oxidation of the β- and δ-methyl isomers is more complicated than that of the α- or γ-isomers. The hHO-1-catalyzed oxidation of the δ-isomer supported by all three oxidizing systems produces a mixture of mesobiliverdin products (Figure 4.3.12, Table 4.3.1). The chromatographic resolution does not allow us to determine whether the product ratio is the same in the three systems. It is nevertheless clear from the mass spectrum that the reaction yields mesobiliverdin IXδ, in which δ-*meso*-carbon and methyl group have been eliminated, and at least two methyl-substituted mesobiliverdin isomers (Table 4.3.1). One of the partially resolved HPLC peaks has the molecular ion at

Figure 4.3.12. HPLC chromatogram of the mesobiliverdin products extracted from the reaction of the δ-*meso*-methylmesoheme-hHO-1 complex under coupled oxidation conditions (ascorbic acid). The HPLC peaks are labeled with the mass spectrometric molecular ion determined for the material in that peak. The reaction that produces the indicated product is shown in the inset. It is assumed but not proven that the two isomers that retain the methyl group come from oxidation at the α- and γ-positions (as shown).

86

m/z 586 of an unsubstituted mesobiliverdin and is thus mesobiliverdin IXδ. The other peak, which consists of at least two isomers, has a molecular ion at *m/z* 600 and thus corresponds to a mixture of two methyl-substituted mesobiliverdin isomers. The hHO-1 catalyzed oxidation of the β-methyl isomer supported by all three oxidizing systems results in rapid degradation of the heme chromophore but gives mesobiliverdin products in amounts too small for mass spectrometric characterization.

	Absorption spectrum of product(s) (CH$_3$OH)	NADPH-P450 reductase	H$_2$O$_2$[a]	ascorbate
	nm	*m/z*	*m/z*	*m/z*
α-methyl	366, 636	586	NR[b]	586
β-methyl	NR[b]	NR[b]	NR[b]	NR[b]
γ-methyl	366, 650	586	586	586
δ-methyl	322, 358, 570	600	600	600
	366, 610	586	586	586
α-formyl	364, 640	ND[c]	NA[d]	NA[d]
β-formyl	366, 650	ND[c]	NA[d]	NA[d]
γ-formyl	NR[b]	NR[b]	NA[d]	NA[d]
δ-formyl	366, 635, 680	ND[c]	NA[d]	NA[d]

Table 4.3.1. Absorption spectra amd molecular ions of the products from hHO-1-catalyzed oxidation of *meso*-substituted mesoheme isomers supported by different oxidizing agents.

[a]After further reaction of the H$_2$O$_2$ product with NADPH and cytochrome P450 reductase.
[b]NR indicates reaction gives insufficient mesobiliverdin isomers for definitive characterization.
[c]ND indicates that the molecular ion was not detected.
[d]NA indicates that the experiment was not carried out.

Regiochemistry of hHO-1-Catalyzed *Meso*-Formylmesoheme Oxidation

Regiospecific analysis of the *meso*-methyl products using three different oxidants revealed that the regiospecificity of oxidation by heme oxygenase is independent of the type of oxidant used. Therefore, the regiospecificity of the oxidation of each of the *meso*-formylmesohemes by hHO-1 was only examined with one of the three oxidizing systems: NADPH-cytochrome P450 reductase. Figures 4.3.13-4.3.16 show the HPLC analyses of

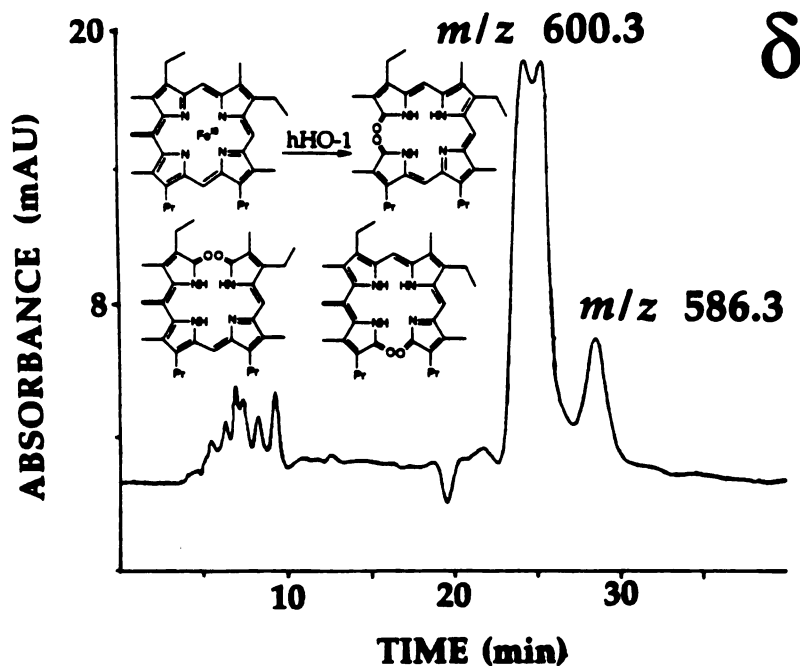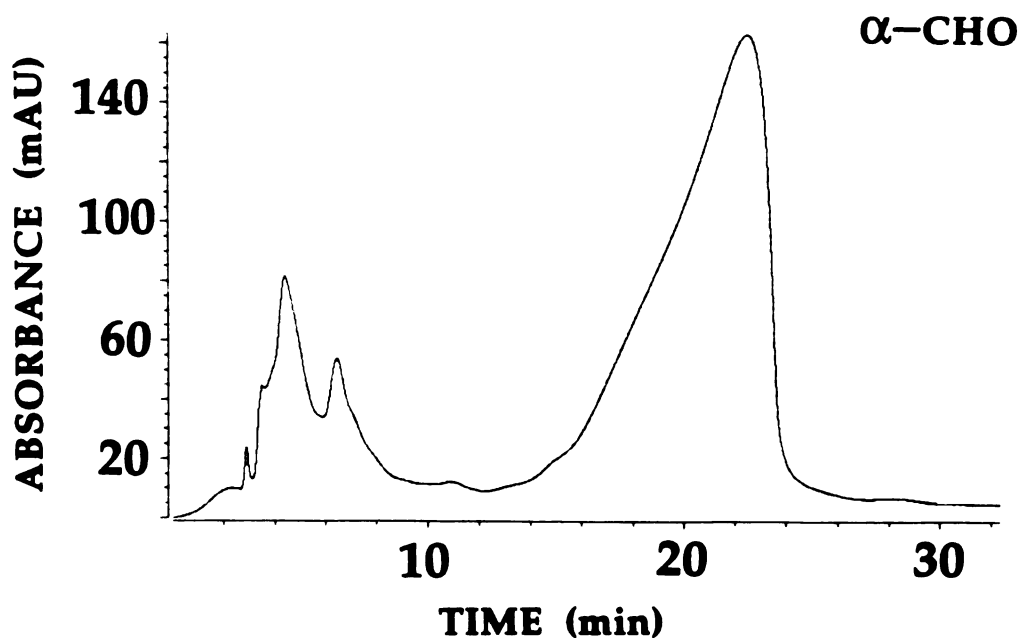

Figure 4.3.13. HPLC chromatogram of the mesobiliverdin product extracted from the reaction of the α-*meso*-formylmesoheme-hHO-1 complex using NADPH-cytochrome P450 reductase.

the reaction products of hHO-1 and the *meso*-formyl isomers with NADPH and cytochrome P450 reductase. The peak eluting earliest is presumed to be oxidized NADP+ which also absorbs at strongly at 364 nm. Each reaction appears to yield only a single regioisomer, but it is unknown whether a mixture of regioisomeric mesobiliverdins would separate in this HPLC system. The purified mesobiliverdin peaks were collected off the HPLC and their UV-visible spectra recorded (Table 4.3.1). Following formation of the dimethylesters, the isomers were subjected to mass spectrometric analysis by (+) LSIMS. Although no parent ions were detected after many attempts, the product obtained from the scaled-up reaction of the α-*meso*-formylmesoheme-hHO-1 complex gave a mass fragment

88

of m/z 273 using electron impact mass spectrometry (Figure 4.3.17).
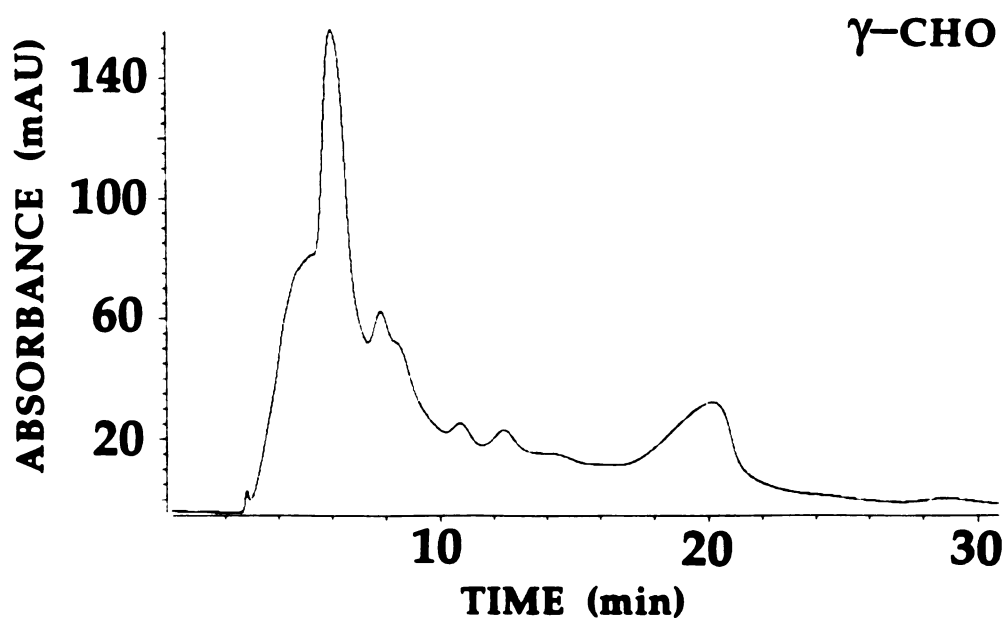
Figure 4.3.14. HPLC chromatogram of the mesobiliverdin product extracted from the reaction of the γ-*meso*-formylmesoheme-hHO-1 complex using NADPH-cytochrome P450 reductase.

Figure 4.3.15. HPLC chromatogram of the mesobiliverdin product extracted from the reaction of the β-*meso*-formylmesoheme-hHO-1 complex using NADPH-cytochrome P450 reductase.
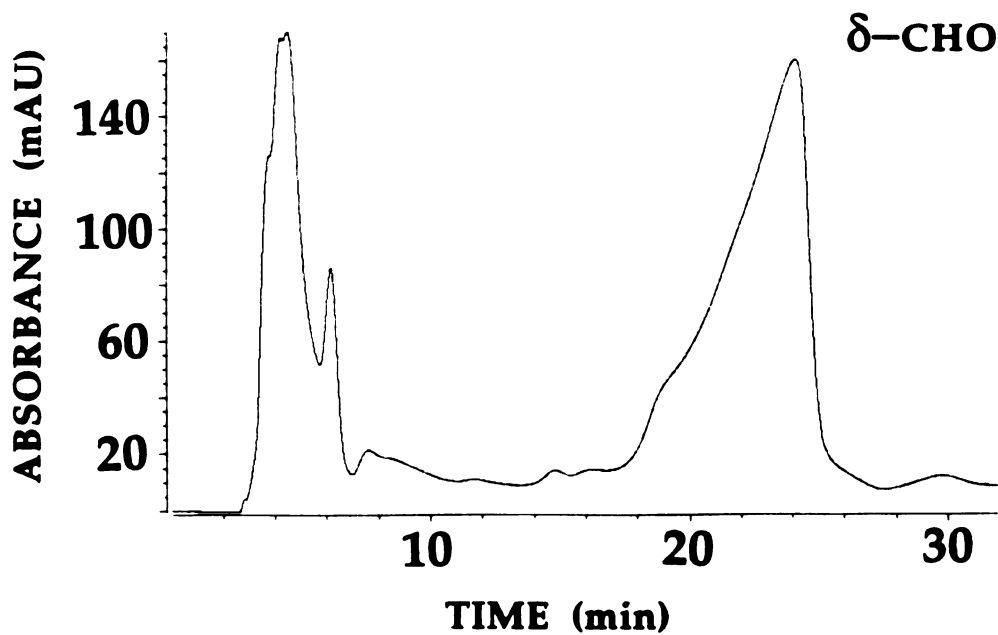
Figure 4.3.16. HPLC chromatogram of the mesobiliverdin product extracted from the reaction of the δ-*meso*-formylmesoheme-hHO-1 complex using NADPH-cytochrome P450 reductase.

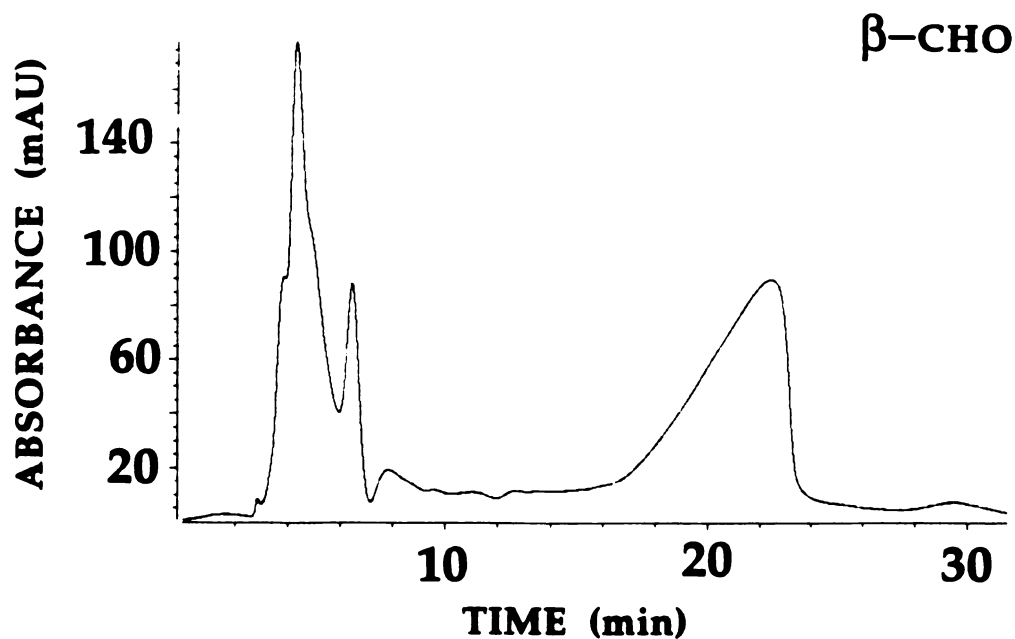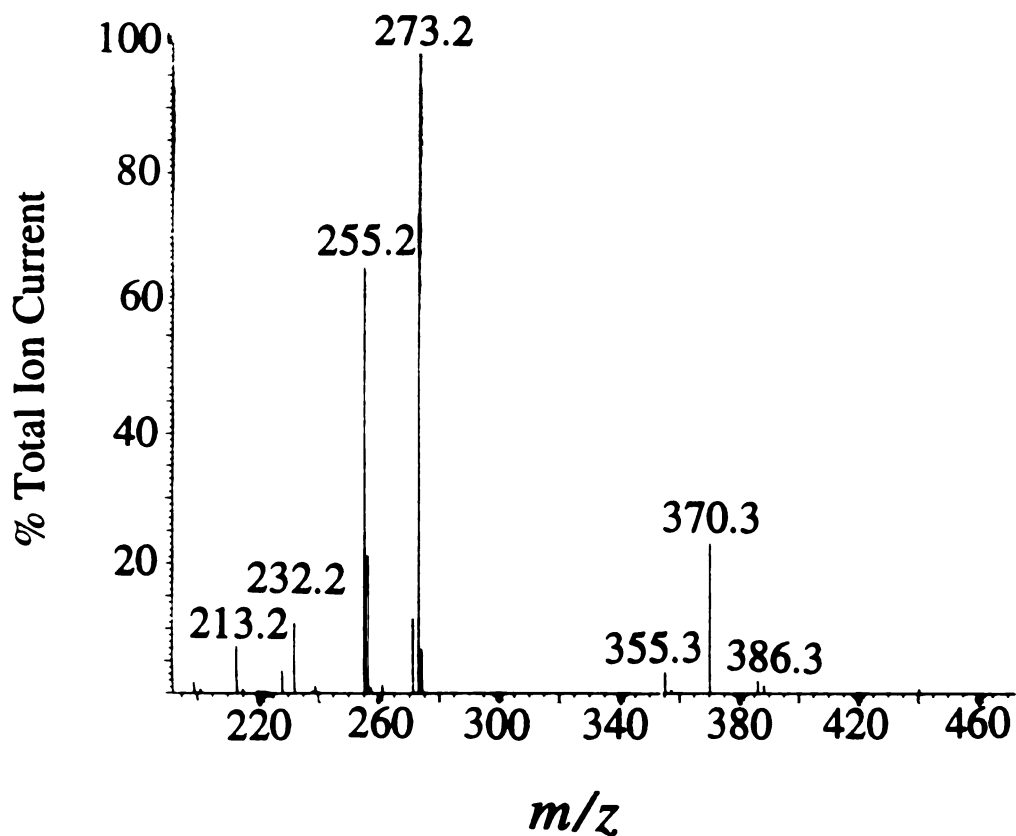Figure 4.3.17. Mass spectrometric fragments generated by electron impact ionization (225 °C) of the mesobiliverdin product of the reaction of the α-*meso*-formylmesoheme-hHO-1 complex with cytochrome P450 reductase and NADPH. (100% of Total Ion Current = 1.92 x 10⁶)

CO Formation

An assay based on the affinity of ferrous deoxymyoglobin for CO was used to detect the formation of CO in the NADPH/P450 reductase-supported reactions of hHO-1 with mesoheme and α-*meso*-methylmesoheme. The assay is based on the shift of the Soret maximum of ferrous deoxymyoglobin (λ_{max} 434 nm) on complexation with CO (λ_{max} 422 nm). Addition of deoxymyoglobin (Figure 4.3.18, trace a) to the mesoheme-hHO-1 reaction mixture after completion of the reaction resulted in immediate formation of the ferrous myoglobin-CO complex (Figure 4.3.18, trace b) accompanied by visible bands at 540 and 580 nm. No detectable shift of the deoxymyoglobin Soret maximum was observed
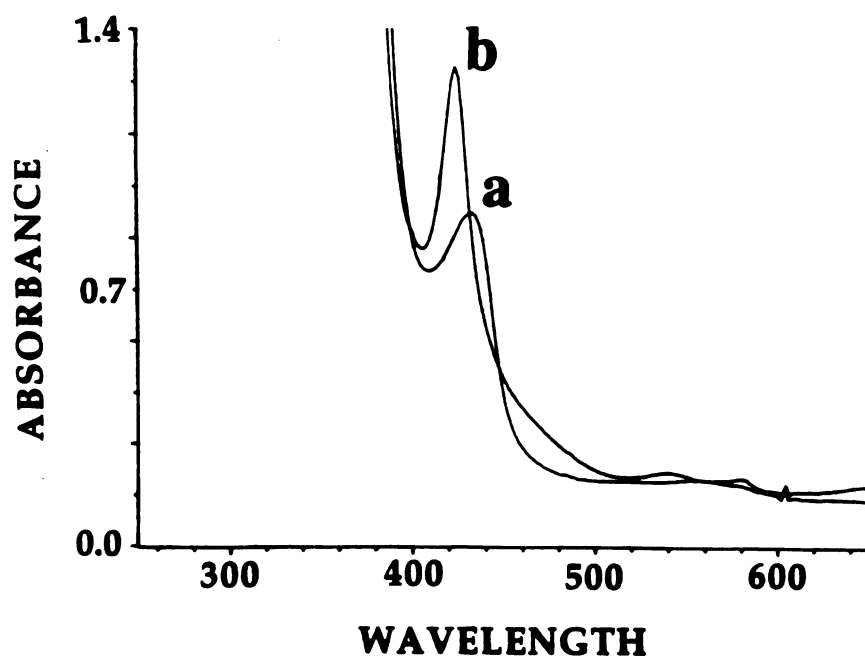
Figure 4.3.18. Assay for the formation of CO in the hHO-1 reactions by inclusion of ferrous deoxymyoglobin as a CO-trap. The spectra are shown of ferrous deoxymyoglobin before (a) and after (b) addition of the mesoheme-hHO-1 complex reaction mixture following completion of the reaction with NADPH-P450 reductase. The spectra obtained from the corresponding reactions with α- and γ-*meso*-methylmesohemes are indistinguishable from spectrum (a), indicating the absence of detectable CO in either reaction.

when the identical experiment was carried out with the α-*meso*-methylmesoheme-hHO-1 complex (not shown). The same result was obtained with the γ-methyl isomer. Thus, CO is not detectably formed in the reactions of the α- and γ-isomers under conditions where it is easily detected in the corresponding reaction with mesoheme. In contrast to the results of

CO assays of the reactions of hHO-1 with the α- and γ-*meso* methyl isomers, the *meso*-formyl isomers all gave qualitatively positive results for the production of CO upon hHO-1 catalyzed oxidation. Production of CO was quantitated for the α- and δ-formyl isomers by use of 0.9 molar equivalents of ferrous deoxymyoglobin and determination that the assay produced a clean shift to 422 nm as expected for the Soret band of the ferrous carbonmonoxy myoglobin complex.

Acetaldehyde Assay

An assay for the detection and quantitation of acetaldehyde in aqueous buffer was developed using Brady's reagent (2,4-DNP). A standard curve was constructed by integration of HPLC peaks to demonstrate the limit of detection and linearity of the response. The unreacted 2,4-DNP has an HPLC retention time of 4.8 min and the acetaldehyde dinitrophenylhydrazone derivative has an HPLC retention time of 7.1 min.
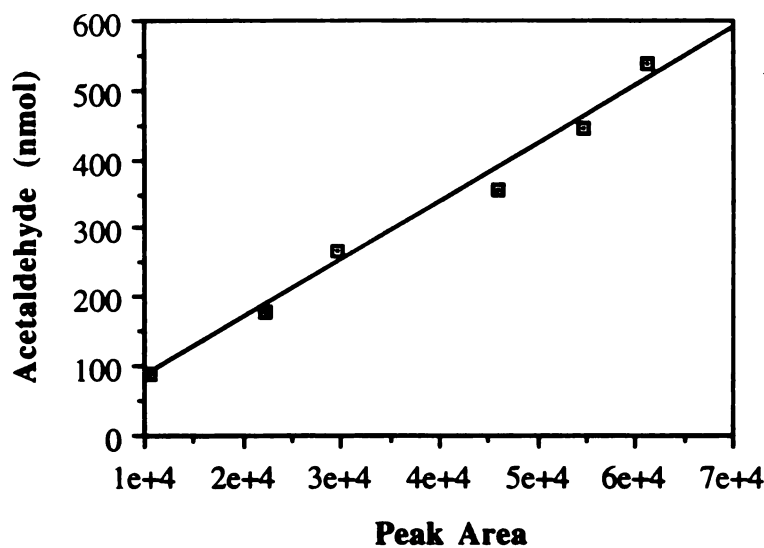
Figure 4.3.19. Standard curve of the acetaldehyde assay as described under Experimental Procedures.

The limit of detection was shown to be about 36 nmol and the response curve was linear through 500 nmol (Figure 4.3.19). The α-*meso*-methylmesoheme-hHO-1 complex (357 nmol) was turned over using ascorbate and assayed as described yielding only 47 nmol of acetaldehyde from the α-methyl reaction.

Acetic Acid Assay

The assay for detection and quantitation acetic acid is based primarily on the work of Li et al. (1995). This assay relies on the nucleophilic attack of acetate anion on 2,4'-dibromoacetophenone to displace the 4'-bromine ion. A standard curve was again constructed to demonstrate the limit of detection and linearity of the response. Gas chromatography was employed to quantitate derivatized acetate. Unreacted 2,4'-
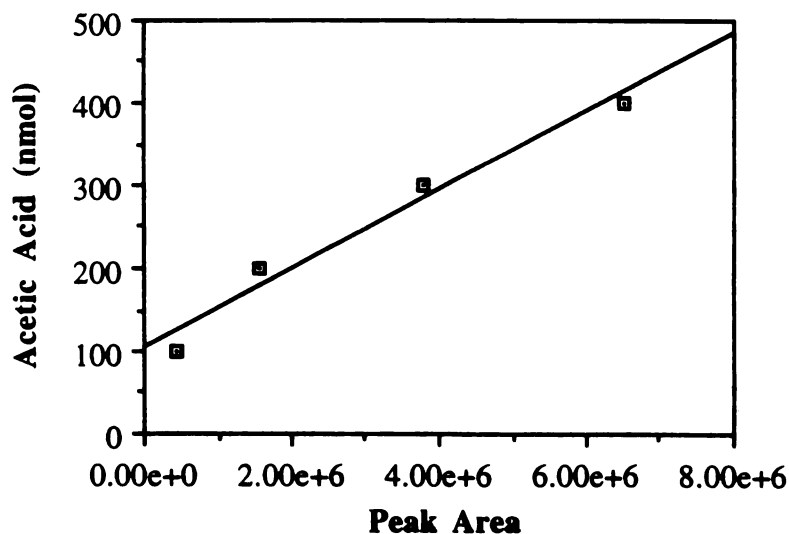
Figure 4.3.20. Standard curve of the acetic acid assay as described under Experimental Procedures.

dibromoacetophenone had a GC retention time of 16.8 min whereas the derivatized product had a GC retention time of 17.7 min. The limit of detection was shown to be about 100 nmol and the response curve was linear through 400 nmol (Figure 4.3.20). The α-meso-methylmesoheme-hHO-1 complex (321 nmol) was turned over using ascorbate and assayed as described yielding absolutely no detectable amounts of acetic acid from the α-methyl reaction.

4.4 DISCUSSION

Coupled oxidation of a pyridine solution of the iron salt of PPIX results in production of a random mixture of regioisomeric verdohemes which can be hydrolyzed to the regioisomeric set of biliverdins. The biliverdin isomers are readily separated by the HPLC system described under General Methods. Since the substrates synthesized in

Chapter 3 are all of the mesoheme type (2,4-ethyls instead of vinyls), coupled oxidation of mesoheme was carried out to produce the corresponding mixture of mesobiliverdins. Unfortunately, this mixture did not resolve nearly as well as that of their vinyl-substituted cousins (Figure 4.3.1). Interestingly, no mesobiliverdin products were obtained from the coupled oxidation of any of the *meso*-methyl mesohemes free in solution. HPLC confirms that the *meso*-methyl mesohemes are destroyed in the process. As the reactions were only monitored for the production of mesobiliverdin products, the reason for this altered reactivity is unknown.

As shown in Chapter 2, heme oxygenase-catalyzed oxidation of α-*meso* methyl heme results in regiospecific attack at the α-*meso* position with concomitant removal of the α-*meso* carbon and the appended methyl group. In addition, the reaction appears to converge on the normal reaction pathway because it leads to the formation of verdoheme (see Figure 2.3.9). Coupled oxidation (without heme oxygenase) of the *meso*-methyl mesohemes was characterized by a color change to yellow instead of green. Furthermore, the yellow substances, unlike the green verdoheme intermediate, were not amenable to extraction. Thus, it appears that in the absence of heme oxygenase, the *meso*-methyl coupled oxidation does not produce a verdoheme intermediate. This implies that some property of heme oxygenase is required in the mechanism of *meso*-methyl oxidation and the subsequent removal of the *meso*-methyl group. It seems that no biliverdin products are obtained because, in the absence of heme oxygenase, the reaction intermediates cascade down an alternative pathway not involving verdoheme.

The reactions of the α-*meso*-methylmesoheme-hHO-1 complex exactly parallel the results found with the α-*meso*-methyl-1,2-dimethyl heme-hHO-1 complex studied in Chapter 2. Thus, reaction of the α-*meso*-methylmesoheme-hHO-1 complex with cytochrome P450 reductase and NADPH under a partial atmosphere of CO results in a time-dependent decay of the Soret band with a simultaneous appearance of a visible band (614 nm) signaling the formation of the Fe(II)-verdoheme-CO complex (Figure 4.3.2). Furthermore, the α-*meso* carbon and the appended methyl group are removed and the product of the reaction is mesobiliverdin IXα (Figure 4.3.10). The absence of CO (Figure 4.3.18) in this reaction is evidence that the reaction does not proceed by removal of the *meso*-methyl group followed by the normal catalytic pathway. This finding also excludes the possibility that hydroxyheme is an intermediate in the mechanism of *meso*-methyl oxidation. This implies that *meso*-methyl oxidation occurs by a distinct mechanism that probably involves oxygen transfer to the α-*meso* position but that does not converge on the

hydroxyheme intermediate *en route* to verdoheme.

Also in accordance with the results of Chapter 2, the reaction of the α-*meso*-methylmesoheme-hHO-1 complex with H_2O_2 did not result in production of the Fe(III)verdoheme complex obtained with methyl-unsubstituted hemes (Figure 4.3.6). The exact reason for this is not understood. It does not, however, appear to be a general phenomenon with *meso*-methyl substituted hemes. For example, the γ-methyl isomer reacts with H_2O_2 to give a large increase in the 600-700 nm region indicating formation of an Fe(III)verdoheme intermediate. The inability of the α-methyl isomer to react with peroxide to give a verdoheme intermediate may be analogous to the inability of the H132A mutant of heme oxygenase to utilize H_2O_2 to oxidize heme to verdoheme (Wilks et al., 1996). These investigators suggested that without the distal histidine, the distal-side hydrogen-bonding network is disrupted. This might explain the mutant enzyme's inability to activate hydrogen peroxide for catalysis. Such a disruption may occur for the α-*meso* methyl mesoheme due to an isomer-specific perturbation of important active site residues.

A major finding of this study is that the regiospecificity of the reaction can be redirected by *meso*-methyl substitution. The best illustration of this is provided by the results found for the γ-*meso*-methylmesoheme-hHO-1 complex. Whether reacting with NADPH-cytochrome P450 reductase, sodium acorbate, or H_2O_2, the regiospecificty of the reaction is redirected to the γ-*meso* position, producing mesobiliverdin IXγ, even in the presence of an unsubstituted α-*meso* position (Figure 4.3.11). No observation of a change in the regiospecificity of heme oxygenase-catalyzed oxidations has previously been reported. The inverted regiospecificity can be explained in the context of an electrophilic mechanism, with reaction taking place at the most electron-rich *meso*-carbon. This finding clearly contradicts the steric hindrance model for regiospecific control of heme catabolism and suggests that electronic effects play a dominant role.

Further support for this idea is found in the results obtained for the reaction of the δ-*meso* methyl mesoheme-hHO-1 complex. Reaction of the δ-methyl-hHO-1 complex with each of the three oxidants results in a mixture of methyl-substituted and methyl-unsubstituted mesobiliverdins (Figure 4.3.12). The production of a mixture of mesobiliverdins indicates that there is more than one factor controlling the regiospecificity of this reaction. The presence of methyl-substituted mesobiliverdins in the heme oxygenase-catalyzed oxidation of the δ-methyl isomer suggests that the protein exerts an influence that opposes the inherent reactivity of this particular methyl-substituted heme. Because the protein clearly exerts a preference for reaction at the α-position, this effect does

not oppose oxidation at the methyl-substituted α-*meso* carbon in the case of the α-*meso* methyl mesoheme-hHO-1 complex. Furthermore, as the γ-position is axially related to the α-position, the γ-*meso* carbon must share some electronic similarities with the α-*meso* carbon (see Figure 1.12.2a). Therefore, with a methyl substituent at the γ-*meso* position, the protein's preference does not override the preference for oxidation at the methyl-substituted site. However, with a methyl substituent at the δ-position, the preference for attack at the site of methyl substitution is in direct conflict with the protein's activation of the α/γ axis. The result is a mixture of methyl-substituted and unsubstituted mesobiliverdins (Figure 4.3.12). It is also evident that the small electron donating effect of a methyl group is not strong enough to completely overcome the protein's preference for oxidation along the α/γ axis.

The reactivity of the β-*meso*-methylmesoheme-hHO-1 complex, for unknown reasons, is distinct from that of the other *meso*-methyl regioisomers. Figures 4.3.3 and 4.3.7 show the reactions of the β-methyl-hHO-1 complex with NADPH-cytochrome P450 reductase and H_2O_2, respectively. Both reactions show a time-dependent decay of the Soret band with only slight changes in the visible region. Work-up of the reactions to obtain mesobiliverdin products confirms that, while the heme is efficiently degraded, very little mesobiliverdin product is obtained. The results appear similar to the case of coupled oxidation of free *meso*-methyl mesohemes in aqueous pyridine. The heme is destroyed, and apparently a separate reaction pathway is followed in the absence of an unkown factor related to heme oxygenase. It is possible that the β-position is inaccessible to the essential catalytic machinery required for *meso*-methyl oxidation or that a steric effect blocks β-hydroxylation.

The differences in the reactivities of the β- and δ-isomers are curious. Hernández et al. (1994) demonstrated that the heme molecule can flip 180° about the α/γ axis in the enzyme active site resulting in heterogeneity of substrate binding. This can render the δ- and β- positions essentially indistinguishable. However, the δ- and β-*meso* methyl substituted positions are distinguishable empirically by the fact that the δ-isomer reacts to give mesobiliverdin products whereas the β-isomer does not. Further examination of the ^{1}H NMR data provided by Hernández et al. suggests that the two heme orientations may not be catalytically equivalent. They reported that the unique contact shift pattern resulting in the activation of the α-*meso* position is present to different degrees for the two heme orientations. The difference in activity of the methyl-substituted δ- and β- positions supports the idea that the two heme orientations may not have equivalent catalytic

properties.

The inability to detect CO as a product of the heme oxygenase catalyzed oxidations of α- and γ-meso-methylmesoheme suggests that the methyl group is not first excised from the porphyrin macrocycle followed by the normal catalytic pathway. Assuming that the meso-carbon and the attached methyl carbon are not separated during the catalytic process, the two most likely products derived from the excised fragment would be acetaldehyde and acetic acid. Both of these products assume that the meso-methyl itself undergoes no oxidation. However, both acetic acid and acetaldehyde are ruled out as the metabolites produced by the heme oxygenase-catalyzed oxidation of the α- and γ-meso methyl mesohemes. The methods employed to detect and quantitate acetaldehyde and acetic acid would also be expected to find further oxidized products, such as hydroxy-acetic acid or hydroxy-acetaldehyde, but no such products were observed.

The possibility must be considered that the two-carbon piece remains attached to the biliverdin product and the mass spectra indicating its absence are artifactual. However, Brown et al. (1980) reported the mass spectra of the photooxidation products of meso-methyl substituted porphyrin and chlorin macrocycles. Specifically, they photooxidized Zn(II) meso-methyl octaethylporphyrin in the presence of either $^{16,16}O_2$ or $^{18,18}O_2$ and showed that the the mass spectrum of the ^{18}O labeling experiment was consistent with a One-Molecule Mechanism. The product of the reaction is an 8-acetylbilitriene (Figure 4.4.1), the molecular ion of which was detected without difficulty using electron impact ionization. This mass spectrum demonstrates that if an acetyl group is attached to the macrocycle, one would expect to detect it. This precedent supports the validity of the mass spectrometric data on the meso-methyl oxidation products. Therefore, the piece is not still attached to the product, and furthermore it is not released as acetic acid, acetaldehyde, or oxidized derivatives thereof. The most likely fate for the piece appears to be that it is cleaved off the porphyrin macrocycle as a highly reactive intermediate that covalently binds to an active site residue. A hypothetical mechanism for this reaction is shown in Figure 4.4.2. The iron-peroxo complex (1) is formed by two-electron reduction of molecular oxygen bound to the heme and reacts by electrophilic attack as described in Chapter 2. Structure (2) shows the formal tertiary carbocation and tetrahedral meso carbon likely to be formed. The cation can be stabilized by the resonance structure (3), or possibly by addition of a protein nucleophile (4). If the meso-methyl group were a proton it is assumed that the proton would eliminate forming iron(III) hydroxyheme (not shown). However, the methyl is essentially stuck, which is likely to leave the complex susceptible

to another round of oxidation by reduced molecular oxygen. Binding of reduced molecular oxygen to the site of the formal tertiary carbocation as well as to the heme iron (6) followed by a series of hypothetical homolytic cleavages (6), (7), (8), and (9) results in formation of iron(III) verdoheme (10) and (12), and a hypothetical carbene (11). If the proposed oxidation state of the *meso*-methyl piece (11) is correct, reaction with a proton from the solvent would yield acetaldehyde (13). However, acetaldehyde has been ruled out as a possible reaction product. If acetaldehyde were to form a Schiff base with a lysine residue, the control experiments indicate it would be recovered as the 2,4-dinitrophenyl hydrazone. If the highly reactive intermediate (11) existed and first reacted with an active-site residue such as histidine, one can propose a mechanism whereby the piece is covalently attached to the protein resulting in structure (15), for example.
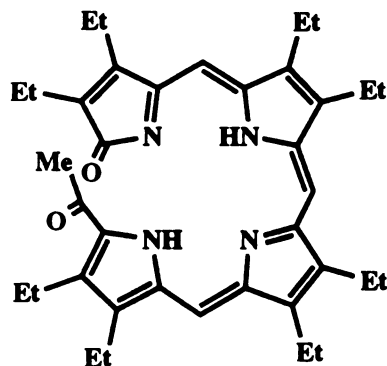

Figure 4.4.1. The 8-acetylbilitriene obtained from the photooxidation of zinc(II) octaethylporphyrin has a molecular ion of m/z 580 which is detected using electron impact ionization at 205 °C (Brown et al., 1980).

Figure 4.4.2. Hypothetical mechanism for hHO-1-catalyzed *meso*-methyl oxidation.

Reaction of the *meso*-formyl mesoheme-hHO-1 complexes provides data complementary to that for the *meso*-methylmesohemes. All four *meso*-formyl-hHO-1 complexes undergo NADPH-cytochrome P450 reductase supported oxidation in the presence of CO to form Fe(II)verdoheme-CO complexes (Figures 4.3.4 & 4.3.5). In addition, all four *meso*-formyl-hHO-1 complexes undergo H_2O_2 supported oxidation to form Fe(III)verdoheme complexes (Figures 4.3.8 & 4.3.9). These data mean simply that the four *meso*-formyl regioisomers are efficient substrates for heme oxygenase using both NADPH-cytochrome P450 reductase and H_2O_2. Extraction and HPLC analysis of the products of the reactions of the *meso*-formyl-hHO-1 complexes with NADPH-cytochrome P450 reductase shows that for each reaction only one mesobiliverdin regioisomer is produced (Figures 4.3.13-4.3.16). The detection in each instance of carbon monoxide as a reaction product demonstrates that the site of cleavage is a *meso*-carbon other than the *meso*-formyl substituted one, and thus the mesobiliverdin regioisomers must be *meso*-formyl subtituted. For the α- and δ-formyl isomers CO production was quantitated to be at least 90% of the theoretical maximum. The finding that hHO-1-catalyzed *meso*-formylmesoheme oxidation occurs exclusively at the non-formyl-substituted *meso*-positions is in contrast to the γ- and α-*meso*-methyl isomers, which are oxidized exclusively at the methyl-substituted *meso*-positions. The finding that the methyl and formyl groups channel the reaction regiospecificity in opposite directions indicates that the regiospecificity is primarily under electronic rather than steric control.

Mass spectrometric data for the set of *meso*-formyl mesobiliverdins was uninformative. Despite repeated efforts, no parent ions were detected. The absence of a molecular ion for the *meso*-formyl mesobiliverdins is indirect evidence that the molecules retain the *meso*-formyl substituent. Unlike the mesobiliverdins obtained from the *meso*-formylmesoheme reactions, which were converted to the dimethylesters to enhance volatility, the *meso*-methyl-substituted and -unsubstituted mesobiliverdins all gave satisfactory parent ions as the free acids even though obtained in comparable yields (~100 µg). Therefore, the absence of a molecular ion for any of the *meso*-formylmesoheme-hHO-1 oxidation products is presumably due to the presence of the meso-formyl group. Similar difficulty in obtaining mass spectrometric data on the synthetic *meso*-formyl MSPR-DME regioisomers was also experienced. In this case the obstacle was hurdled by the availability of milligram quantities of porphyrin for analysis. The reaction of the α-*meso*-formylmesoheme-hHO-1 complex was therefore scaled up using 80 mgs of recombinant heme oxygenase and producing ~1.0 mg of purified mesobiliverdin product . While this product still gave no molecular ion, fragments were obtained by electron impact

mass spectrometry (Figure 4.3.17) consistent with fragmentation patterns previously observed in the biliverdin IX series (Bonnett & McDonagh, 1973). Specfically, the individually purified biliverdin IX isomers were subjected to electron impact mass spectrometric analysis and it was found that in addition to giving the correct molecular ion, the isomers consistently fragmented at the *meso*-edge directly opposite the site of oxidation. Thus biliverdin IXα fragmented in half by cleavage at the γ-position. This data was used to determine the axis of cleavage, distinguishing biliverdin IXα from biliverdin IXδ, but not biliverdin IXα from biliverdin IXγ. The major mass spectrometric fragment of the α-*meso*-formyl mesobiliverdin dimethylester (*m/z* 273) (Figure 4.3.17) is consistent with a formyl-substituted mesobiliverdin. This data also indicates that hHO-1 catalyzed oxidation occurs along the β/δ axis, the same axis as that of the cleavage pattern observed in the mass spectrum (Figure 4.4.3). As opposed to the α-methyl reaction which reacts
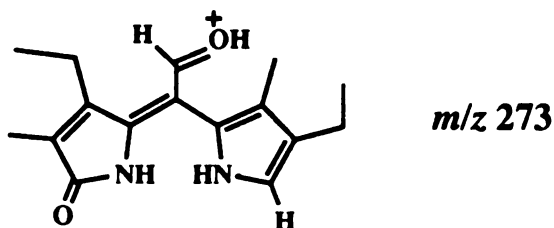

m/z 273

Figure 4.4.3. Mass fragment obtained by electron impact ionization of the mesobiliverdin product of the reaction of the α-*meso*-formylmesoheme-hHO-1 complex with cytochrome P450 reductase and NADPH.

exclusively at the site of *meso*-substitution, the α-formyl reaction results in cleavage at a *meso*-position adjacent to that of the formyl-substituted one. These results demonstrate that *meso*-substituents with opposite electronic properties have opposite effects on the regiospecificity of the reaction. This type of control over the reaction regiospecificity is compelling evidence that the reaction regiospecficity is controlled mainly by electronic factors.

The *meso*-substituted mesohemes synthesized in Chapter 3 were each reconstituted with heme oxygenase to form 1:1 complexes that resemble hemoproteins with respect to their spectroscopic properties. As described earlier, the experiments that followed can be described as a site-directed mutagenesis of the substrate-cofactor as a study of electronic control of the reaction regiospecificity. Each *meso*-methylmesoheme was assayed for activity using three different oxidants (H_2O_2, NADPH-cytochrome P450 reductase, and

ascorbate) and monitored spectroscopically for the formation of verdoheme intermediates. Furthermore, the regioselectivity of each reaction was evaluated by HPLC, UV-visible absorption spectroscopy, and mass spectrometry. The findings indicate that the regiospecificity of the hHO-1-catalyzed oxidation of heme is controlled primarily by electronic factors. The findings that the *meso*-methyl group and *meso*-carbon are not converted to carbon monoxide, acetic acid, or acetaldehyde, and do not remain attached to the mesobiliverdin product, suggest that the two carbons may have been excised as a highly reactive species, such as a carbene, that is covalently bound to one or more active-site residues. In addition, the synthetic *meso*-formylmesoheme regioisomers were assayed for activity using NADPH-cytochrome P450 reductase and monitored spectroscopically for the formation of verdoheme intermediates. The products of each reaction were analyzed by HPLC and UV-visible absorption spectroscopy. While mass spectrometric analysis of the products gave no molecular ions, fragments were obtained for the α-*meso*-formylmesoheme product using electron impact mass spectrometry. The finding that hHO-1-catalyzed oxidation of α-*meso*-formylmesoheme occurs at a site adjacent to the *meso*-substituent supports the idea that the reaction regiospecifiity is under electronic rather than steric control. While there may still be a steric component controlling enzyme regiospecificity, the results clearly show that whatever effect the protein exerts can be attenuated by the inherent electronic properties of the heme. Additionally, the observed control of the reaction regiospecificity by the opposite electronic effects of the *meso*-methyl and *meso*-formyl hemes provides further experimental support for an electrophilic mechanism for hHO-1-catalyzed heme hydroxylation.

REFERENCES

Ator, M. A., David, S. K., Ortiz de Montellano, P. R. (1989) *J. Biol. Chem.* **264**, 9250-9257.

Balch, A. L., Lechoslaw, L. G., Noll, B. C., Olmstead, M. M., Szterenberg, L., and Safari, N. (1993) *J. Am. Chem. Soc.* **115**, 1422-1429.

Balch, A. L., Mazzanti, M., and Olmstead, M. M. (1994) *J. Chem. Soc., Chem. Commun.* 269-270.

Balch, A. L., Mazzanti, M., St. Claire, T. N., and Olmstead, M. M. (1995) *Inorg. Chem* **34**, 2194-2200.

Bonnett, R., and Chaney, B. D. (1987) *J. Chem. Soc. Perkin Trans. I* 1063-1067.

Bonnett, R., and Dimsdale, M. J. (1968) *Tet. Lett.* 731-733.

Bonnett, R., and Dimsdale, M. J. (1972) *J. Chem. Soc. Perkin I* 2540-48.

Bonnett, R., and McDonagh, A. F. (1973) *J. Chem. Soc. Perkin Trans. I* 881-888.

Brown, S. B. (1976) *Biochem. J.* **159**, 23-27.

Brown, S. B., Chabot, A. A., Enderby, E. A., and North, A. C. T. (1981) *Nature* **289**, 93-95.

Brown, S. B., and Docherty, J. C. (1978) *Biochem J.* **173**, 985-987.

Brown, S. B., and King, R. F. G. J. (1975) *Biochem J.* **150**, 565-567.

Brown, S. B., and King, R. F. G. J. (1976) *Biochem. Soc. Trans.* **4**, 197-201.

Brown, S. B., and King, R. F. G. J. (1978) *Biochem J.* **170**, 297-311.

Brown, S. B., Smith, K. M., Bisset, G. M. F., and Troxler, R. F. (1980) *J. Biol. Chem.* **255**, 8063-8068.

Coburn, R. F., Williams, W. J., White, P., and Kahn, S. B. (1967) *J. Clin. Invest.* **46**, 346.

Cruse, I., and Maines, M. D. (1988) *J. Biol. Chem.* **263**, 3348-3353.

Dawson, J. H. (1988) *Science* **240**, 433-439.

Docherty, J. C., Schacter, B. A., Firneisz, G. D., and BRown, S. B. (1984) *J. Biol. Chem.* **259**, 13066-13069.

Fischer, H., and Orth, H. (1937) *Die Chemie des Pyrrols* (Leipzig: Akademische Verlagsgesell-schaft) p. 409.

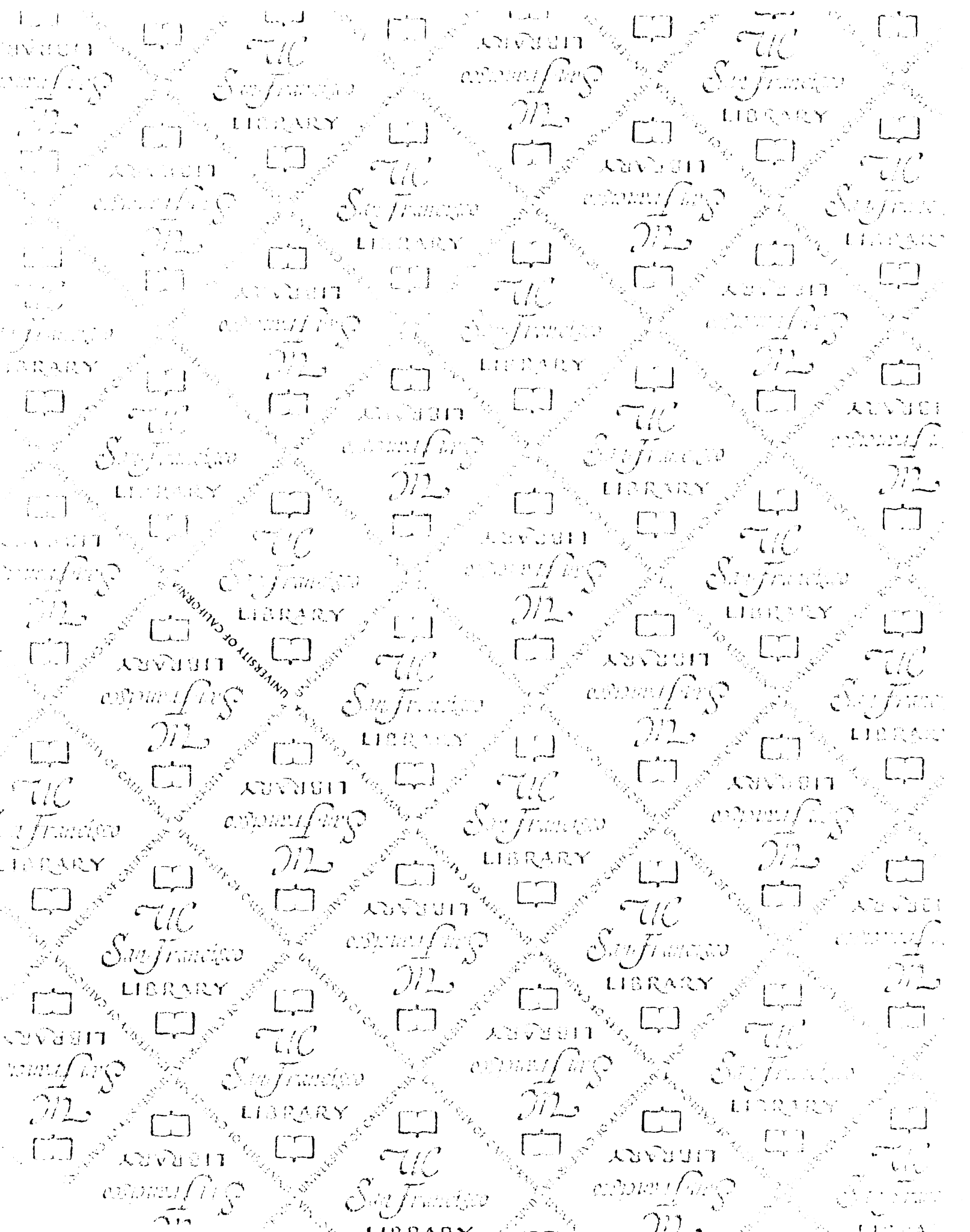Fischer, H., and Plieninger, H. (1942) *Hoppe. Seyl. Z.* **274**, 231.

Frydman, R. B. and Frydman, B. (1987) *Acc. Chem. Res.* **20**, 250-256.

Frydman, R. B., Tomaro, M. L., Buldain, G., Awruch, J., Diaz, L., and Frydman, B. (1981) *Biochemistry* **20**, 5177-5182.

Furhop, H. H., and Smith, K. M. (1975) *Porphyrins and Metalloporphyrins* (Smith, K. M. Ed.) Elsevier, New York, pp 798, 800, 818, 836-837.

Gray, C. H. (1953) *The Bile Pigments*, John Wiley and Sons, New York, 1-15, 37-50.

Hernández, G., Wilks, A., Paolesse, R., Smith, K. M., Ortiz de Montellano, P. R., & and La Mar, G. N. (1994) *Biochemistry.* **33**, 6631-6641.

Inhoffen, H. H., Fuhrhop, J.-H., Voigt, H., and Brockman Jr., H. (1966) *Ann. Chem.* **695**, 133.

Ishikawa, K., Sato, M., Ito, M., and Yoshida, T. (1992) *Biochem. Biophys. Res. Commun.* **182**, 981-986.

Ishikawa, K., Sato, M., and Yoshida, T. (1991) *Eur. J. Biochem.* **202**, 161-165.

Ishikawa, K., Takeuchi, N., Takahashi, S., Matera, K. M., Sato, M., Shibahara, S., Rousseau, D. L., Ikeda-Saito, M., and Yoshida, T. (1995) *J. Biol. Chem.* **270**, 6345-6350.

Ito, S., Suzuki, M., Kobayashi, T, Itoh, H., Harada, A., Ohba, S. and Nishida, Y. (1996) *J. Chem. Soc. Dalton Trans.* 2579.

Ito-Maki, M., Ishikawa, K., Matera, K. M., Sato, M., Ikeda-Saito, M., and Yoshida, T. (1995) *Arch. Biochem. Biophys.* **317**, 253-258.

Jackson, A. H., Kenner, G. W., McGillivray, G., and Smith, K. M. (1968a) *J. Chem. Soc. (C)* 294-301.

Jackson, A. H., Kenner, G. W., and Smith, K. M. (1968b) *J. Chem. Soc. (C)* 302-310.

Kendrew, J. C., Dickerson, R. E., Strandberg, B. D., Hart, R. G., Davies, D. R., Philips, D. C., and V. C. Shore (1960) *Nature* **185**, 422.

Kenner, G. W., Smith, K. M., and Sutton, M. J. (1973) *Tet. Lett.* **16**, 1303-1306.

King, R. F. G. J., and Brown, S. B. (1978) *Biochem. J.* **174**, 103-109.

Kondo, T., Nicholson, D. C., Jackson, A. H., Kenner, G. W. (1971) *Biochem. J.* **121**, 601-607.

Lagarias, J. C. (1982) *Biochim. Biophys. Acta.* **717**, 12-19.

Landaw, S. A., Callahan, E. W., Jr., and Schmid, R. (1970) *J. Clin. Invest.* **49**, 914.

Legge, J. W., and Lemberg, R. (1941) *Biochem. J.* **35**, 353-362.

Lemberg, R. (1935) *Biochem. J.* **29**, 1322.

Lemberg, R. (1943) *Australian. J. Exptl. Biol. Med. Sci.* **21**, 239.

Lemberg, R. (1956) *Rev. Pure Appl. Chem.* **6**, 1-23.

Lemberg, R., Cortis-Jones, B., and Norrie, M. (1938) *Biochem. J.* **32**, 171-186.

Lemberg, R., and Legge, J. W. (1949) in *Hematin Compounds and Bile Pigments*, Interscience, New York, p. 465.

Lemberg, R., Legge, J. W., and Lockwood, W. H. (1941a) *Biochem. J.* **35**, 328-338.

Lemberg, R., Legge, J. W., and Lockwood, W. H. (1941b) *Biochem. J.* **35**, 339-352.

Lemberg, R., Lockwood, W. H., and Legge, J. W. (1941c) *Biochem. J.* **35**, 363-379.

Li, Y., Stamford, P. J., and Battersby, A. R. (1995) *J. Chem. Soc. Perkin Trans. 1* 283-284.

Lin, Q., Simonis, U., Tipton, A. R., Norvell, C. J., and Walker, F. A. (1992) *Inorg. Chem.* **31**, 4216-4217.

Liu, Y., Moënne-Loccoz, P., Loehr, T., and Ortiz de Montellano, P. R. (1997) *J. Biol. Chem.* **272**, 6909-6917.

London, I. M. (1950) *J. Biol. Chem.* **184**, 373.

Luo, D., and Vincent, S. R. (1994) *Eur. J. Pharmacol.* **267**, 263-267.

Maines, M. D. (1988) *FASEB J.* **2**, 2557-2568.

Maines, M. D. (1992a) *Heme Oxygenase: Clinical Applications and Functions*, CRC Press, Boca Raton, FL, 203-266.

Maines, M. D., and Kappas, A. (1974) *Proc. Natl. Acad. Sci. USA* **71**, 4293-4297.

Maines, M. D., and Kappas, A. (1975) *J. Biol. Chem.* **250**, 4171-4177.

Maines, M. D., Trakshel, G. M., and Kutty, R. K. (1986) *J. Biol. Chem.* **261**, 411-419.

Marks, G. S. (1994) *Cell. Molec. Biol.* **40**, 863-870.

Marks, G. S., Brien, J. F., Nakatsu, K., and McLaughlin, B. E. (1991) *Trends Pharmacol. Sci.* **12**, 185-188.

Masuoka, N. and Itano, H. A. (1987) *Biochemistry* **26**, 3672-3680.

McCoubrey, W. K., and Maines, M. D. (1993) *Arch. Biochem. Biophys.* **302**, 402-408.

McDonagh, A. F., and Lightner, D. A. (1985) *Pediatrics* **75**, 443-455.

McDonagh, A. F., Palma, L. A., and Schmid, R. (1981) *Biochem. J.* **194**, 273.

Medforth, C. J., Senge, M. O., Smith, K. M., Sparks, L. D., and Shelnutt, J. A. (1992) *J. Am. Chem. Soc.* **114**, 9859-9869.

Morishima, I., Fujii, H., Shiro, Y. and Sano, S. (1986) *J. Am. Chem. Soc.* **108**, 3858-3860.

Morell, D. B., Barrett, J., and Clezy P. S. (1961) *Biochem. J.* **78**, 793-797.

Nakajima, H. (1963a) *J. Biol. Chem.* **238**, 3797.

Nakajima, H., Takemura, T., Nakajima, O., and Yamoaka, K. (1963b) *J. Biol. Chem.* **238**, 3784.

O'Carra, P. A. and Colleran, E. (1969) *FEBS Lett.* **5**, 295.

Ortiz de Montellano, P. R. (1987) *Acc. Chem. Res.* **20**, 289-294.

Petryka, Z., Nicholson, D. C., and Gray, C. H. (1962) *Nature* **194**, 104-7.

Poss, K., Thomas, M., Ebralidze, A., Odell, T., Tonegawa, S. (1995) *Neuron* **15**, 867-873.

Pratt, J. M., Ridd, T. I. and King, L. J. (1995) *J. Chem. Soc. Chem. Comm.* 2297-2298.

Robinson, S. H. (1968) *New Eng. J. Med.* **279**, 143.

Rotenberg, M. O., and Maines, M. D. (1990) *J. Biol. Chem.* **265**, 7501-7506.

Rotenberg, M. O., and Maines, M. D. (1991) *Arch. Biochem. Biophys.* **290**, 336-344.

Sano, S., Sano, T., Morishima, I., Shiro, Y, and Maeda, Y. (1986) *Proc. Natl. Acad. Sci. U. S. A.* **83**, 531-535.

Sano, S.and Sugiura, Y. (1982) *J. Chem. Soc., Chem Comm.* 750-752

Sano, S., Sugiura, Y., Maeda, Y., Ogawa, S., and Morishima, I. (1981) *J. Am. Chem. Soc.* **103**, 2888-2890.

Saito, S., and Itano, H. A. (1982) *Proc. Natl. Acad. Sci. U. S. A.* **79**, 1393-1397.

Saito, S., and Itano, H. A. (1986) *J. Chem. Soc. Perkin Trans. I* 1-7.

Senge, M. O., Ema, T., and Smith, K. M. (1995) *J. Chem. Soc., Chem. Commun.* 733-734.

Shibahara, S., Muller, R., Taguchi, M., and Yoshida, T. (1985) *Proc. Natl. Acad. Sci. USA* **32**, 7865-7869.

Sjöstrand, T. (1949) *Scand. J. Clin. Lab. Invest.* **1**, 201.

Smith, K. M., Bissett, G. M. F., Bushell, M. J. (1980) *Bioorg. Chem.* **9**, 1-26.

Smith, K. M., Bobe, F. W., and Minnetian, O. M. (1984) *Tetrahedron* **40**, 3263-3272.

Stevens, C. F., and Wang, Y. (1993) *Nature* **364**, 147-149.

Stocker, R., Glazer, A. N., Ames, B. (1987a) *Proc. Natl. Acad. Sci. USA* **84**, 5918-5922.

Stocker, R., Yamamoto, Y., McDonagh, A. F., Glazer, A. N., and Ames, B. N. (1987b) *Science* 1043-1046.

Sun, J., Loehr, T. M., Wilks, A., and Ortiz de Montellano, P. R. (1994) *Biochem.* **33**, 13734-13740.

Sun, J., Wilks, A., Ortiz de Montellano, P. R., and Loehr, T. M. (1993) *Biochemistry* **32**, 14151-14157.

Sun, Y., and Maines, M. D. (1990) *Arch. Biochem. Biophys.* **282**, 340-345.

Takahashi, S., Wang, J., Rousseau, D. L., Ishikawa, K., Yoshida, T., Host, J. R., and Ikeda-Saito, M. (1994a) *J. Biol. Chem.* **269**, 1010-1014.

Takahashi, S., Wang, J., Rousseau, D. L., Ishikawa, K., Yoshida, T., Takeuchi, N., and Ikeda-Saito, M. (1994b) *Biochem.* **33**, 5531-5538.

Tan, H., Simonis, U., Shokhirev, N. V., and Walker, F. A. (1994) *J. Am. Chem. Soc.* **116**, 5784-5790.

Tenhunen, R., Marver, H., and Schmid, R. (1968) *Proc. Natl. Acad. Sci. USA* **61**, 748-755.

Tenhunen, R., Marver, H., and Schmid, R. (1969) *J. Biol. Chem.* **244**, 6388-6394.

Tenhunen, R., Marver, H., Pimstone, N. R., Trager, W. F., Cooper, D. Y., and Schmid, R. (1972) *Biochemistry* **11**, 1716-1720.

Tenhunen, R., Ross, M. E., Marver, H. S., and Schmid, R. (1970) *Biochemistry* **9**, 298-303.

Tephly, T. R. and Hibbeln, P. (1971) *Biochem. Biophys. Res. Commun.* **244**, 6388-6394.

Tomaro, M. L., Frydman, R. B., Frydman, B., Pandey, R. K., and Smith, K. M. (1984) *Biochimica et Biophysica Acta* **791**, 342-349.

Trakshel, G. M., Kutty, R. K., and Maines, M. D. (1986) *J. Biol. Chem.* **261**, 11131-11137.

Trakshel, G. M., Kutty, R. K., and Maines, M. D. (1988) *Arch. Biochem. Biophys.* **260**, 732-739.

Verma, A., Hirsch, D. J., Glatt, C. E., Ronnett, G. V., and Snyder, S. H. (1993) *Science* **259**, 381-384.

Vernon, D. I., and Brown, S. B.(1984) *Biochem. J.* **223**, 205-209.

Warburg, O., and Negelein, E. (1930) *Berichte* **63B**, 1816.

Wilks, A., Black, S. M., Miller, W. L., and Ortiz de Montellano, P. R. (1995a) *Biochem.* **34**, 4421-4427.

Wilks, A., and Ortiz de Montellano, P. R. (1993) *J. Biol. Chem.* **268**, 22357-22362.

Wilks, A., and Ortiz de Montellano, P. R., Sun, J., and Loehr, T. M. (1996) *Biochemistry* **35**, 930-936.

Wilks, A., Sun, J., Loehr, T. M., and Ortiz de Montellano, P. R. (1995b) *J. Am. Chem. Soc.* **117**, 2925-2926.

Wiseman, J. S., Nichols, J. S., Kolpak, M. X. (1982) *J. Biol. Chem.* **257**, 6328-6332.

Yoshida, T., Biro, P., Cohen, T., Müller, R. M., and Shibahara, S. (1988) *Eur. J. Biochem.* **171**, 457-461.

Yoshida, T. Ishikawa, K., and Sato, M. (1991) *Eur. J. Biochem.* **199**, 729-733.

Yoshida, T., and Kikuchi, G. (1978) *J. Biol. Chem.* **253**, 4224-4230.

Yoshida, T., and Kikuchi, G. (1979) *J. Biol. Chem.* **254**, 4487-4491.

Yoshida, T., and Noguchi, M. (1984) *J. Biochem. (Tokyo)* **96**, 563-570.

Yoshida, T., Noguchi, M., Kikuchi, G. (1980) *J. Biochem. (Tokyo)* **88**, 537-563.

Yoshida, T., Noguchi, M., Kikuchi, G. (1982) *J. Biol. Chem.* **257**, 9345-9348.

Yoshida, T., Noguchi, M., Kikuchi, G., and Sano, S. (1981) *J. Biochem. (Tokyo)* **90**, 125-131.

Yoshida, T., and Sato, M. (1989) *Biochem. Biophys. Res. Comm.* **163**, 1086-1092.

Yoshida, T. Takahashi, S. and Kikuchi, G. (1974) *J. Biochem. (Tokyo)* **75**,1187-1191.

Yoshinaga, T., Sassa, S., and Kappas, A. (1982) *J. Biol. Chem.* **257**, 7794-7802.

Yoshinaga, T., Sudo, Y., and Sano, S. (1990) *Biochem. J.* **270**, 659-664.

Zhuo, M., Small, S. A., Kandel, E. R., and Hawkins, R. D. (1993) *Science* **260**, 1946-1950.